

**AMMONIA RECOVERY FROM MUNICIPAL WASTEWATER THROUGH  
A STRUVITE FORMATION-THERMAL DECOMPOSITION CYCLE**

by

CONNOR WALTER WILSON

B.A.Sc., The University of British Columbia, 2010

A THESIS SUBMITTED IN PARTIAL FULFILLMENT OF THE  
REQUIREMENTS FOR THE DEGREE OF

MASTER OF APPLIED SCIENCE

in

The FACULTY OF GRADUATE AND POSTDOCTORAL STUDIES

(Civil Engineering)

THE UNIVERSITY OF BRITISH COLUMBIA

(Vancouver)

September 2013

© Connor Walter Wilson, 2013

## ABSTRACT

Bench-scale batch experiments were performed to assess the potential for ammonia removal and recovery from municipal post-digestion waste streams via struvite ( $\text{MgNH}_4\text{PO}_4 \cdot 6\text{H}_2\text{O}$ ) crystallization using thermally decomposed struvite as a source of magnesium and orthophosphate. To simulate this process, newberyite ( $\text{MgHPO}_4 \cdot 3\text{H}_2\text{O}$ ), a synthesized surrogate for thermally decomposed struvite, was added to various ammonia solutions including synthetic struvite crystallizer effluent and synthetic dewatering centrate. The main objective of this study was to develop the concept of the proposed technology through evaluation of the effects of chemical and physical factors on the rates and mechanisms of ammonia removal, orthophosphate solubilization, and overall newberyite-to-struvite conversion efficiency.

A model was developed using PHREEQC software to simulate each batch experiment and to predict the solid and liquid phase compositions that would result from these systems attaining chemical equilibrium. Experimental and model-predicted results were employed for the delineation of near optimal conditions for efficient transformation of newberyite into struvite.

Ammonia removal efficiencies as high as 87% were achieved while maintaining orthophosphate residuals as low as 10 mg/L  $\text{PO}_4\text{-P}$ . Measurements of liquid phase compositions at reaction times approaching equilibrium compared well with that predicted by the model. Results suggested an optimum within a region of 1 to 3 hour reaction times, pH between 7 and 8, temperature between 10° and 25° C, and at a newberyite dose that provides a suspension Mg:N:P molar ratio of 1:1:1.

Although the results of the present study illustrate the potential of this technology, it is recommended that further research be performed employing the newberyite-containing material produced by the pilot-scale struvite thermal decomposition reactor located at the University of British Columbia.

## PREFACE

This thesis is original, unpublished, independent work by the author, C. Wilson.

---

**TABLE OF CONTENTS**

ABSTRACT.....	ii
PREFACE.....	iii
TABLE OF CONTENTS.....	iv
LIST OF TABLES.....	viii
LIST OF FIGURES.....	ix
LIST OF ABBREVIATIONS AND SYMBOLS.....	xi
ACKNOWLEDGEMENTS.....	xii
CHAPTER 1: INTRODUCTION.....	1
CHAPTER 2: BACKGROUND.....	5
2.1    Motivation for ammonia removal and recovery.....	5
2.1.1    Conventional ammonia synthesis.....	6
2.1.2    Demand for nitrogenous fertilizers.....	7
2.1.3    Ammonia as a fuel.....	8
2.1.4    Economic benefits of recovery of ammonia at municipal WWTPs.....	10
2.2    Existing ammonia recovery options for post-digestion side streams.....	12
CHAPTER 3: RESEARCH OBJECTIVES.....	15
CHAPTER 4: LITERATURE REVIEW.....	16
4.1    Chemistry of magnesium and phosphate compounds.....	16
4.1.1    Aqueous equilibria affecting speciation of magnesium, ammonium, orthophosphate, and carbonate.....	17
4.1.2    Solubility products.....	18
4.2    Struvite and newberyite morphology.....	18
4.3    Factors affecting struvite formation.....	20
4.3.1    Supersaturation.....	20
4.3.2    Mg:P and N:P molar ratio.....	21
4.3.3    Hydrodynamics.....	22
4.4    UBC struvite crystallization process.....	23

4.4.1	Pilot-scale UBC struvite crystallizer design .....	23
4.4.2	Pilot-scale UBC struvite crystallizer operation.....	26
4.5	Struvite decomposition products as ammonia removal agents .....	26
4.5.1	Struvite decomposition in solution – “Wet process”.....	28
4.5.2	Ammonia removal following “wet process” .....	31
4.5.3	Thermal decomposition of struvite in air – “Dry process” .....	33
4.5.4	Ammonia removal following “dry process” .....	35
4.6	Potential ammonia gas capture techniques .....	37
4.7	Conclusions for development of present study.....	38
CHAPTER 5: MATERIALS AND METHODS.....		40
5.1	Description of performed batch tests.....	40
5.2	Ammonia solutions – Synthetic wastewaters.....	41
5.3	Synthetic newberyite .....	42
5.3.1	Synthesis .....	42
5.3.2	Analysis .....	42
5.4	Materials and equipment .....	43
5.4.1	Batch test method and apparatus .....	43
5.4.2	pH monitoring.....	44
5.4.3	Conductivity monitoring .....	44
5.4.4	Ammonium monitoring.....	44
5.4.5	PHREEQC-2 chemical equilibrium model.....	45
5.5	Sample collection and preservation .....	45
5.6	Analytical methods .....	46
5.6.1	Magnesium .....	46
5.6.2	Ammonia and orthophosphate.....	47
5.6.3	Carbonate alkalinity .....	47
5.6.4	XRD identification of solid phases.....	47
5.6.5	Crystal morphology.....	47
5.7	Statistics .....	48
5.8	Terminology .....	48
5.8.1	Molar ratio .....	48

5.8.2	Solubility product ( $K_{sp-N}$ and $K_{sp-S}$ ) .....	49
5.8.3	Supersaturation ratio .....	49
5.8.4	Removal efficiency .....	50
CHAPTER 6: RESULTS AND DISCUSSION .....		51
6.1	Fundamentals of newberyite dissolution-struvite formation mechanism in the presence of ammonium.....	51
6.2	Transformation of newberyite into struvite in ammonia solution: Phase 1 – Suspension Mg:N:P molar ratio of 1:1.1:1 .....	51
6.2.1	pH effect on rate and efficiency of ammonia removal .....	52
6.2.2	pH effect on rate and extent of orthophosphate solubilization .....	55
6.2.3	Temperature effect on rate and efficiency of ammonia removal .....	58
6.2.4	Temperature effect on rate and extent of orthophosphate solubilization .....	60
6.2.5	XRD analysis of solid phase mixtures .....	62
6.2.6	Chemical composition of solid phase mixtures .....	63
6.2.7	Comparison of experimental results and model predictions .....	65
6.2.8	Initial rates of newberyite dissolution and struvite formation .....	68
6.3	Transformation of newberyite into struvite in ammonia solution: Phase 2 – Suspension Mg:N:P molar ratio of 1:1.4:1 .....	69
6.3.1	Newberyite dose effect on rate and efficiency of ammonia removal .....	70
6.3.2	Newberyite dose effect on rate and extent of orthophosphate solubilization .....	73
6.4	Transformation of newberyite into struvite in synthetic crystallizer effluent .....	76
6.4.1	Ammonia removal.....	78
6.4.2	Orthophosphate residual .....	79
6.4.3	Chemical composition of solid phase mixtures .....	81
6.4.4	Newberyite and struvite supersaturation.....	82
6.4.5	Caustic consumption.....	85
6.4.6	Crystal morphology.....	86
6.5	Transformation of newberyite into struvite in synthetic centrate .....	89
6.5.1	Ammonia removal.....	91
6.5.2	Online ammonium residual monitoring.....	92
6.5.3	Orthophosphate residual .....	94
6.5.4	Chemical composition of solid phase mixtures .....	95

6.5.5	Newberyite and struvite supersaturation.....	96
6.5.6	Caustic consumption.....	98
6.5.7	Crystal morphology.....	98
CHAPTER 7: CONCLUSIONS.....		102
CHAPTER 8: RECOMMENDATIONS.....		104
REFERENCES.....		105
APPENDIX A: INSTRUMENT OPERATIONAL SETTINGS.....		115
APPENDIX B: LIQUID AND SOLID SAMPLE COMPOSITIONS.....		116
APPENDIX C: RESULTS OF XRD ANALYSIS OF SOLID SAMPLES.....		130
APPENDIX D: MODELLING RESULTS.....		151

---

**LIST OF TABLES**

Table 1 – Modelled savings for two WWTPs implementing ammonia recovery from dewatering centrate (ThermoEnergy Corporation, 2007).....	11
Table 2 – 2013 prices for various ammonium-derived fertilizers (USDA ERS, 2013).....	11
Table 3 – Experimentally determined $pK_{sp}$ at 25° C for various magnesium and phosphate compounds .....	18
Table 4 – Range of operation and performance for UBC struvite crystallizer pilot studies .....	26
Table 5 – Summary of struvite decomposition studies using thermal-alkali treatment .....	31
Table 6 – Summary of ammonia removal studies using struvite decomposed under thermal-alkali conditions.....	32
Table 7 – Summary of experimental parameters for duplicate batch tests.....	40
Table 8 – Annacis Island WWTP centrate compared to studied solutions .....	42
Table 9 – Synthetic newberyite chemical composition and concerned experiments .....	43
Table 10 – Suspension characteristics at t = 0 h for Mg:N:P molar ratio 1:1.1:1 newberyite dose batch tests .....	52
Table 11 – Suspension characteristics at t = 0 h for Mg:N:P molar ratio 1:1.4:1 newberyite dose batch tests .....	70
Table 12 – Suspension characteristics at t = 0 h for Mg:N:P molar ratio 1:1:1 newberyite dose in synthetic crystallizer effluent batch tests .....	78
Table 13 – Suspension characteristics at t = 0 h for Mg:N:P molar ratio 1:1.05:1 newberyite dose in synthetic centrate batch tests .....	91

## LIST OF FIGURES

Figure 1 – Historic trends in world population, fertilizer consumption, and meat production (Erisman et al., 2008).....	8
Figure 2 – Star-shaped dendritic (a), X-shaped twinned (b), coffin-shaped (c), and rod-like (d) struvite crystals (Abbona et al., 1985) .....	19
Figure 3 – Pseudo-octagonal newberyite crystals amongst dissolving tabular struvite crystal (a); rhombohedral newberyite crystals (b and c) (Boistelle et al., 1983; Kontrec et al., 2005; Babić-Ivančić et al., 2002).....	20
Figure 4 – General schematic of UBC struvite crystallization process (top) and crystallizer injector (bottom) (Fattah, 2004).....	25
Figure 5 – Conceptual schematic of $\text{NH}_4$ removal through reuse of Mg and $\text{PO}_4$ .....	28
Figure 6 – Schematic diagram of reusing MAP residues for ammonia removal by acid dipping as proposed by Zhang et al. (2004) .....	29
Figure 7 – $\text{NH}_4\text{-N}$ removed for various pH conditions at (a) $10^\circ$ , (b) $25^\circ$ , and (c) $35^\circ$ C .....	54
Figure 8 – Residual $\text{PO}_4\text{-P}$ for various pH conditions at (a) $10^\circ$ , (b) $25^\circ$ , and (c) $35^\circ$ C .....	57
Figure 9 – $\text{NH}_4\text{-N}$ removed for various temperatures for (a) no pH control, (b) pH 7, (c) pH 8, and (d) pH 9.....	59
Figure 10 – Residual $\text{PO}_4\text{-P}$ for various temperatures for (a) no pH control, (b) pH 7, (c) pH 8, and (d) pH 9.....	61
Figure 11 – N:P molar ratio of solid phase mixtures sampled at 1 h (No pH = no pH control) ....	64
Figure 12 – N:P molar ratio of solid phase mixtures sampled at 3 and 12 h (No pH = no pH control).....	64
Figure 13 – Comparison of real and model-predicted $\text{NH}_4\text{-N}$ for $25^\circ$ C.....	66
Figure 14 – Comparison of real and model-predicted $\text{PO}_4\text{-P}$ for $25^\circ$ C.....	66
Figure 15 – Comparison of real and model-predicted N:P molar ratios of solid phase mixtures	67
Figure 16 – pH vs time for no pH control at $10^\circ$ C .....	69
Figure 17 – $\text{NH}_4\text{-N}$ removed for various pH conditions at (a) $10^\circ$ , (b) $25^\circ$ , and (c) $35^\circ$ C .....	72
Figure 18 – $\text{NH}_4\text{-N}$ removed at $25^\circ$ C for Mg:N:P molar ratio of (a) 1:1.1:1 and (b) 1:1.4:1 .....	73
Figure 19 – Residual $\text{PO}_4\text{-P}$ for various pH conditions at (a) $10^\circ$ , (b) $25^\circ$ , and (c) $35^\circ$ C .....	75
Figure 20 – $\text{PO}_4\text{-P}$ residual at $25^\circ$ C for Mg:N:P molar ratio of (a) 1:1.1:1 and (b) 1:1.4:1 .....	76
Figure 21 – Reactor Configuration 1: Ammonia recovery from primary crystallizer effluent .....	77
Figure 22 – Comparison of real and model-predicted $\text{NH}_4\text{-N}$ .....	79

Figure 23 – Comparison of real and model-predicted $\text{PO}_4\text{-P}$ .....	81
Figure 24 – N:P molar ratio of solid phase sampled at 1 and 4 h .....	82
Figure 25 – Newberyite and struvite supersaturation ratio at pH 7 .....	83
Figure 26 – Newberyite and struvite supersaturation ratio at pH 8 .....	84
Figure 27 – Theoretical struvite supersaturation ratio immediately after mixing of liquid reagents .....	85
Figure 28 – Comparison of real and model-predicted caustic consumption .....	86
Figure 29 – x40 magnified newberyite (a); 1 hour samples from pH 7-10° C (b), pH 7-25° C (c), and pH 8-25° C (d) .....	87
Figure 30 – x10 magnified 4 hour samples from pH 7-10° C (a), pH 7-25° C (b), pH 8-10° C (c), and pH 8-25° C (d) .....	88
Figure 31 – x40 magnified 4 hour samples from pH 7-10° C (a), pH 7-25° C (b), pH 8-10° C (c), and pH 8-25° C (d) .....	89
Figure 32 – Reactor Configuration 2: Ammonia recovery from dewatering centrate .....	90
Figure 33 – Comparison of real and model-predicted $\text{NH}_4\text{-N}$ .....	92
Figure 34 – Comparison of probe and sample measured $\text{NH}_4\text{-N}$ .....	93
Figure 35 – Comparison of real and model-predicted $\text{PO}_4\text{-P}$ .....	95
Figure 36 – N:P molar ratio of solid phase sampled at 1 and 4 h .....	96
Figure 37 – Newberyite and struvite supersaturation ratio at pH 7 .....	97
Figure 38 – Newberyite and struvite supersaturation ratio at pH 8 .....	97
Figure 39 – Comparison of real and model-predicted caustic consumption .....	98
Figure 40 – x40 magnified synthetic newberyite batches (a and b); 1 hour samples from pH 7-10° C (c), and pH 7-25° C (d) .....	99
Figure 41 – x10 magnified 4 hour samples from pH 7-10° C (a), pH 7-25° C (b), pH 8-10° C (c), and pH 8-25° C (d) .....	100
Figure 42 – x40 magnified 4 hour samples from pH 7-10° C (a), pH 7-25° C (b), pH 8-10° C (c), and pH 8-25° C (d) .....	101

**LIST OF ABBREVIATIONS AND SYMBOLS**

ARP	Ammonia Recovery Process
CRT	crystal retention time
EUR	Euro
FBR	fluidized bed reactor
GBP	Great British Pound
HRT	hydraulic retention time
$K_{sp-N}$	newberyite solubility product
$K_{sp-S}$	struvite solubility product
MLD	million litres per day
n	number of samples
$P_{S-eq}$	conditional solubility product of struvite at equilibrium
$P_{S-reactor}$	in-reactor conditional solubility of struvite
QTG	quasi-isothermal thermogravimetry
s	standard deviation
$S_N$	supersaturation ratio with respect to newberyite
$S_S$	supersaturation ratio with respect to Struvite
t	Student's t-value
UBC	University of British Columbia
USD	United States Dollar
USDA ERS	United States Department of Agriculture Economic Research Service
USEPA	United States Environmental Protection Agency
USGS	United States Geological Survey
WERF	Water Environment Research Foundation
WWTP	wastewater treatment plant
XRD	X-ray diffraction

## ACKNOWLEDGEMENTS

- My partner, Aubrie, for encouraging me to pursue an impactful and fulfilling career and for her support throughout my degree
- My supervisor, Dr. Donald Mavinic, for his insight, enthusiasm, and for bringing the nutrient recovery group to life
- My mentors, Dr. Sergey Lobanov and Frederic Koch, for their unparalleled knowledge and experience
- Paula Parkinson and Timothy Ma for kindly providing their analytical and experimental expertise
- Natural Sciences and Engineering Research Council of Canada for their generous funding
- My loving family
- My friends for cheering me on

## CHAPTER 1: INTRODUCTION

Nitrogen is essential to life and is among the nutrients consumed in the largest quantities by organisms. Wastewater nitrogen is derived primarily from organic matter originating from human, animal and food processing wastes. Organic nitrogen is decomposed by bacteria to release ammonia. Aqueous ammonia takes the form of both ammonium ( $\text{NH}_4^+$ ) and un-ionized ammonia gas ( $\text{NH}_3$ ). In typical environmental conditions the majority of ammonia exists as ammonium. However, un-ionized ammonia is known to be more toxic to organisms living in receiving bodies (Environment Canada, 2001; Randall and Tsui, 2002). Ammonia discharge is reduced through wastewater treatment to prevent these toxic effects as well as to avoid eutrophication of downstream aquatic or marine environments. To achieve lower nitrogen discharge goals, wastewater treatment plants (WWTPs) employ biological nitrogen removal processes, such as nitrification, which is commonly followed by denitrification to ultimately convert ammonia to atmospheric nitrogen.

Aerobic or anaerobic digestion of the biosolids produced during wastewater treatment results in the release of a significant fraction of the nutrients that were previously removed. Ammonia is contained in liquid biosolids streams at levels which generally far exceed that of the raw influent wastewater. Therefore, digester supernatant, as well as the filtrate or centrate generated during digested sludge dewatering, are returned upstream for further treatment. These streams carry high ammonium and orthophosphate concentrations and, in the presence of magnesium, they may be supersaturated with respect to magnesium ammonium phosphate ( $\text{MgNH}_4\text{PO}_4 \cdot 6\text{H}_2\text{O}$ ), also known as struvite. Struvite is a sparingly soluble salt that commonly forms in systems which convey post-digestion streams. Deposits may appear as scale on the walls of pipes or within equipment. This has the potential to damage pumps and dewatering equipment, as well as significantly reduce the diameter of pipes resulting in a loss of hydraulic capacity and lower operational efficiency. Therefore, chemical removal of orthophosphate or routine system cleaning with acid is often required, consequently increasing process complexity and maintenance costs.

To avoid the operational issues surrounding unwanted formation, controlled crystallization of struvite may be employed to reduce its supersaturation in wastewater. One technology that has successfully been used for this purpose is the fluidized bed reactor (FBR) designed at University of British Columbia, also known as the UBC struvite crystallizer (Dastur, 2001; Adnan, 2002;

Britton, 2002; Huang, 2003; Fattah, 2004). The UBC struvite crystallization process provides the chemical and hydrodynamic conditions favourable for the incorporation of struvite crystals into agglomerates and eventually pellets. After sufficient reaction time, struvite pellets are harvested and may be sold as a high-purity, slow-release fertilizer containing equimolar parts magnesium, ammonium and orthophosphate. This process was made commercially available by Ostara Nutrient Recovery Technologies Inc., who has commissioned six municipal struvite recovery facilities to date (Ostara Nutrient Recovery Technologies Inc., 2007; Britton et al., 2009; Ostara Nutrient Recovery Technologies Inc., 2011).

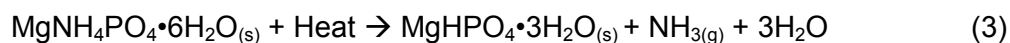
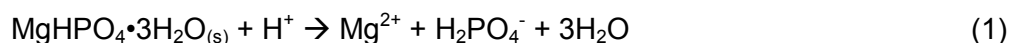
Municipal wastewater is generally much higher in nitrogen relative to phosphorus. Therefore, with the addition of sufficient magnesium, the amount of struvite that can be formed from these streams is limited by its orthophosphate concentration. Pilot and full-scale studies have proven that the UBC struvite crystallization process is capable of consistently providing orthophosphate removals from post-digestion streams between 80% and 99%. However, this process only removes, on average, between 5% and 10% of the nitrogen; this means that the crystallizer effluent is still rich in ammonia (Britton, 2002; Huang, 2003; Fattah, 2004; Ostara Nutrient Recovery Technologies Inc., 2007, 2011; Britton et al., 2009). Following struvite recovery, the crystallizer effluent is returned to upstream processes where ammonia is restabilized. If external magnesium and orthophosphate was added to this stream, a significant portion of the residual ammonia could theoretically be recovered as struvite, while considerably increasing plant ammonia removal capacity and reducing aeration costs.

Recent research has focussed on the recovery of phosphorus from wastewater to offset the world's reliance on localized and limited phosphate rock reserves for global food security (Le Corre et al., 2009; WERF, 2010; Liu et al., 2012). Since ammonia is synthesized commercially from atmospheric nitrogen, the main constituent in air, through the Haber-Bosch process, it is impractical to convert high quality sources of orthophosphate to struvite in order to recover it. Nevertheless, the ammonia production industry relies heavily on natural gas as a non-renewable precursor for hydrogen (Smil, 2001; Erisman et al., 2008). It is a frightening concept that the availability of an ingredient so widely used in a fertilizer that is crucial in feeding the world is dependent on a fossil fuel that has, in the past, experienced market volatility (Mohr and Evans, 2011; Maggio and Cacciola, 2012). Further, the processes of synthesizing ammonia and removing it from wastewater are both energy and resource intensive. If an inexpensive source

of external magnesium and orthophosphate were available, the potential is there to recover ammonia from nutrient-rich sidestreams, rather than biologically convert it back to atmospheric nitrogen or lock it up in waste solids.

A possible source of magnesium and orthophosphate could be derived from recovered struvite itself. However, this requires the removal of the ammonium that is bound within struvite. Several studies have shown that struvite can be used as a precursor to produce other magnesium phosphate materials under various experimental conditions (Abdelrazig and Sharp, 1988; Sarkar, 1991; Sugiyama et al., 2005; Bhuiyan et al., 2008; Kurtulus and Tas, 2011, Novotny, 2011). Newberyite ( $\text{MgHPO}_4 \cdot 3\text{H}_2\text{O}$ ) is an ideal material as it contains no ammonium, but previous studies suggest that significant chemical addition would be required to produce it from a struvite suspension (Boistelle et al., 1983; Zhang et al., 2004; Babić-Ivančić et al., 2006). Using a proprietary technology recently developed at UBC, pelletized struvite can be converted to a nearly pure source of crystalline newberyite through relatively low temperature thermal decomposition in air.

Newberyite is expected to fully dissolve in ammonia-rich wastewater and recrystallize as struvite with control of temperature and/or pH. This presents an opportunity to efficiently recycle magnesium and orthophosphate while removing and recovering ammonia. In essence, a significant portion of the struvite formed through these reactions could be thermally decomposed to produce more newberyite. Further, there is the potential to recover the ammonia gas evolved during this process which represents commercial value as a high-purity source of reactive nitrogen. Eqns. 1, 2, and 3 illustrate the theory of magnesium and orthophosphate recycling through the systematic reactions of newberyite dissolution, struvite recrystallization, and struvite thermal decomposition.



For the described technology to be justified economically, it is essential that the outlined process offers high ammonia recovery efficiency and a short reaction time. Further, it is hypothesized that newberyite will dissolve in wastewater and that nearly 100% of the orthophosphate released can be utilized in the formation of struvite. To explore these hypotheses, this research employed a systematic approach. For a variety of experimental conditions, the reaction rates were observed for the conversion of newberyite to struvite in the presence of ammonium. This work employed batch tests to examine several combinations of synthetic newberyite with an ammonia solution, synthetic crystallizer effluent, and synthetic dewatering centrate. The extent of reactions with respect to time was evaluated based on liquid and solid phases compositions, as well as solid morphologies. This data was compared to the outputs of a chemical equilibrium model to verify its usefulness in future development of the proposed ammonia removal and recovery technology.

## CHAPTER 2: BACKGROUND

### 2.1 Motivation for ammonia removal and recovery

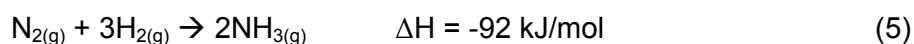
Nitrogen is one of the primary nutrients essential to life and ammonia is taken up by terrestrial organisms either directly or indirectly to satisfy nutritional needs. As a part of the nitrogen cycle, ammonia can be produced from atmospheric nitrogen ( $N_2$ ) by select organisms or it can be converted to atmospheric nitrogen by combined nitrification and denitrification. Ammonia is synthesized at a massive scale by the fertilizer industry. Approximately 100 Mt of reactive nitrogen is synthesized annually worldwide using the Haber-Bosch process. To put this anthropogenic effect in perspective, about 150 to 200 Mt nitrogen is fixed naturally per year on earth, mostly by symbiotic diazotrophs (Smil, 2001). Not all of the ammonia applied to land is utilized by crops and losses can be attributed to runoff and leaching. It has been estimated that only 17% of the 100 Mt of reactive nitrogen synthesized for global agriculture in 2005 were actually consumed as food by humans (Erisman et al., 2008; Aiking 2011).

Humans excrete a significant fraction of the nutrients contained in the food they ingest. Alongside agricultural sources, these nutrients find their way back into the environment as municipal wastewater effluents and organic matter deposited to landfills. Anthropogenic loading of nutrients is the main cause for eutrophication of receiving water bodies. Eutrophication of lakes and coastal estuaries results in enhanced productivity and the formation of algal blooms that are detrimental to local ecosystems. This is extremely difficult to remedy as nutrients are cycled between organic matter deposited in sediment and the water column. In severe cases, this boost in organic carbon content can result in increased heterotrophic activity in the sediments contributing to oxygen-deficient zones. These are also referred to as “dead zones”, as their formation will decimate local aerobic organism populations. Pollution from these sources also increases un-ionized ammonia levels in aquatic and marine environments, which is known to be toxic to many organisms (Environment Canada, 2001; Randall and Tsui, 2002). For these reasons, nitrogen discharge is heavily regulated in many countries and biological nutrient removal processes were developed for municipal wastewater treatment. These processes essentially lock up the nitrogen originating from chemical fertilizers in solids for disposal and/or destroy it through conversion to atmospheric nitrogen.

The current paradigm of synthesis and subsequent loss, disposal, and destruction of ammonia is wasteful. Ammonia fertilizer manufacturing and municipal wastewater treatment are both resource and energy intensive tasks. Municipal wastewater should be viewed as an ammonia resource and nutrient-rich waste streams should be exploited through the recovery of ammonia in forms that could be employed by agriculture or other industries.

### **2.1.1 Conventional ammonia synthesis**

The atmosphere contains 78% nitrogen and, unlike phosphorus, it is not considered a limited resource on earth. Using the Haber-Bosch process, ammonia can be synthesized from atmospheric nitrogen gas as needed. Eqn. 5 provides a general explanation of this process.



At a temperature and pressure of approximately 400 to 450° C and 10 to 30 MPa respectively, hydrogen and nitrogen gas are combined to form ammonia (Smil, 2001). This reaction is generally performed in the presence of an iron catalyst. The Haber-Bosch process of today is not particularly efficient and allows for a nitrogen-to-ammonia molar conversion of about 15% per pass and, therefore, unreacted gases are recycled further to achieve overall conversions of about 98% (Smil, 2001). Approximately 85% of the ammonia worldwide is produced from hydrogen gas generated through steam reforming of light hydrocarbons of which 80% of processes utilize natural gas (Smil, 2001; Wood and Cowie, 2004). Ammonia synthesis is responsible for about 5% of the world's natural gas consumption (Maxwell, 2005). Further, providing the conditions of high temperature and pressure are energetically expensive. It is estimated that global ammonia production accounts for 1.3% of the world's fossil fuel-derived energy use, contributing considerable greenhouse gas emissions (Smil, 2001; Erisman et al., 2008). However, there is debate concerning the role that ammonia production plays in global warming, since enrichment of aquatic and marine environments by synthetic ammonia is a cause for eutrophication and, therefore, enhanced carbon dioxide sequestration. Although reactive nitrogen is a renewable resource, the cost and availability of ammonia-based fertilizers depend heavily on that of fossil fuels and energy.

### **2.1.2 Demand for nitrogenous fertilizers**

The cultivation of food crops results in the transfer of nutrients from the soil to plant matter. When these crops are harvested, generally only a portion of the nutrients from these plant residues are reintroduced in the soil. The nitrogen cycle is broken with respect to conventional agriculture, since the majority of the nutritional elements that went into growing crops are lost to the environment, disposed of in landfills, or emitted to the atmosphere. Synthetic fertilizers are believed to provide 60% to 80% of the nitrogen requirements for cultivation of high staple crops (Smil, 2001). Without these inputs, the world population would be significantly lower than it is today. As a result of the Haber-Bosch process for ammonia synthesis, the number of people one hectare of arable land can support has increased from approximately 1.9 to 4.3 between 1908 and 2008. Today, it is estimated that 80% of the ammonia produced is used for manufacturing nitrogenous fertilizers (Erisman et al., 2008). Further, assuming the global adoption of extremely basic, vegetarian diets, preindustrial agriculture could provide for only about 40% of the today's world population (Smil, 2001).

Synthetic fertilizers have allowed for massive growth of the livestock industries resulting in a worldwide shift towards more meat-based and dairy-based diets. These changes to human diets further increase demands as meat and dairy production indirectly require more fertilizer than cereal and vegetable crops. During the mid-1990's, about one third of the nitrogen used to grow crops was fed to domestic animals (Smil, 2001). This is of concern because livestock protein conversion efficiencies for chicken, pork, and beef are approximately 20%, 10%, and 5% respectively, and little more than half of the nitrogen contained in animal manures is used globally for cultivation of crops (Smil, 2001; Aiking 2011). Figure 2 illustrates historic trends with respect to world population, fertilizer application, and meat production. It is predicted that the world population will increase by about 2.3 billion in the next 40 years and feeding the world will not be possible without global shifts towards more efficient transfer of synthesized ammonia to food, preservation of land fertility, lower overall meat and dairy consumption, and more sustainable production of fertilizers (Aiking, 2011).

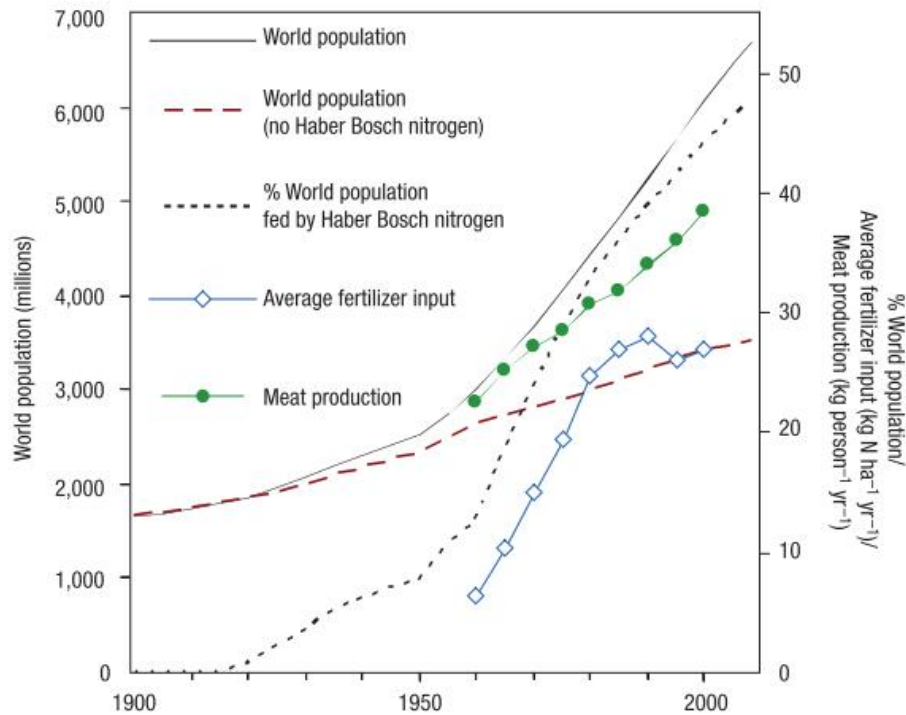


**Figure 1 – Historic trends in world population, fertilizer consumption, and meat production (Erisman et al., 2008)**

### **2.1.3 Ammonia as a fuel**

It is inevitable that humans will be forced to turn away from non-renewable fossil fuels to more sustainable energy sources with fewer environmental impacts. Although hydrogen is commonly mentioned as a synthesizable alternative, it has a far lower octane level when compared to other fuels burned by vehicles and its adoption suggests significant challenges with regard to safe storage and distribution (Yin et al., 2004; Christensen et al., 2006; Lan et al., 2012). Ammonia can provide more energy per unit volume than hydrogen (Zamfirescu and Dincer, 2009). Hydrogen is also three times more expensive than ammonia, with respect to the volume of stored energy (Zamfirescu and Dincer, 2008). Further, ammonia is safer than hydrogen due to its narrow flammability limits and it is generally considered non-explosive. It also possesses a characteristic odour which alarms those nearby of its presence. Since ammonia is already widely used in industry, distribution methods are well established and it is stored for combustion in a similar fashion to propane, making it attractive for vehicular operations (Zamfirescu and

Dincer, 2008; Zamfirescu and Dincer, 2009). Some advanced ammonia internal combustion engines are designed to use compression ratios several times higher than that of the conventional. Alternatively, conventional internal combustion engines can run on a mixture of 80% ammonia and 20% gasoline with minor modifications (Zamfirescu and Dincer, 2009). Up to 60% of the energy used in a turbocharged diesel engine can be supplied by ammonia with a conversion efficiency of close to 100% (Reiter and Kong, 2011). As compared to gasoline, liquid petroleum gas, compressed natural gas, and methanol, ammonia has the lowest cost per energetic unit when used in the 100 km driving range (Zamfirescu and Dincer, 2008; Zamfirescu and Dincer, 2009). Ammonia is also an excellent refrigerant. It is estimated that engine performance may be improved by 10% by using onboard ammonia for engine cooling and air conditioning (Zamfirescu and Dincer, 2009).

A major advantage ammonia has over fossil fuels is that its combustion produces no carbon dioxide or sulfur oxides. Nevertheless, the burning of ammonia in internal combustion engines could potentially result in the release of some nitrogen oxides. However, this emission may be minimized through the optimization of air-to-fuel ratios (Zamfirescu and Dincer, 2009). Although combustion of ammonia proposes a concern based on its toxicity, ammonia pollution may be mitigated using well established reversible adsorption techniques (Elmøe et al., 2006). Current trends in research suggest a future advancement of hydrogen fuel cell technology but, again, one of the major obstacles for the shift towards hydrogen-based energy is the need for safe techniques of hydrogen storage and transport. These issues could be avoided by using ammonia and other storage materials as indirect sources of hydrogen. In place of hydrogen, ammonia may be transported in compressed cylinders or as decomposable materials such as  $\text{Mg}(\text{NH}_3)_6\text{Cl}_2$  or  $(\text{NH}_4)_2\text{CO}_3$ . This allows for on-site production of hydrogen for fuel cells through thermal cracking or catalytic methods (Yin et al., 2004; Christensen et al., 2006; Elmøe et al., 2006; Lan et al., 2012) Alternatively, ammonia may be used directly in alkaline, alkaline membrane, and solid oxide fuel cells (Zamfirescu and Dincer, 2008; Hejze et al., 2008; Zamfirescu and Dincer, 2009; Lan et al., 2012). Recovered sources of ammonia from waste products represent ideal candidates for hydrogen production, compared to widely used and non-renewable hydrogen precursors such as natural gas.

### **2.1.4 Economic benefits of recovery of ammonia at municipal WWTPs**

The main benefit of ammonia recovery from post-digestion streams is the nitrogen removal aspect. At municipal WWTPs, it is not uncommon for return streams to contribute 15% to 20% of the nitrogen loading to secondary operations; yet, these inputs make up only 1% of the influent flow (Fux and Siegrist, 2004). To satisfy strict effluent quality regulations, sidestream processes for nitrogen removal are an attractive alternative to costly expansion of mainstream biological processes. For perspective, a New Hampshire study (2010) examined 18 secondary WWTPs processing from 0.5 to 25 MLD, with an average effluent total nitrogen of about 18 mg/L. To upgrade these plants to meet 8 and 3 mg/L total nitrogen limits, capital costs were estimated at between 45M to 60M and 58M to 67M USD respectively (Kessler, 2010). The operational costs for these plants are approximated at 13 to 15 USD/kg total nitrogen removed for a limit of 8 mg/L and 70 to 86 USD/kg for a limit of 3 mg/L. This cost may vary significantly from larger BNR plants (35 to 490 MLD). Case studies from nine BNR plants suggests operational costs between 0.30 and 2.20 USD/kg of total nitrogen removed, with the majority attributed to aeration costs (USEPA, 2008). Decentralized nitrogen removal processes are an option for treatment of post-digestion streams; however, these generally involve high external carbon consumption and/or high aeration costs. With the assumption of an 85% ammonia removal from a 150 m<sup>3</sup>/d digester supernatant stream at 1000 mg/L NH<sub>4</sub>-N, operational costs for a partial nitrification-anammox system have been estimated at 2.50 EUR/kg total nitrogen removed, while a nitrification-denitrification system would cost between 3.05 to 4.10 EUR/kg (Fux and Siegrist, 2004).

Physical-chemical techniques for sidestream ammonia removal have the potential to considerably reduce the operating costs of central biological operations, while reducing nitrous oxide emissions. A preliminary cost analysis by Evans and Thompson (2009) compared technologies for 90% recovery of the ammonia in digester supernatant from a moderately sized secondary WWTP. This comparison suggested that capital expenditure divided over 20 years, plus operating costs for steam stripping-condensation, vacuum distillation-acid scrubbing, or air stripping-acid scrubbing systems would amount to an expense of between 1 and 2 GBP/kg of NH<sub>4</sub>-N recovered. Another study by ThermoEnergy Corporation (2007) modelled the savings that could be obtained for two 500 MLD WWTP scenarios by recovering approximately 90% of the ammonia contained in dewatering centrate using their patented technology (see Section

2.2). The first scenario was characterized by digestion of sludge from combined carbon and nutrient removal (single sludge plant) while the other handled sludges from separate carbon and nutrient removal operations (two sludge plant). Table 1 outlines the results of this modelling study. Considerable savings in aeration energy, sludge disposal, and chemical costs could be gained by removing the ammonia resolubilized during digestion (ThermoEnergy Corporation, 2007).

**Table 1 – Modelled savings for two WWTPs implementing ammonia recovery from dewatering centrate (ThermoEnergy Corporation, 2007)**

Savings	Single Sludge Plant	Two Sludge Plant
Methanol Reduction	38%	19%
Alkalinity Reduction	10%	13%
Sludge Reduction	6%	3%
Aeration Energy Reduction	10%	13%

The other major incentive of ammonia recovery is the potential for internal revenue generation. Table 2 lists 2013 values for various ammonium fertilizers as provided by the US Department of Agriculture Economic Research Center (2013). Recently, the value of recovered reactive nitrogen has been estimated between 260 to 770 USD per tonne (WERF, 2010; Orentlicher, 2012). If only 15% of the influent total nitrogen was recovered from a WWTP treating 1.5 tonne N/d, internal revenues as high as 63,000 USD per year could be generated.

**Table 2 – 2013 prices for various ammonium-derived fertilizers (USDA ERS, 2013)**

Fertilizer	Price (USD/tonne)
Anhydrous ammonia	932
Urea 44%-46% nitrogen	651
Ammonium nitrate	598
Ammonium sulfate	574
Nitrogen solutions (%30)	451

## 2.2 Existing ammonia recovery options for post-digestion side streams

Several techniques exist for the recovery of ammonia from concentrated wastewater such as municipal biosolids streams. One of the simplest methods is through the addition of magnesium, orthophosphate, and caustic to remove ammonia via the formation of struvite. Struvite crystals are easily separated from the wastewater and can be employed as a fertilizer (Le Corre et al., 2009; WERF, 2010; Liu et al., 2013). After moderate capital expenditures of around 200,000 EUR for a crystallizer, this type of operation has been estimated to cost as much as 6 EUR/kg nitrogen recovered (Cilona et al., 2009). Although struvite has been valued at between 180 and 300 EUR/tonne, recent research is focussed on the recovery of phosphorus from waste, rather than the conversion of high quality orthophosphate to struvite (Le Corre et al., 2009; WERF, 2010; Liu et al., 2012). Some techniques for ammonia recovery that stand out include ammonia air stripping-scrubbing, absorption using membrane contactors and adsorption by ion exchange. Similar to the technology proposed in this study, each requires their own combination of resource and energy inputs.

Air stripping is a well established method of wastewater ammonia removal. Air is contacted with wastewater to allow for the transfer of ammonia from the liquid to gas phase. However, at the near neutral pH of wastewater, ammonium dominates and, therefore, significant caustic addition is required to raise the pH high enough to convert the majority of ammonium to un-ionized ammonia. Additionally, ammonia stripping systems may employ various combinations of aeration, steam application, vacuum induction, wastewater conveyance and heating which contribute significant operational and maintenance costs (Elston and Karmarkar, 2003; Evans and Thompson, 2009; Orentlicher, 2012; Ulbricht et al., 2013). These operating costs have been approximated to be between 1 GBP/kg to 6 EUR/kg  $\text{NH}_4\text{-N}$  removed or 13.50 EUR/h alongside relatively high capital costs of 230,000 to 300,000 EUR for infrastructure (Evans and Thompson, 2009; Cilona et al., 2009). A similar process is used to recover the ammonia. The ammonia off-gas is contacted with an acid solution (acid scrubbing) and the result of absorption is an ammonium salt solution which can be marketed to various industries (Elston and Karmarkar, 2003; Cilona et al., 2009). Ammonia stripping is well suited to ammonia-rich wastewater such as human urine. For instance, a bench scale study by Başakçılardan-Kabakci et al. (2007) demonstrated 97% volatilization of urine ammonia, of which nearly 100% was recovered in a packed bed, sulfuric acid scrubber.

A recently developed technology utilizes gas permeable membranes to transfer ammonia from wastewater to an acid absorption phase. Essentially, the wastewater is in contact with bundles of hollow fibre membranes and the ammonia is driven across the membrane into a flowing acid solution by the concentration gradient between the two liquid phases. This gradient remains strong as the ammonia reacts with the acid to form an ammonium salt solution that can be recovered. Cilona and colleagues (2009) achieved greater than 85% ammonia recovery from power plant condensed flue gas using membrane gas transfer. Compared to other ammonia recovery processes, they claimed that membrane contactors would contribute relatively low capital costs of around 150,000 EUR while operation (including chemical, pumping, and membrane replacement costs) is estimated at 1.21 EUR/kg nitrogen recovered or 0.17 EUR/m<sup>3</sup> for the 200 mg/L NH<sub>4</sub> wastewater processed at 25 m<sup>3</sup>/h. In another application with industrial wastewater, up to 95% recovery of ammonia has been reported using a similar membrane contactor (Ulbricht et al., 2013). Similarly to ammonia stripping, this technique requires ammonia to be present as un-ionized ammonia and, therefore, requires high caustic dosing. Further, operation and maintenance costs are involved in absorbent pumping, and membrane replacement (Cilona et al., 2009; Ulbricht et al., 2013).

Ion exchange techniques have been used frequently to remove ammonia from wastewater. Adsorbents for these processes include zeolites which are natural mineral materials and synthetic ion exchange resins. One promising adsorbent is clinoptilolite, which can be placed in packed bed columns and adsorb wastewater ammonium (Hedström, 2006; Beler-Baykal et al., 2011; Allar and Beler-Baykal, 2013). Using this technology, ammonia removals as high as 97% have been achieved in treating human urine and greater than 86% ammonia recovery has been obtained through regeneration of exhausted clinoptilolite (Beler-Baykal et al., 2011; Allar and Beler-Baykal, 2013). Interestingly, a recent study showed that clinoptilolite can also be used to remove and recover up to 99% of the orthophosphate in human urine (Allar and Beler-Baykal, 2013). Additionally, clinoptilolite is a common soil conditioner and exhausted material can be used directly as a fertilizer.

A more complex ion exchange method for the recovery of ammonia from wastewater is the Ammonia Recovery Process (ARP) patented by ThermoEnergy Corporation (Fassbender, 2001; ThermoEnergy Corporation, 2007). The first stage of ARP involves the adsorption of wastewater ammonium on selective ion exchange resins. These resin columns are then regenerated using

a zinc and sulfuric acid solution. After regeneration, a solution containing recovered ammonia as well as zinc and sulfate remains. With the addition of more acid to this solution, the zinc double salt, ammonium zinc sulfate hexahydrate  $((\text{NH}_4)_2\text{SO}_4\text{ZnSO}_4 \cdot 6\text{H}_2\text{O})$ , can be crystallized. The double salt crystals are harvested and heated to produce ammonia and sulfur trioxide ( $\text{SO}_3$ ) gases leaving behind solid zinc sulfate. The off-gas from this process is absorbed in sulfuric acid and this mixture can be concentrated by evaporation to produce marketable solid ammonium sulfate. In a pilot study at the Oakwood Beach WWTP in New York, the ARP proved successful in recovering nearly 100% of the ammonia from municipal dewatering centrate. This technology consists of multiple processes some of which require heavy chemical addition or heating contributing to operating costs of around 2.64 USD/m<sup>3</sup> for a 650 mg/L  $\text{NH}_4$  wastewater processed at a rate of 8 m<sup>3</sup>/d. However, the complexity of this technology's design lends to its very high capital cost of as much as 44M USD (Fassbender, 2001).

## CHAPTER 3: RESEARCH OBJECTIVES

The purpose of this research is to demonstrate the potential for wastewater ammonia removal by struvite crystallization using synthetic newberyite as a surrogate for thermally decomposed struvite. It also works to explore the possibility that these materials can be employed to produce struvite suitable as a feedstock for the UBC-developed thermal decomposition process.

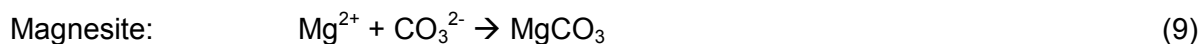
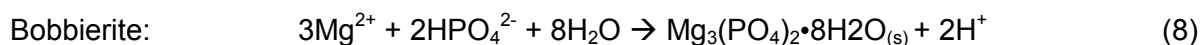
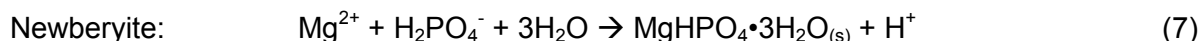
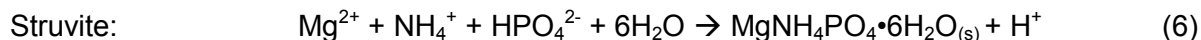
The objectives of this study are defined as follows:

1. To develop the physical-chemical concept for the ammonia removal stage of the proposed ammonia recovery technology specifically ammonium uptake during the conversion of newberyite to struvite
2. To verify optimal conditions of the process as defined by chemical equilibrium modelling and experimental results
3. To delineate the rates and mechanisms of the process
4. To provide recommendations regarding process operation, including optimal physical-chemical parameters and cost-effectiveness

## CHAPTER 4: LITERATURE REVIEW

### 4.1 Chemistry of magnesium and phosphate compounds

In most cases, struvite can form between pH 6 to 9 in nutrient-rich wastewater if sufficient magnesium is present. Struvite crystallization is promoted also by decreases in temperature which occur during the conveyance of post-digestion streams. In water at 25° C, struvite solubility decreases with the increase of pH up until its minimum solubility around pH 10.3 after which struvite becomes more soluble (Ohlinger et al., 1998; Ohlinger et al; 1999; Bhuiyan et al., 2007). However, struvite is not the only magnesium compound that could exist in conditions inherent of most wastewaters. Other crystalline solid phases such as newberyite, bobbierite ( $Mg_3(PO_4)_2 \cdot 8H_2O$ ), or magnesite ( $MgCO_3$ ) could form and perhaps limit the magnesium and orthophosphate available for struvite formation (Taylor et al., 1963; Boistelle and Abbona, 1983; Kontrec et al., 2005; Babić-Ivančić et al., 2006; Königsberger and Königsberger, 2006; Shand, 2006). Eqns. 6 to 9 demonstrate the formation of these magnesium compounds.

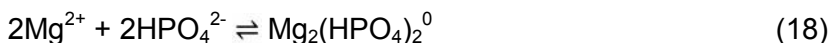
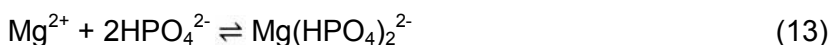
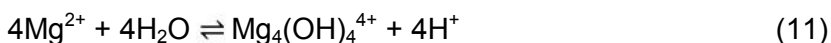


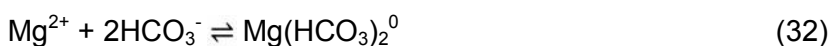
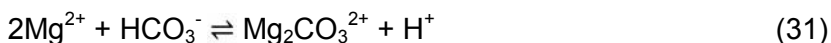
Newberyite can exist even in the presence of high ammonium if pH drops to between 5 and 6 (Boistelle and Abbona, 1983; Kontrec et al., 2005; Babić-Ivančić et al., 2006). In contrast, bobbierite and, in the presence of carbonate, magnesite may form in significant quantities above a pH of 8 in magnesium enriched nutrient solutions (Taylor et al., 1963; Königsberger and Königsberger, 2006; Shand, 2006). Further, newberyite or bobbierite crystallization could occur alongside struvite due to increases in solution temperature. This is because struvite solubility increases as solution temperature is enhanced above 25° C, while newberyite and bobbierite

solubility decreases slightly (Boistelle and Abbona, 1983; Kontrec et al., 2005; Babić-Ivančić et al., 2006; Königsberger and Königsberger, 2006).

#### **4.1.1 Aqueous equilibria affecting speciation of magnesium, ammonium, orthophosphate, and carbonate**

There are many simultaneous reactions occurring in wastewater which affect the speciation and, therefore, the activity of aqueous magnesium, ammonium, orthophosphate, and carbonate. Eqns. 10 to 32 lists some of the potential aqueous equilibria that are indirectly involved in the formation of magnesium and phosphate compounds such as struvite, newberyite, bobbierite, and magnesite (USGS, 2013).





### 4.1.2 Solubility products

The solubility products ( $K_{sp}$ ) of magnesium salts vary with temperature according to the negative enthalpy change of their formation reaction but are generally measured at 25° C in water. The fundamentals of  $K_{sp}$  and how it is related to solid phase saturation are explained in more detail in Section 4.3. Table 3 lists some experimentally determined  $K_{sp}$  values for the solid phases of interest to this study.

**Table 3 – Experimentally determined  $pK_{sp}$  at 25° C for various magnesium and phosphate compounds**

Solid Phase	$pK_{sp} = -\text{Log}_{10}K_{sp}$	Reference
Struvite	13.15	Taylor et al., 1963a
	13.26	Ohlinger et al., 1998
	13.36	Babić-Ivančić et al., 2002
	13.36	Bhuiyan et al., 2007
	13.68	Koutsoukos et al., 2007
	13.47	Lobanov et al., 2013
Newberyite	5.82	Taylor et al., 1963b
	5.78	Verbeeck et al., 1984
	5.88	Lobanov et al., 2013
Bobbierite	25.20	Taylor et al., 1963b
	25.47	Lobanov et al., 2013
Magnesite	7.52	Pokrovsky et al., 1999
	7.80	Bénezeth et al., 2011

## 4.2 Struvite and newberyite morphology

Struvite and newberyite crystallize with a variety of habit and morphology depending greatly on factors such as supersaturation, pH, temperature, elemental molar ratios and crystal age. Struvite takes orthorhombic morphologies and single, twinned, and dendritic crystal shapes have been reported. Single crystals may be rod-like, prismatic platelets, coffin-shaped or

needle-like while dendrites may be X-shaped twins, multi-branched, or star-shaped (Abbona et al., 1985; Babić-Ivančić et al., 2002; Kontrec et al., 2005). Generally, smaller, more elongated and dendritic crystals are believed to form at higher supersaturation. At low supersaturation larger, rod-like or tabular types are observed (Abbona et al., 1985). Newberyite crystals are trigonal and generally take rhombohedral or pseudo-octagonal morphologies (Boistelle et al., 1983; Babić-Ivančić et al., 2002; Kontrec et al., 2005). Figures 2 and 3 provide some examples of reported crystal morphologies for struvite and newberyite respectively.

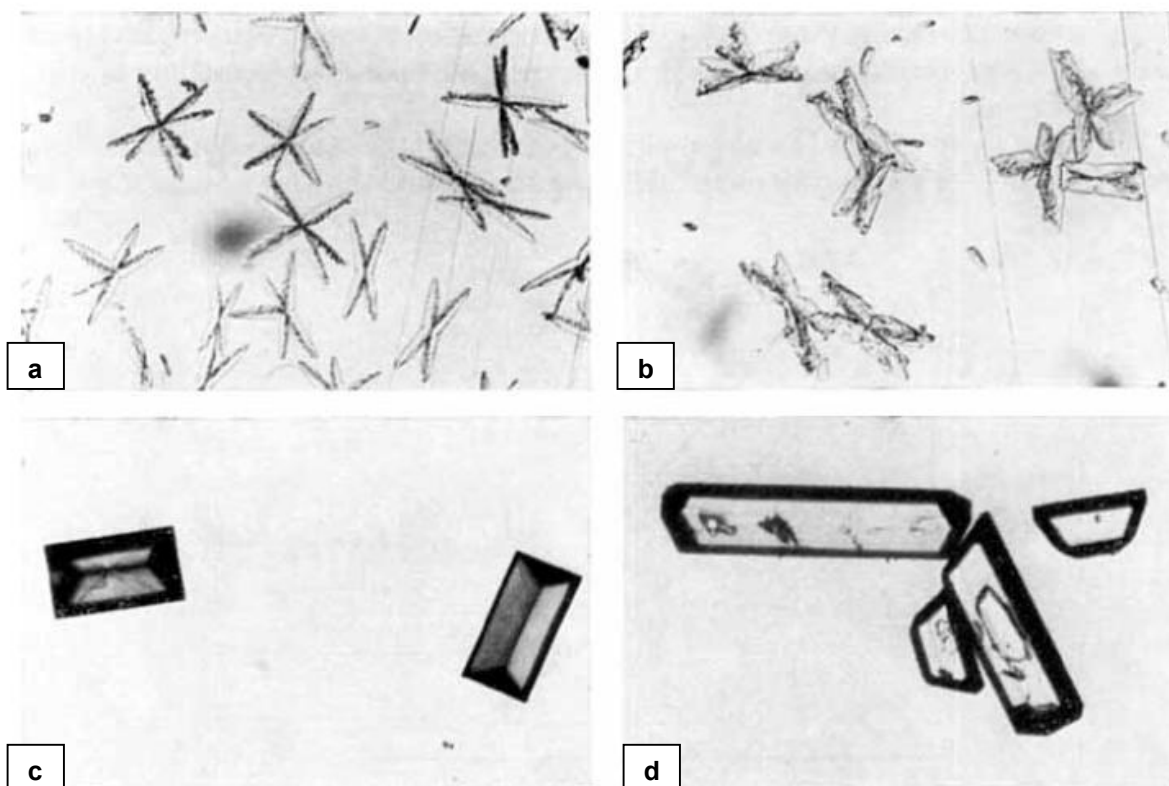


**Figure 2 – Star-shaped dendritic (a), X-shaped twinned (b), coffin-shaped (c), and rod-like (d) struvite crystals (Abbona et al., 1985)**

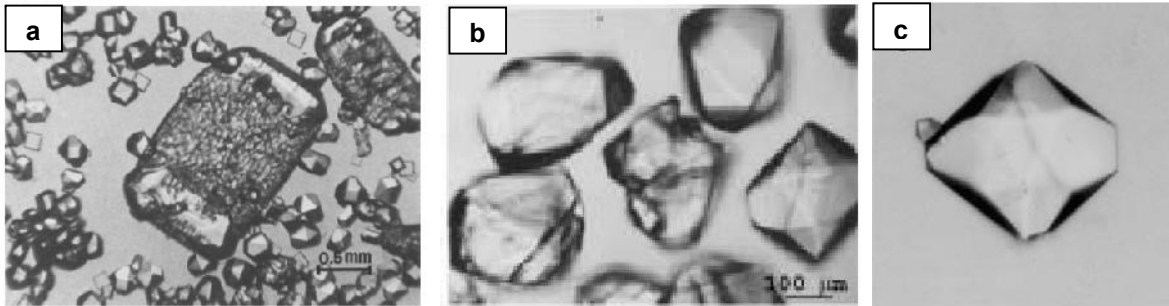


Figure 3 – Pseudo-octagonal newberyite crystals amongst dissolving tabular struvite crystal (a); rhombohedral newberyite crystals (b and c) (Boistelle et al., 1983; Kontrec et al., 2005; Babić-Ivančić et al., 2002)

### 4.3 Factors affecting struvite formation

#### 4.3.1 Supersaturation

A solution's degree of supersaturation with respect to struvite is the primary factor in its crystallization. Struvite supersaturation ratio ( $S_S$ ) is directly dependant on magnesium, ammonium, and orthophosphate activity. However, solution pH, temperature, and ionic strength also play a role in supersaturation and, therefore, struvite formation. Eqn. 33 demonstrates  $S_S$  as a relationship between constituent activities and solubility product (Söhnel and Garside, 1992).

$$S_S = \left( \frac{\{Mg^{2+}\}\{NH_4^+\}\{PO_4^{3-}\}}{K_{sp-S}} \right)^{\frac{1}{3}} \quad (33)$$

The most common way of controlling supersaturation ratio in a struvite crystallization process is through pH adjustment. Although nutrient-rich wastewaters such as post-digestion streams may be initially basic, the formation of struvite results in the release of hydrogen ions and, therefore, chemical addition is generally required to maintain basic conditions and maximize orthophosphate removal through nucleation and growth of struvite crystals. It is widely accepted that an in-reactor pH of 8 to 9 will allow for effective struvite crystallization (Andrade and

Shuiling, 2001; Le Corre et al., 2009; Huang et al., 2011). This may be accomplished through the addition of a basic solution of sodium hydroxide, magnesium oxide (MgO), or brucite (Mg(OH)<sub>2</sub>). Raising the pH affects supersaturation ratio indirectly by increasing the orthophosphate activity through a shift in the orthophosphate equilibria. For instance, additional hydroxide neutralizes hydrogen ions resulting in a shift from dihydrogen phosphate to hydrogen phosphate, which is utilized in the formation of struvite as demonstrated by Eqns. 34 and 35.



Solution temperature is also indirectly involved in supersaturation. As temperature increases, struvite solubility product increases according to the negative enthalpy change of the struvite formation reaction. An increase in struvite solubility product,  $K_{sp-s}$ , results in a reduction of struvite supersaturation ratio,  $S_s$ . In general, struvite recovery potential is higher for wastewaters with lower temperature due to its decreased solubility.

The ionic strength of the crystallizer feed affects the activity of struvite's constituents, magnesium, ammonium, and orthophosphate. Higher ionic strength results in more interaction between solution ions and, therefore, lower effective availability or activity of these constituents. This effect is quantified using activity coefficients denoted as  $\gamma$  which are a function of solution ionic strength, ion valence, and ion effective diameter. Activity is defined as the product of the specific activity coefficient for an element and its molar concentration. An increase in ionic strength results in a decrease in activity coefficient and, therefore, a reduction of constituent activity. Hence, a less saline wastewater has higher constituent activities and is more supersaturated with respect to struvite.

#### **4.3.2 Mg:P and N:P molar ratio**

Struvite is composed of equimolar parts magnesium, ammonium, and orthophosphate. Therefore, struvite crystallization is limited to the lowest molar concentration between these constituents regardless of solution supersaturation. Unless the local water contains significant

hardness, wastewater is generally magnesium limited and supplemental magnesium must be added to effectively remove orthophosphate as struvite. In a struvite recovery process, this is accomplished with the addition of a concentrated magnesium feed stock containing dissolved magnesium chloride ( $\text{MgCl}_2$  or  $\text{MgCl}_2 \cdot 6\text{H}_2\text{O}$ ), magnesium oxide, or brucite. Studies have determined that struvite crystallization is enhanced in solutions with magnesium in excess of orthophosphate. To maximize orthophosphate removal efficiency, a Mg:P molar ratio of 1.05:1 to 1.3:1 has been recommended (Jaffer et al., 2002). Further, Huang et al. (2003) found that pellet size, hardness and density were increased above this Mg:P range in a pilot study using a UBC struvite crystallizer.

Municipal wastewater streams generally carry an ammonia molar concentration many times higher than that of orthophosphate. This is advantageous with regard to controlled struvite crystallization, as increased N:P molar ratio has been shown to enhance orthophosphate removal (Münch and Barr, 2001). Fattah (2004) observed a positive correlation between N:P molar ratio and orthophosphate removals during their struvite recovery pilot study. However, there are a lack of studies which systematically examine the effect of N:P molar ratio on struvite formation.

### **4.3.3 Hydrodynamics**

The hydrodynamic conditions and turbulence induced within a reactor are believed to play a role in struvite crystallization. Ohlinger and colleagues (1999) demonstrated that an increase in mixing rate results in more rapid accumulation of struvite. Further, it is posited that crystal nucleation rates may also be increased in cases of enhanced turbulence. However, aggressive mixing may also result in crystal breakage and attrition (Franke and Mersmann, 1995). With fluidized bed struvite reactors such as the UBC struvite crystallizer, turbulence is dependent on upflow velocity as well as struvite load, particle size distribution and reactor scale. The performance of these technologies relies on a lower bound upflow velocity that allows for the fluidization of struvite particles and adequate exposure of particle surfaces to the feed solution. Further, an upflow velocity too high will result in the loss of fine struvite crystals, in turn, affecting struvite agglomeration rates. Although the UBC struvite crystallizer is capable of producing relatively large struvite pellets, the effect of turbulence on struvite pelletization is not well understood due to the complex hydrodynamics inherent to its design. Nevertheless,

examination of struvite grown in this type of reactor suggests that higher upflow velocity results in a harvest of larger pellets with higher density and hardness (Huang, 2003; Fattah, 2004).

#### **4.4 UBC struvite crystallization process**

In 1999, UBC acquired funding from British Columbia Hydro to commence research on phosphorus recovery from various waste streams, with the intention of producing a fertilizer suitable for the enrichment of oligotrophic streams. Bench-scale studies led to the development of the UBC struvite crystallizer (Dastur, 2001; Adnan, 2002). Many projects have been completed in this area, but the pilot studies utilizing real waste streams from Penticton, Lulu Island and Annacis Island WWTPs were integral in the progression from batch tests to commercialization of struvite recovery in less than a decade (Britton, 2002; Huang, 2003; Fattah, 2004).

##### ***4.4.1 Pilot-scale UBC struvite crystallizer design***

The pilot-scale crystallizers used at these WWTPs followed the general characteristics illustrated in Figure 4. They are composed of a FBR, an injector, an external clarifier, and storage for chemical additives and feed. The success of this technology originates from the design of the injector and the FBR. Feed, recycle feed, supplemental magnesium, and caustic are mixed at the injector. The high turbulence and supersaturation ratio resulting from influent mixing allows for the rapid nucleation of struvite. These nuclei grow into crystals as the fluid flows upward through the FBR. The FBR is made up of four zones of varying diameter. From bottom to top, this includes the harvest zone or wasting zone, the active zone, the fines or reaction zone, and the seed hopper. With the largest diameter, the seed hopper is essentially a clarifier, which retains the small crystals (seeds) long enough for them to grow larger. As zone diameter decreases, turbulence increases due to higher upflow velocities with the highest being at the injector. The active and harvest zones are characterized by high turbulence and, therefore, high particle collision frequency. Struvite fines entering these zones agglomerate into larger particles along with nuclei. Over a period of hours to days, these agglomerates grow into round, hard pellets formed by layers of struvite smoothed by attrition and abrasion. The pellets eventually remain in the harvest zone where they can be recovered by draining a portion of the crystallizer. Feed and recycle bypasses allow for continuous operation during harvesting. The

lengths of each zone have been varied from 45.7 to 275 mm to provide various hydraulic retention times (HRT). However, HRT and, therefore, orthophosphate and magnesium residuals in the crystallizer effluent are controlled primarily by recycling. The external clarifier facilitates removal of struvite fines lost to the effluent, while a portion of the supernatant is returned to the crystallizer.

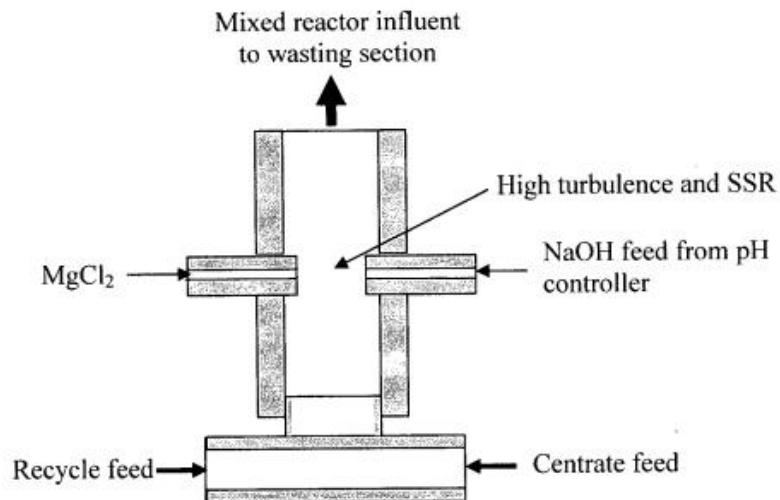
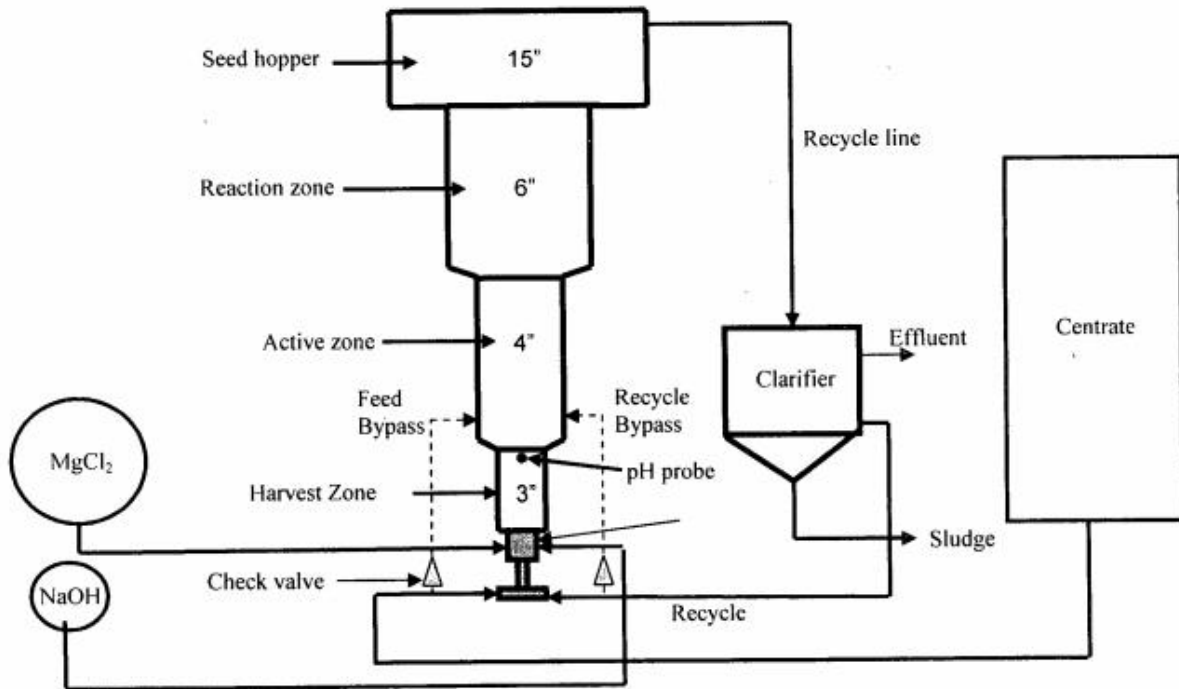


Figure 4 – General schematic of UBC struvite crystallization process (top) and crystallizer injector (bottom) (Fattah, 2004)

#### 4.4.2 Pilot-scale UBC struvite crystallizer operation

The operation of a struvite crystallizer is largely waste specific. The principle operational parameters of interest to this process are the in-reactor supersaturation ratio, in-reactor Mg:P molar ratio, feed temperature, total reactor flow, recycle ratio, HRT and crystal retention time (CRT). Parameters used to evaluate struvite recovery performance are effluent PO<sub>4</sub>-P, percent removal of orthophosphate and ammonia-nitrogen and pellet diameter. Table 4 summarizes the range of operation and performance for important struvite recovery pilot studies.

**Table 4 – Range of operation and performance for UBC struvite crystallizer pilot studies**

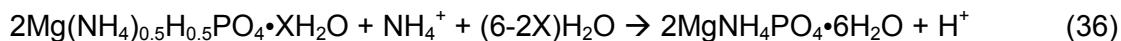
Operational Parameter	Pilot-Study		
	Britton, 2002 Penticton digester supernatant	Huang, 2003 Lulu & Annacis digester supernatant	Fattah, 2004 Lulu dewatering centrate
<sup>a</sup> Supersaturation ratio (S <sub>S</sub> )	1.1~2.2	1.1~1.9	1.0~1.9
<sup>b</sup> Mg:P molar ratio	1.0~16.8	2.0~21.7	1.1~30
Temperature (° C)	16~25	10~20	15~29
Total reactor flow (L/min)	2.4~10.2	3.1~4.8	8.3~23.1
<sup>c</sup> Recycle ratio	3.0~23	4.0~10.3	6~12
HRT (mins)	Not reported	3.6~9.4	4.0~9.5
<sup>d</sup> CRT (days)	12~47	8~20	Not reported
<b>Performance</b>			
Effluent PO <sub>4</sub> -P (mg/L)	3.9~43.6	3~13.5	2~54
% PO <sub>4</sub> Removal	0~91	88~98	24~100
% NH <sub>4</sub> Removal	0~26	1~22	5~10
Pellet diameter (mm)	0.5~2.1	1.5~3.5	1.4~3.6

- Cube root of the ratio of conditional solubility product of the solution leaving the injector to that of equilibrium ( $P_{S\text{-reactor}}/P_{S\text{-eq}}$ )<sup>1/3</sup>
- Mg:P molar ratio of the solution leaving the injector
- Recycle flow divided by the influent flow to the reactor
- The volume of crystal bed divided by the volumetric rate of crystal harvest

#### 4.5 Struvite decomposition products as ammonia removal agents

An ideal material for the stabilization of aqueous ammonium would contain both magnesium and orthophosphate. Struvite can be decomposed to various products either in air or in solution. The majority of the ammonium contained in struvite may be eliminated through release to solution or volatilization to the atmosphere. However, if some ammonium remains in the solid phase, its

capacity to remove wastewater ammonium via dissolution and struvite reformation is limited. Decomposed struvite containing minimal residual ammonium has a greater aqueous ammonia removal potential. In other words, the required dose of this material would be smaller than one that contains more residual ammonium as demonstrated by Eqns. 36 and 37.



A struvite decomposition product is suitable for removal of ammonia from wastewater if it:

1. Contains ammonium at an N:P molar ratio of less than one (ie. ammonia removal efficiency of material increases as N:P approaches zero)
2. Is less thermodynamically stable than struvite and will dissolve readily to release magnesium and orthophosphate in the wastewater

Ammonia removal agents can be produced by either wet or dry processes of struvite decomposition. Several studies have proven that these residues can be used to remove wastewater ammonia via struvite recrystallization and that the struvite formed can be repeatedly decomposed. As illustrated by Figure 5, ammonia could theoretically be removed continuously from wastewater by reusing magnesium and orthophosphate as cycled between struvite and struvite decomposition products. This section reviews the current state of knowledge on struvite thermal decomposition products and their effectiveness as ammonia removal agents.

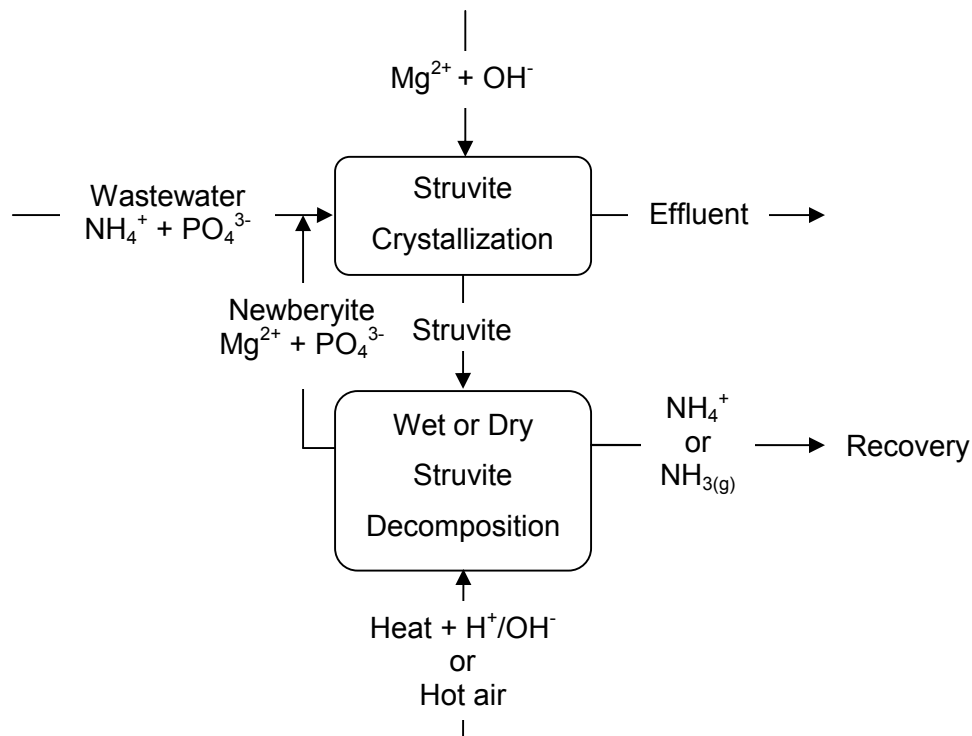
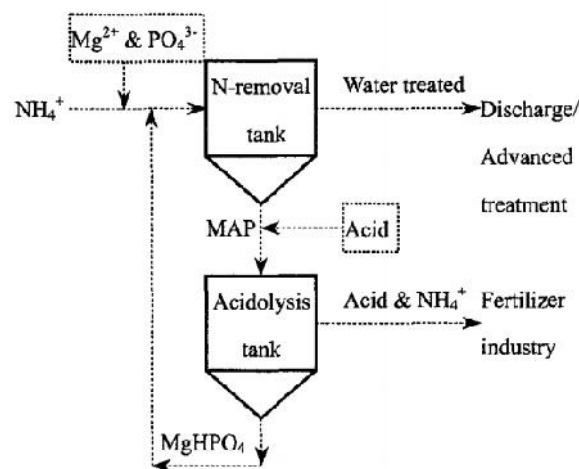


Figure 5 – Conceptual schematic of  $\text{NH}_4$  removal through reuse of Mg and  $\text{PO}_4$

#### 4.5.1 Struvite decomposition in solution – “Wet process”

By adjusting solution conditions such as pH and temperature, struvite instability can be induced. For instance, struvite may convert partially or fully to another magnesium phosphate by changing one or both of these parameters. In the interest of ammonia recovery, this decomposition should result in the release of struvite ammonium to solution while preserving magnesium and orthophosphate in a solid phase and this suspension can be settled and decanted. The ammonia in the supernatant can be recovered while the solid phase can be reused as a source of magnesium and orthophosphate for removal of more ammonia from wastewater. In this case, the transformation from struvite to a magnesium phosphate phase, which is low in or devoid of ammonium occurs in excess water and is, therefore, referred to as the “wet process”.

Struvite can be replaced by newberyite through simply adding acid to a suspension. Work by Boistelle et al. (1983) demonstrated that the drop in pH induced by struvite formation can eventually provide the conditions for complete conversion of struvite to newberyite if the initial solution pH is low enough. As pH decreases, struvite supersaturation ratio eventually reaches unity ( $S_S = 1$ ) and struvite will begin to dissolve as long as newberyite forms simultaneously. Struvite will completely dissolve if the solution is sufficiently supersaturated with respect to newberyite ( $S_N > 1$ ). Complete replacement of struvite by newberyite was shown to occur at a pH between 4 and 5.5, with the process favoured at higher temperature. Babić-Ivančić and colleagues (2006) expanded on this topic revealing the reaction kinetics of the struvite-newberyite conversion with adequate mixing. Using various combinations of initial pH and initial  $S_N:S_S$  ratios, it was confirmed that struvite is fully converted to newberyite in a pH range of 4 to 6. At a temperature of 25° C, this process could be completed in 30 minutes, given an initial solution of low pH and high  $S_N:S_S$  ratio.



**Figure 6 – Schematic diagram of reusing MAP residues for ammonia removal by acid dipping as proposed by Zhang et al. (2004)**

A chemical reuse and ammonium recovery application was proposed by Zhang et al. (2004) employing a struvite-newberyite system as shown in Figure 6. The two-stage process involves ammonia removal from wastewater by struvite crystallization followed by acidification of the separated struvite to produce a suspension containing newberyite. By adjusting the pH and temperature of a struvite suspension to 5 and 60° C respectively, a mixture of newberyite and

struvite was produced in 90 minutes. The ammonium-rich acid supernatant is recovered as a fertilizer and the newberyite formed is reused to remove additional wastewater ammonia. Although the extent of the struvite-to-newberyite conversion was not reported, this solid phase was reused successfully as an ammonia removal agent.

Struvite can be decomposed to other magnesium phosphates by thermal-alkali treatment of the suspension. Türker and Celen (2007) demonstrated this with struvite formed in anaerobically pretreated industrial wastewater containing molasses. The ammonia was removed via struvite formation by adding magnesium and orthophosphate in excess. With the addition of caustic to the struvite suspension at a  $\text{OH}:\text{NH}_4$  (initial  $\text{NH}_4^+$  concentration in wastewater) molar ratio of 1:1, ammonia is released to the liquid phase. At this high pH, the ammonia may be volatilized by heating. 81% and 100% removal of ammonia from the alkali suspension was achieved at 110° C and by distillation respectively in only minutes. They suggested that the evolved ammonia gas could be recovered in boric acid. Although it was noted that it could contain  $\text{Mg}_3(\text{PO}_4)_2$  and/or magnesium pyrophosphate, the dominant material in the resultant solid phase was not identified. Nonetheless, these residues proved to be a suitable source of magnesium and orthophosphate for high removal of ammonia when added to another sample of wastewater.

Researchers from the State Key Laboratory of Environmental Aquatic Chemistry in Beijing, China, have adopted a similar approach for ammonia recovery from various wastewaters by reusing struvite decomposition residues. Their studies verify and expand upon the results obtained by Türker and Celen (2007). Each of these studies followed a similar conceptual process flow involving two main stages. In the first stage, ammonia was removed from the wastewater by producing struvite. The second stage involved the decomposition of collected struvite by thermal-alkali treatment. The decomposed struvite produced in each study was later used successfully to remove more ammonia from the same wastewater. The supernatant produced in the second stage was considered a recoverable source of ammonia. The type of wastewater, the  $\text{OH}:\text{NH}_4$  molar ratio of the alkali struvite suspension, the heating temperature and time, the percent release of ammonia during struvite decomposition and the suggested composition of decomposed struvite are summarized for each of these studies in Table 5.

**Table 5 – Summary of struvite decomposition studies using thermal-alkali treatment**

Wastewater	OH:NH <sub>4</sub> Molar Ratio	Heating Temp. (°C)	Heating Time (hours)	% Release of NH <sub>4</sub> -N	Solid Phases; Possible Impurities	Reference
Molasses industry	1:1	≥110	<3	<sup>a</sup> 81-100	Not identified; Mg <sub>3</sub> (PO <sub>4</sub> ) <sub>2</sub> , Mg <sub>4</sub> P <sub>2</sub> O <sub>7</sub>	Türker and Celen, 2007
Landfill leachate	1:1	90	2	>96%	<sup>b</sup> Amorphous MgNaPO <sub>4</sub> ; Ca, K, Al	He et al., 2007
Saponification	1:1.1	100	3	Not reported	Not identified; Mg <sub>3</sub> (PO <sub>4</sub> ) <sub>2</sub> , Mg <sub>4</sub> P <sub>2</sub> O <sub>7</sub>	Huang et al., 2009
Coking	2:1	110	3	90	<sup>b</sup> Amorphous MgNaPO <sub>4</sub> ; Mg <sub>3</sub> (PO <sub>4</sub> ) <sub>2</sub> , Mg <sub>4</sub> P <sub>2</sub> O <sub>7</sub>	Zhang et al., 2009
Piggery	1:1	110	3	Not reported	<sup>b</sup> Amorphous MgNaPO <sub>4</sub> ; Ca, K,	Huang et al., 2011

- a. Percent removal of solubilized NH<sub>3</sub> from liquid phase by volatilization; Percent elimination of NH<sub>4</sub><sup>+</sup> from struvite was not reported
- b. XRD identified amorphous phase; MgNaPO<sub>4</sub> was suggested as dominant material by authors

#### 4.5.2 Ammonia removal following “wet process”

Ammonia can be removed from wastewaters using residues that were produced by decomposing struvite in excess water. One of these residues is newberyite. By dissolving struvite in acid and heating the resulting solution, newberyite can be formed. This process can be reversed by collecting newberyite and adding it along with caustic to an ammonia solution. The newberyite dissolves and the released magnesium and orthophosphate are utilized to recrystallize struvite. Zhang and colleagues (2004) proposed that this reversible process could be exploited for continuous ammonia removal and recovery using the two-stage application shown in Figure 6. Newberyite was added to an ammonia solution to provide a Mg:N:P molar ratio of 1:0.5:1 and pH was maintained at 8.5 for 4 hours to produce struvite. The mixture of struvite and newberyite was collected and the struvite portion was converted back to newberyite in the acidification stage as described in Section 4.5.2. The newberyite material from this stage was added once again to the same solution. This procedure was repeated five more times. In the struvite formation stage, of the first five cycles, greater than 98% ammonia removal was

achieved. However, between 2% and 5% of the magnesium and orthophosphate was lost from the solid phases to the supernatants of both the ammonia removal and acidification stages. It was believed that enough was lost by the fifth cycle to reduce the ammonia removal efficiency of the sixth stage to 88%.

Another decomposition product that could be used to remove ammonia from wastewater is the amorphous phase produced from struvite under alkaline conditions at elevated temperatures. Table 5 reviews the conditions of various thermal-alkali treatments of struvite to form this material. Magnesium and orthophosphate can be cycled through alternating ammonia removal and thermal-alkali stages. The type of wastewater, the pH and reaction time of ammonia removal/struvite formation stage, the percent removal of ammonia from the wastewater for the first and last cycles and the residual orthophosphate concentration in the supernatant from the ammonia removal stage are summarized for each of these studies in Table 6.

**Table 6 – Summary of ammonia removal studies using struvite decomposed under thermal-alkali conditions**

Wastewater	pH	Reaction Time (h)	% Removal of NH <sub>4</sub> -N	Cycle No.	PO <sub>4</sub> Residual (mg/L)	Reference
Molasses industry	8.5	Not reported	92 77	1 <sup>st</sup> 5 <sup>th</sup>	Not reported	Türker and Celen, 2007
Landfill leachate	9.0	2.0	96 84	1 <sup>st</sup> 6 <sup>th</sup>	2-10	He et al., 2007
Saponification	9.0	0.5	99 <sup>a</sup> 99	1 <sup>st</sup> 6 <sup>th</sup>	<1	Huang et al., 2009
Coking	9.5	1.5	85 70	1 <sup>st</sup> 5 <sup>th</sup>	Not reported	Zhang et al., 2009
Piggery	<sup>b</sup> 9.4-8.5	1.0	80 65	1 <sup>st</sup> 5 <sup>th</sup>	<5-70	Huang et al., 2011

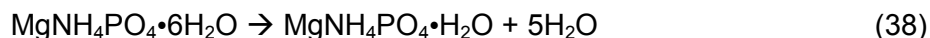
- Initially Mg and PO<sub>4</sub> are in excess and separate stages were employed for dissolution of decomposition products and residual PO<sub>4</sub> recovery
- Required no adjustment of pH; pH varied as struvite formed; Initially Mg was in excess as magnesite

### ***4.5.3 Thermal decomposition of struvite in air – “Dry process”***

Under certain conditions, struvite may become thermodynamically unstable in air, even at ambient temperature. Depending on its morphology, struvite is believed to transform completely into newberyite in open systems. However, this phenomenon occurs slowly over a period of several months (Cohen, 1966; Whitaker, 1967; Ribbe, 1969). In the early 1900's, research on dry thermal decomposition of struvite was performed to improve a common technique used for determination of magnesium or orthophosphate concentration, which involved the formation of struvite and ignition to magnesium pyrophosphate. Errors in the results of this technique were attributed to the fact that the conditions at which orthophosphate transforms to pyrophosphate were not agreed upon universally. Kiehl and Hardt (1933) completed a study which investigated this transition by determining the dissociation pressures of various magnesium phosphates. In open atmosphere at temperatures between 40° and 60° C, it was suggested that struvite loses five moles of its water of crystallization forming dittmarite. Based on the composition of the gaseous phase, struvite loses both ammonia and water above 60° C. In heating dittmarite, pyrophosphate was detected in solid phases whenever ammonia evolved. This study declared 250° C as a suitable temperature to quickly and completely decompose struvite to magnesium pyrophosphate.

The first study that presented evidence of an intermediate phase occurring during heating between dittmarite and magnesium pyrophosphate was completed by Paulik and Paulik (1975a, 1975b). This research used a thermogravimetric method which was novel at the time to investigate thermal decomposition of struvite under quasi-isothermal conditions. The method referred to as quasi-isothermal thermogravimetry (QTG) employs automation to maintain a constant heating temperature when the mass loss rate passes a preset threshold. QTG allows for more accurate determination of the temperature at which phase transformations occur, as well as demonstrating the kinetics of these reactions. Paulik and Paulik verified that approximately five moles of water of crystallization is lost from struvite, with simultaneous elimination of ammonium at temperatures above 90° C. However, the ammonia evolved amounts to no more than 5% of the struvite ammonium. This suggested that a phase believed to be primarily dittmarite is quite stable between 90° and 230° C. Based on the shape of the QTG curve in this range, it was posited that dittmarite may lose its remaining ammonium, water of crystallization and constitution by two overlapping reactions each potentially attributing

intermediate phases. In the range of 200° to 250° C dittmarite was shown to lose 50% to 80% of its volatile components. In theory, dittmarite rapidly loses its water of crystallization to form  $\text{MgNH}_4\text{PO}_4$  at around 230° C followed by the slow elimination of its remaining ammonium to  $\text{MgHPO}_4$ . Finally, the water of constitution evolves producing magnesium pyrophosphate at 500° C. The transformations involved in thermal decomposition of struvite can be represented by Eqns. 38 to 41 (Paulik and Paulik, 1975a; 1975b).



In a study by Abdelrazig and Sharp (1988), a similar approach was employed to investigate the thermal decomposition temperatures of struvite and dittmarite. Conventional differential thermogravimetry confirmed that mass loss from struvite begins to rapidly occur just above 60° C, with a well defined peak occurring at 100° C that was believed to represent high stability of dittmarite. Similarly to Paulik and Paulik (1975a), QTG results suggested that five moles of water of crystallization is simultaneously evolved with a small amount of ammonia during this transformation. Powder X-ray diffraction (XRD) analyses identified dittmarite and an amorphous phase in a cement containing struvite which was heated at 235° C. When the same material was heated at 300° C, it was found to contain only this amorphous phase.

In the research following these earlier studies, similar observations were reported. Results from several more experiments suggest that ammonia and water evolve simultaneously during thermal decomposition of struvite. The temperature at which this begins ranges from 40° to 55° C. The same studies demonstrated rapid decomposition of struvite at temperatures between 85° and 115° C (Sarkar, 1991; Frost et al., 2004; Bhuiyan et al., 2008). Sarkar (1991) and Bhuiyan et al. (2008) also claimed that dittmarite becomes stable in this range. However, Sugiyama and colleagues (2005) were the only other researchers to detect dittmarite in heated struvite (100° to

150° C isotherms) using XRD analysis. Several of these studies also noted the formation of a fully X-ray amorphous phase beginning at heating temperatures ranging from 70° to 160° C extending to as high as 500° C (Sarkar, 1991; Sugiyama et al., 2005; Bhuiyan et al., 2008; Kurtulus and Tas, 2011). This amorphous phase has been suggested to be analogous to  $\text{MgHPO}_4$  but considering the reviewed literature it might be deduced that this phase could realistically be a mixture of multiple phases which might include dittmarite,  $\text{MgNH}_4\text{PO}_4$ ,  $\text{MgHPO}_4$  and magnesium pyrophosphate with composition dependant on heating temperature. Based on this dependence, the amorphous material would vary in its capacity to remove ammonia from wastewater.

In response to the commercialization of struvite recovery from municipal wastewater, a novel study was performed by Novotny (2011) on thermal decomposition of struvite pellets. These pellets were approximately 2 mm in diameter and were isothermally heated for 24 hours in a temperature range of 40° to 200° C. He claimed that about 70% of struvite ammonium had been eliminated at just 80° C along with approximately five moles of water. This contradicts the QTG results of Paulik and Paulik (1975a) and Abdelrazig and Sharp (1988), that suggested that only a small amount of ammonia is released below 100° C. Furthermore, 81% and 87% removal of struvite ammonium from the pellets were calculated for 160° and 200° C respectively. About 70% of the ammonium could be eliminated at heating temperatures between 100° and 200° C in 30 to 60 minutes. Based on previous research, the material produced at these temperatures was believed to be a mixture of struvite and amorphous  $\text{MgHPO}_4$ , but probably contained some magnesium pyrophosphate; this would explain its poor solubility and, therefore, low ammonia removal capacity, as discussed in Section 4.5.4.

#### ***4.5.4 Ammonia removal following “dry process”***

The thermal decomposition of struvite in air is a topic relevant to many fields including analytical chemistry, mineralogy, thermogravimetry and cement production as is demonstrated in Section 4.5.5. More recently, research has shifted to focus on using these struvite decomposition residues as a renewable source of magnesium and orthophosphate for wastewater treatment via struvite precipitation. Stefanowicz and colleagues (1992) proved that the solid phase product of dry thermal decomposition can be utilized to remove ammonium from wastewater. By heating struvite at 150° C for 24 hours, they produced a material which was believed to be mostly

$\text{Mg}_3(\text{PO}_4)_2$  but no XRD analysis was implemented. In acknowledgement of preceding research, this decomposition product was more likely a mixture of amorphous magnesium phosphates and magnesium pyrophosphate. It was demonstrated that the decomposed struvite could be used to treat a concentrated ammonia solution. However, to accomplish this in the set of reaction times investigated, the residues had to first be dissolved in the solution by acidification. 100% removal of ammonia was achieved in 24 hours by maintaining a pH of 9.3 and by adding decomposed struvite to provide a low N:P molar ratio compared to the stoichiometric ratio required for struvite formation. Although the final compositions of solid phases were not reported, it is likely that a significant portion of the magnesium and orthophosphate added to the solution was resolubilized and lost to the supernatant under these conditions. As the authors posited, the struvite produced from decomposition residues could potentially be recycled for repeated ammonia removal. However, a supplementary source of magnesium and orthophosphate would probably be required for consistent process efficiency.

Recycling of the struvite produced through dry thermal decomposition has been proven possible by a group of researchers, most of which are affiliated with the Department of Chemical Science and Technology at the University of Tokushima, Japan. A preliminary study by Sugiyama et al. (2005) showed that newberyite would dissolve and reform as struvite in the presence of ammonium, given a solution Mg:N:P molar ratio of 1:1:1 and a constant pH of 8. This resulted in a 77% ammonia removal efficiency after 3 hours. In the following experiment, struvite was decomposed in air at 150° C to produce an amorphous phase which contained what was believed to be  $\text{MgHPO}_4$ . When the struvite crystallization process was repeated using this material, a removal of only 41% was achieved. The resulting solid phase was collected and decomposed once again and the process was repeated a third time, affording a 33% removal of ammonia, perhaps, indicating incomplete elimination of struvite ammonium during decomposition. Hence, a portion of the added magnesium and orthophosphate could be recycled repeatedly by combined dry thermal decomposition and struvite formation. The loss of magnesium and orthophosphate incurred during this process was not reported.

The potential of the dry process of struvite decomposition was later verified by Sugiyama et al. (2007). A layer of  $\text{MgHPO}_4 \cdot 1.2\text{H}_2\text{O}$  was synthesized on a glass plate using a novel sol-gel technique. The sheet was immersed in an ammonia solution and, through the formation of dittmarite, more than 30% of the ammonia was removed in 3 hours. The sheet was then heated

to 150° C for 3 hours to eliminate the ammonium that was taken up and re-immersed in the same solution. This process was repeated two more times affording ammonia removal efficiencies between 10% and 20%. XRD analysis of the material following decomposition identified pronounced dittmarite peaks indicating that 150° C is likely too low to eliminate the ammonium on the spent sheet. By increasing  $\text{MgHPO}_4 \cdot 1.2\text{H}_2\text{O}$  availability for ammonia removal and optimizing the decomposition process, this application could be a promising technique for continuous wastewater treatment.

As described in Section 4.5.5, Novotny (2011) examined the dry thermal decomposition of commercially available struvite pellets. Pellets heated at 160° C in air for 24 hours were used successfully to remove ammonia through dissolution of an amorphous magnesium phosphate and reformation of struvite. When immersed in a 700 mg/L  $\text{NH}_4\text{-N}$  solution with a constant pH of 8, 40 and 80 g/L doses of decomposition product corresponded to approximately 50% and 93% ammonia removals in 2 hours. These doses provide a very low solution N:P molar ratio resulting in the solubilization of orthophosphate at about 60 and 190 mg/L  $\text{PO}_4\text{-P}$  for 40 and 80 g/L doses respectively. At a constant pH of 9, residual orthophosphate concentrations were reduced to below 10 mg/L  $\text{PO}_4\text{-P}$  due to the higher supersaturation with respect to struvite. This research demonstrated that decomposed struvite pellets could be used to treat for wastewater ammonia, at the cost of magnesium and orthophosphate release or high caustic addition.

## 4.6 Potential ammonia gas capture techniques

There are several options for the recovery of ammonia gas released during thermal decomposition of struvite. Proven methods include condensation and acid scrubbing or absorption. An ammonia-rich distillate or compressed ammonia could be generated from the mixture of air, water vapour, and ammonia using cryogenic or temperature-pressure-based condensation techniques (Türker and Celen, 2007; Evans and Thompson, 2009; Orentlicher, 2012) This recovered ammonia could also be packaged as a compressed liquid using similar methods. This type of product would be ideal for fuel combustion or for using ammonia as a precursor for hydrogen production. Alternatively ammonia-containing gas is contacted with sulfuric, nitric, or phosphoric acid using a scrubber or a membrane contactor to eventually produce an ammonium salt solution (Fassbender, 2001; ThermoEnergy Corporation, 2007; Cilon et al., 2009; Evans and Thompson, 2009; Ulbricht et al., 2013). This solution can be used

directly by industry or can be processed further to produce solid ammonium salts through evaporation or caustic addition. Alternatively, ammonia could be effectively adsorbed by magnesium chloride to form magnesium hexamine chloride ( $\text{Mg}(\text{NH}_3)_6\text{Cl}_2$ ) (Christensen et al., 2006; Elmøe et al., 2006; Zamfirescu and Dincer, 2009; Lan et al., 2012). The stored ammonia can be easily desorbed later through thermal decomposition of the metal amine. However, this method requires the removal of water vapour from recovery gas mixtures prior to adsorption, as magnesium chloride binds water to form hydrates.

#### **4.7 Conclusions for development of present study**

In moving forward with the present study, several knowledge gaps exist in literature pertaining to the study of ammonia removal using thermally decomposed struvite. Several studies claimed to have employed a  $\text{MgHPO}_4$ -containing struvite decomposition product to remove ammonia from solutions (Zhang et al., 2004; Sugiyama et al., 2005; Sugiyama et al., 2007). However, only the material produced by Sugiyama and colleagues (2007) provided any evidence of crystalline  $\text{MgHPO}_4$  and none of the previous research concerning thermal decomposition of struvite named newberyite as a potential product. Although the conversion of struvite to newberyite has been examined in detail (Boistelle and Abbona, 1983; Kontrec et al., 2005; Babić-Ivančić et al., 2006), no research has yet focussed on investigating the conversion of newberyite to struvite in the presence of ammonium. Of the work directed towards ammonia removal technologies (Zhang et al., 2004; Sugiyama et al., 2005; Sugiyama et al., 2007; Türker and Celen, 2007; He et al., 2007; Huang et al., 2009; Huang et al., 2011), few took a systematic approach to delineating the multi-parameter effects on rates and mechanisms. In general, these studies offered a limited scope of experimental conditions with respect to pH control, decomposed struvite dosing, temperature, and initial solution chemical composition. For instance, previous research has centred on presenting the potential of these techniques with little discussion of how these parameters would affect overall effluent quality and operating costs.

With regard to controlled struvite formation, several researchers have completed detailed studies on systems with post-dosing Mg:P and N:P molar ratios above 1 (Dastur, 2001; Adnan, 2002; Britton, 2002; Huang, 2003; Fattah, 2004). However, there is a lack of literature which evaluates the potential for combined ammonia and orthophosphate removal at Mg:P and N:P

molar ratios of 1 and below. The present study works to fill in some of this missing information and act as a foundation for the selection of various technological features of the proposed ammonia recovery system.

## CHAPTER 5: MATERIALS AND METHODS

### 5.1 Description of performed batch tests

Multiple sets of batch tests were employed to examine the rate and mechanisms of newberyite-to-struvite conversion in the presence of ammonium. Twenty-four experiments were conducted to represent the fundamental system of synthetic newberyite in a simple ammonia solution. A broad range of experimental conditions were provided in this phase of the study to “cast a wide net” in identifying a potential optimal region of operation for the proposed technology. This technology relies on the dissolution of newberyite to provide the magnesium and orthophosphate required to induce struvite formation and, hence, ammonia removal.

However, complete conversion of newberyite to struvite can only be accomplished through the maintenance of newberyite and struvite supersaturation. To adjust  $S_N$  and  $S_S$ , various combinations of pH control and temperature were selected. These ranges were meant to represent the potential temperatures of municipal post-digestion streams and the caustic doses that might be required to promote struvite formation. Further, a newberyite dose range that would result in a total suspension Mg:N:P molar ratio between 1:1:1 and 1:1.4:1 was employed to observe how excess ammonia relative to the stoichiometry of struvite formation affects rates and mechanisms. These doses were selected to target high newberyite-to-struvite conversion efficiency, while maintaining low magnesium and orthophosphate residuals. Eight subsequent experiments were performed in an “optimal” range of conditions for synthetic solutions intended to represent the basic characteristics of specific wastewaters. Each combination of parameters was represented by duplicate batch tests. Table 7 outlines the value of specific parameters which were combined to construct experimental matrices (refer to Sections 5.2 and 5.3.2 for ammonia solutions and synthetic newberyite compositions respectively).

**Table 7 – Summary of experimental parameters for duplicate batch tests**

Solution	No. of Experiments	pH Control	Temperature (° C)	Mg:N:P Molar Ratio
Ammonia solution	24	None, 7, 8, 9	10, 25, 35	1:1.1:1, 1:1.4:1
Synthetic crystallizer effluent	4	7, 8	10, 25	1:1:1
Synthetic centrate	4	7, 8	10, 25	1:1:1

## 5.2 Ammonia solutions – Synthetic wastewaters

The compositions of the simple ammonia solution and synthetic wastewaters allocated to previously described batch tests are compared to typical dewatering centrate from Annacis Island WWTP in Table 8. The ammonia solution was prepared to be around 700 mg/L  $\text{NH}_4\text{-N}$  to represent the typical ammonia concentration in the effluent of a pilot-scale struvite crystallization process (Huang, 2002; Fattah, 2004). It should be noted that Annacis Island centrate is characterized by high organic matter, a total suspended solids content greater than 2000 mg/L and alkalinity above 6000 mg/L as  $\text{CaCO}_3$ . A typical anaerobic digester supernatant carries alkalinity at 2000 to 5000 mg/L (Tchobanoglous et al., 2003). To minimize synthetic wastewater salinity, an alkalinity of 2000 mg/L, typical of Lulu Island WWTP digester supernatant, was adopted for these solutions (Huang, 2003). However, some alkalinity losses as carbon dioxide occurred during preparation due to the low initial pH of nutrient solutions.

Synthetic wastewaters were prepared using reagent grade chemicals and distilled water. This included ammonium phosphate monobasic ( $\text{NH}_4\text{H}_2\text{PO}_4$ ) and ammonium chloride ( $\text{NH}_4\text{Cl}$ ). Magnesium was added as magnesium chloride hexahydrate ( $\text{MgCl}_2 \cdot 6\text{H}_2\text{O}$ ). Alkalinity was provided as sodium bicarbonate ( $\text{NaHCO}_3$ ). Synthetic crystallizer effluent was prepared by a batch procedure simulating conventional struvite recovery. An equimolar quantity of magnesium with respect to initial orthophosphate content was mixed with 3 L of synthetic centrate in a beaker on a stir plate. Temperature was maintained constant at 35° C using an aquarium heating rod, while pH was maintained at 8.5 using a 2 M caustic solution made from sodium hydroxide (NaOH) pellets. Once pH was stabilized, mixing and heating were continued overnight and the resulting suspension was filtered using Whatman 5 qualitative 12.5 cm diameter filters and a vacuum apparatus. All feed solutions were stored in 8 L Nalgene containers.

**Table 8 – Annacis Island WWTP centrate compared to studied solutions**

Feed	pH	Mg (mg/L)	NH <sub>4</sub> -N (mg/L)	PO <sub>4</sub> -P (mg/L)	Alkalinity (mg/L as CaCO <sub>3</sub> )
Annacis Island centrate	8.5	1	1000	150	> 6000
Ammonia solution	4.5-5.5	0	737	0	0
Synthetic crystallizer effluent	8.1-8.4	16	919	19	1470
Synthetic centrate	7.4-7.9	0	1008	147	1475

### 5.3 Synthetic newberyite

#### 5.3.1 Synthesis

The synthetic newberyite used as a surrogate for thermally decomposed struvite pellets was prepared in the laboratory. Reagent grade 71.3 g/L sodium phosphate dibasic (Na<sub>2</sub>HPO<sub>4</sub>) and 544 g/L MgCl<sub>2</sub>·6H<sub>2</sub>O solutions were prepared using distilled water. The pH of the orthophosphate solution was adjusted to around 8.3 using several drops of concentrated hydrochloric acid (HCl). 800 mL of the orthophosphate solution and 150 mL of the magnesium solution were mixed in a 1 L beaker on a heated stir plate. Temperature was maintained above 25° C and concentrated HCl was added dropwise to maintain a pH below 6.5 for an hour. The resulting suspension was filtered using Whatman 5 qualitative 12.5 cm diameter filters and a vacuum apparatus. The retained solids were washed several times with distilled water and reagent alcohol. The synthetic newberyite was then dried in an oven at 90° C overnight to evaporate any residual water and alcohol. This procedure yielded about 70 g newberyite and this was stored in a closed plastic sample bottle.

#### 5.3.2 Analysis

The purity of synthesized newberyite was evaluated by XRD and chemical analyses. XRD analyses showed that no other solid phases were formed while preparing synthetic newberyite. XRD output graphs for this newberyite product is provided in Appendix C. A known mass of newberyite was dissolved in distilled water with the addition of concentrated hydrochloric acid to reduce pH to below 2. This solution was then diluted and analyzed for orthophosphate using the flow injection method outlined in Section 5.6.2. Table 9 presents the results of chemical analysis

and the batch experiments of which they were used in. Magnesium and orthophosphate content with mass was not the same for each batch of newberyite due to variations in its water of crystallization (theoretically there are 3 moles of water per mole of newberyite). This variation in molecular weight and composition is believed to be due to small differences between batches in the method of synthesis, such as crystallization temperature and pH, as well as drying and storage time.

**Table 9 – Synthetic newberyite chemical composition and concerned experiments**

<b>Date prepared</b>	<b>Mg and PO<sub>4</sub>-P content (mmoles/g newberyite)</b>	<b>Experiments used in (Section)</b>
Theoretical	5.73	-
May 2012	5.34	6.2
July 2012	5.47	6.3
September 2012	5.44	6.5
November 2012	5.95	6.4

## **5.4 Materials and equipment**

### **5.4.1 Batch test method and apparatus**

Duplicate batch tests were performed in two glass jacketed containers sitting atop stir plates. Temperature control was accomplished using a cooled/heated water bath that provided continuous flow of water through the jackets. Prior to each set of experiments, the containers were cleaned using a 5% hydrochloric acid solution to dissolve any residual newberyite or struvite that had adhered to the glass during previous experiments. This was followed by three rinses with distilled water. 500 mL of synthetic wastewater feed was added to each reactor and the water bath and stir plates were turned on to initiate temperature adjustment. Temperature was monitored using the temperature sensor feature of two handheld pH probes (see Section 5.4.2). Once the feed had stabilized with respect to the desired reaction temperature, premeasured amounts of newberyite were added simultaneously to both apparatuses. The synthetic centrate tests required supplementation of magnesium which was provided using pipette-measured volumes of a 0.5 M MgCl<sub>2</sub> solution. The time was noted and the apparatuses were covered with glass caps to reduce heat loss/gains. However, batch tests were open to the

atmosphere. Finally, caustic burettes and pH probes were positioned for pH control and monitoring. pH was controlled for the duration of study through the dropwise addition of a 2 M NaOH solution using two 50 mL burettes. At every sample time, pH and caustic consumption were recorded. For two sets of experiments, an ammonium selective electrode and conductivity probe were positioned in Reactor 1 (see Sections 5.4.3 and 5.4.4).

### ***5.4.2 pH monitoring***

pH was monitored in both apparatuses using two Oakton pH 11 Series meters complete with ATC probes. pH meters were calibrated prior to each set of experiments using pH 4, 7 and 10 standard buffer solutions that were heated in the a water bath to 25° C. The probes were submerged in the test suspension by insertion into openings separate from that used for caustic addition.

### ***5.4.3 Conductivity monitoring***

Conductivity was monitored in one of the two apparatuses along with online ammonium measurement. For this purpose a specialized foam cap was designed to hold and submerge a conductivity, ammonium, and pH probe collectively. The ATC conductivity probe was connected to an Oakton CON 110 meter and calibrated prior to each experiment using potassium chloride (KCl) standard solutions of similar ionic strengths to that expected in the suspensions. These standards were also heated/cooled to the same temperature as the suspension for each experiment. The meter was connected via an analog-USB cord to a laptop PC and conductivity data was stored every 5 seconds using the software provided with the meter.

### ***5.4.4 Ammonium monitoring***

Ammonium activity was monitored in one of the two reactors along with online conductivity measurement. The Cole-Parmer ammonium selective electrode was connected to an Oakton pH 2100 bench meter and calibrated prior to each experiment using standard solutions that spanned the expected range of ammonium concentrations and background orthophosphate, alkalinity, and ionic strength conditions. These standards were also heated/cooled to the same

temperature as the feed for each experiment. The meter was connected via an analog-USB cord to a laptop PC and ammonium activity data was stored every 5 seconds using the software provided with the meter.

#### **5.4.5 PHREEQC-2 chemical equilibrium model**

A chemical equilibrium model was constructed for this study using PHREEQC Version 2 to predict the equilibrium liquid and solid phase compositions that would result from specific sets of initial and constant conditions. The experimental parameters outlined in Section 5.1 were simulated and model-generated outputs were compared with batch test results to identify discrepancies between observed and theoretical compositions and to evaluate the model as a tool for future studies. PHREEQC is a software provided by the United States Geological Survey, capable of modelling low temperature aqueous chemical reactions. PHREEQC stands for a pH-REdox-Equilibrium program written in C language. Environmental and geochemical reactions of interest involving magnesium, ammonium, and orthophosphate were added to a customized model from a database file (thermo.com.V8.R6.230) containing data compiled by Jim Johnson of Lawrence Livermore National Laboratory. The attributed constants of these reactions, such solubility products and negative enthalpy changes for reactions, were collected from relevant literature; those of special interest, including struvite, newberyite, and bobbierite were determined experimentally in a previous study at UBC (Lobanov et al., 2013). With the input of initial composition of dissolved elements and solid complexes, the model will output initial batch suspension pH and saturation with respect to the considered solid phases, as well as elemental and solid phase concentrations after equilibrium has been reached. pH control, through caustic addition, can be simulated and caustic consumption may be estimated. Overall, it is a powerful tool for estimating activity coefficients, supersaturation ratios, and corrected solubility products for suspensions with controlled experimental conditions. Initial suspension composition model inputs and equilibrium outputs are reported in Sections 6.2, 6.3, 6.4, 6.5 and Appendix D.

### **5.5 Sample collection and preservation**

Samples were collected from both apparatuses at 1, 3, 6, 9, and 12 hours after initiation for batch tests with synthetic newberyite in ammonia solution. With synthetic crystallizer effluent

and centrate, samples were collected at 10 minutes, 1, 3, and 4 hours after dosing. This was accomplished using two 60 mL syringes with tube extensions allowing for sampling at the centre of the suspension column. Samples were pushed through a Millipore 47 mm diameter 0.45µm nylon membrane filter into 50 mL centrifuge tubes for storage. Two drops of concentrated HCl were added immediately after collection to induce undersaturation in samples with respect to both newberyite and struvite to prevent further formation of solid phases. The same syringes were used to force two full volumes of distilled water and one volume of reagent alcohol through the filter to wash and partially dry the retained solid phase. The filter and retained solids were allowed to dry overnight and were stored in individual sealed sample bags.

## **5.6 Analytical methods**

All synthetic wastewater feeds were analyzed prior to experiments for magnesium, ammonia, orthophosphate, and inorganic carbon where applicable. All liquid samples from the batch tests were analyzed for ammonia and orthophosphate. Ammonia and orthophosphate measurements were also involved in determining N:P molar ratios of solid phase samples dissolved in a weak HCl solution. Liquid samples from tests with crystallizer effluent and centrate were also analyzed for magnesium in order to estimate the newberyite and struvite supersaturation ratio at each sample time. Each sample was prepared in triplicate and all analyses were undertaken at the UBC Environmental Engineering Laboratory, unless otherwise specified.

### **5.6.1 Magnesium**

Samples and calibration standard solutions were diluted in 25 mL glass tubes at a 1:10 volumetric ratio with a 20 g/L lanthanum solution prepared from reagent grade lanthanum nitrate ( $\text{La}(\text{NO}_3)_3$ ) and distilled water. This was followed by addition of three drops of concentrated nitric acid ( $\text{HNO}_3$ ) to each tube and agitation using a vortex mixer. This background matrix reduces the interference of other ionic species during analysis for magnesium using a Varian Inc. SpectrAA220 Fast Sequential Atomic Absorption Spectrophotometer. Prior to each set of analyses, fresh deionized water was provided for autosampler rinsing and the magnesium lamp was optimized and warmed up for at least 30 minutes (see Appendix A for instrument operational settings).

### **5.6.2 Ammonia and orthophosphate**

Ammonia and orthophosphate were measured in samples by flow injection analysis on a Lachat QuikChem 8000 using Method 4500-NH<sub>3</sub> H and 4500-P G from Standard Methods for the Examination of Water and Wastewater (APHA, AWWA, WEF, 2012). Calibration standard solutions were composed of reagent grade potassium phosphate monobasic (KH<sub>2</sub>PO<sub>4</sub>) and ammonium chloride in distilled water (see Appendix A for method details and instrument settings).

### **5.6.3 Carbonate alkalinity**

Total inorganic carbon was measured as a surrogate for carbonate alkalinity since the only carbon that synthetic feeds contained was that resulting from the addition of NaHCO<sub>3</sub> and dissolution of carbon dioxide from the air. This was accomplished using a Lachat IL550 TOC-TN Analyzer for Method 5310-B from Standard Methods for the Examination of Water and Wastewater (APHA, AWWA, WEF, 2012). Calibration standard solutions were composed of sodium carbonate (Na<sub>2</sub>CO<sub>3</sub>) and NaHCO<sub>3</sub>.

### **5.6.4 XRD identification of solid phases**

Crystalline phases were identified in the solids retained during filtration of suspension samples. This was accomplished with a Bruker D8 Advance X-ray diffractometer using CuK<sub>α</sub> radiation. XRD output peak patterns were identified using the powder diffraction database file, PDF-2, provided by the International Center for Diffraction Data. This instrument was located in the UBC Department of Chemistry (see Appendix A for pattern database details and instrument settings).

### **5.6.5 Crystal morphology**

Crystal morphology was observed using a Motic B3 Professional Series microscope and images were captured using Motic Images Plus software. Small quantities of the solid samples were

placed on glass slides and spread using a drop of reagent alcohol. Crystals were viewed at x10 and x40 magnifications.

## 5.7 Statistics

Comparisons of samples from different combinations of experimental conditions were made based on the error of the mean resulting from two measurements from each of the duplicate batch tests. This error was calculated using an unpaired two-tailed t-test at a confidence interval of 90%. In example, if the errors of the mean of two measurements from different sets of experiments overlapped these two values were deemed not statistically different. Eqns. 42, 43, and 44 demonstrate how standard deviation (s), standard error, and error of the mean were calculated where  $x$ ,  $n$  ( $n = 2$ ), and  $t$  ( $t_{1,0.05} = 6.314$ ) represent the measurement value, the number of samples compared, and the student's-t value respectively (Berthouex and Brown, 2002).

$$s = \frac{1}{n} \sqrt{\sum_i^n (x_i - \bar{x})^2} \quad (42)$$

$$\text{standard error} = \frac{s}{\sqrt{n}} \quad (43)$$

$$\pm \text{ error} = \text{standard error} \cdot t_{n-1,0.05} \quad (44)$$

## 5.8 Terminology

### 5.8.1 Molar ratio

The term molar ratio is used with respect to both N:P and Mg:N:P. In the context of newberyite dosing, these molar ratios consider the total of each element in the initial suspension immediately after commencing the batch test. This includes dissolved elements and that contained in the solid phase reagent, newberyite. Eqns. 45 and 46 explain the concept of initial N:P and Mg:N:P molar ratios respectively.

$$[\text{NH}_4^+_{(\text{aq})}] : ([\text{newberyite}_{(\text{s})}\text{-PO}_4] + [\text{PO}_4^{3-}_{(\text{aq})}]) \quad (45)$$

$$([\text{newberyite}_{(\text{s})}\text{-Mg}] + [\text{Mg}^{2+}_{(\text{aq})}]) : [\text{NH}_4^+_{(\text{aq})}] : ([\text{newberyite}_{(\text{s})}\text{-PO}_4] + [\text{PO}_4^{3-}_{(\text{aq})}]) \quad (46)$$

In the context of solid phase sample composition, N:P refers to the molar ratio of the ammonium content in struvite to the orthophosphate content in the mixed solid phase of newberyite and struvite. Since newberyite contains no ammonium, this ratio quantifies the fraction or molar percent of struvite in the solid phase. Eqn. 47 demonstrates this convention.

$$[\text{struvite}_{(\text{s})}\text{-NH}_4] : ([\text{newberyite}_{(\text{s})}\text{-PO}_4] + [\text{struvite}_{(\text{s})}\text{-PO}_4]) \quad (47)$$

### 5.8.2 Solubility product ( $K_{\text{sp-N}}$ and $K_{\text{sp-S}}$ )

The newberyite and struvite solubility products are referred to in this study as  $K_{\text{sp-N}}$  and  $K_{\text{sp-S}}$  respectively.  $K_{\text{sp}}$  is the product of the activities of ionic components concerned in the formation of a solid phase. Eqns. 48 and 49 demonstrate the calculation of  $K_{\text{sp-N}}$  and  $K_{\text{sp-S}}$  based on reagent activities (Söhnel and Garside, 1992).

$$K_{\text{sp-N}} = \{\text{Mg}^{2+}\}\{\text{HPO}_4^{2-}\} \quad (48)$$

$$K_{\text{sp-S}} = \{\text{Mg}^{2+}\}\{\text{NH}_4^+\}\{\text{PO}_4^{3-}\} \quad (49)$$

Section 4.1.2 lists reported and experimentally determined solubility products for a variety of phases that could also form in solutions supersaturated with respect to struvite. From previous experiments by Dr. Sergey Lobanov at UBC,  $K_{\text{sp-N}}$  and  $K_{\text{sp-S}}$  at 25° C are taken as  $10^{-5.88}$  and  $10^{-13.47}$  respectively (Lobanov et al., 2013).

### 5.8.3 Supersaturation ratio

Supersaturation ratio is defined as the square root of the product of reagent activities divided by the concerned solid phase solubility product for newberyite and cubed root of that for struvite.

Newberyite and struvite supersaturation ratios are referred to in this study as  $S_N$  and  $S_S$  and are represented by Eqns. 50 and 51 respectively (Söhnel and Garside, 1992).

$$S_N = \left( \frac{[Mg^{2+}][HPO_4^{2-}]}{K_{sp-N}} \right)^{\frac{1}{2}} \quad (50)$$

$$S_S = \left( \frac{[Mg^{2+}][NH_4^+][PO_4^{3-}]}{K_{sp-S}} \right)^{\frac{1}{3}} \quad (51)$$

Supersaturation ratio is a measure of the crystallization potential of a solution. For instance, struvite will readily crystallize in a solution with a  $S_S$  greater than 1, while it will dissolve in a solution with a  $S_S$  less than 1. In this study, supersaturation ratio of samples was estimated from known elemental concentrations and model-generated parameters, including activity coefficients and temperature-corrected solubility products.

#### 5.8.4 Removal efficiency

In the context of ammonia, removal efficiency is defined as the percent of total ammonia (as converted to ammonium) removed through struvite formation with respect to the total ammonia initially in solution. Essentially, this parameter quantifies the ammonium displaced to the solid phase of the suspension at various sample times during batch tests. Eqn. 52 demonstrates this relationship between initial ammonia concentration and that at sample time,  $x$ .

$$\text{Ammonia removal efficiency} = \left( \frac{[NH_4-N]_{t=0} - [NH_4-N]_{t=x}}{[NH_4-N]_{t=0}} \right) * 100\% \quad (52)$$

## CHAPTER 6: RESULTS AND DISCUSSION

### 6.1 Fundamentals of newberyite dissolution-struvite formation mechanism in the presence of ammonium

The first set of batch tests performed represents the most fundamental cases of this study. They are intended to determine the ranges of pH, temperature and newberyite dose, which promote high ammonia removal and high newberyite-to-struvite conversion efficiency, while limiting magnesium and orthophosphate losses to solution. The following sections answer the following questions:

- How does the composition of liquid and solid phases change when synthetic newberyite is added to a simple ammonia solution?
- How fast do these chemical reactions occur?
- How does the liquid and solid composition compare to that of the model-generated equilibrium?

### 6.2 Transformation of newberyite into struvite in ammonia solution: Phase 1 – Suspension Mg:N:P molar ratio of 1:1.1:1

The rates and mechanisms of ammonia removal and orthophosphate solubilization were observed during 12 batch tests combining synthetic newberyite and a simple ammonia solution. Table 10 outlines the average suspension characteristics immediately after newberyite is added to the solution. This can be considered time zero and Mg:N:P molar ratio represents the proportions of magnesium and orthophosphate contributed by newberyite and the ammonia initially in solution. This set of experiments was intended to represent a Mg:N:P molar ratio of 1:1:1. However, it was determined later, that one mole of synthetic newberyite does not weigh exactly 174.3 g. As reported in Section 5.3.2, one mole of synthetic newberyite may contain slightly less or more than three moles of water of crystallization. Therefore, the following results are for a Mg:P:NH<sub>4</sub> molar ratio of 1:1.1:1, indicating that ammonia was in slight excess.

**Table 10 – Suspension characteristics at t = 0 h for Mg:N:P molar ratio 1:1.1:1 newberyite dose batch tests**

Reagents added as solid newberyite			Initial solution characteristics			Mg:N:P Molar Ratio
Newberyite added (g/L)	Mg (mM)	PO <sub>4</sub> -P (mM)	Mg (mM)	NH <sub>4</sub> -N (mM)	PO <sub>4</sub> -P (mM)	
8.7	46.7	46.7	0	52.6	0	1:1.1:1

### **6.2.1 pH effect on rate and efficiency of ammonia removal**

By increasing the pH to 7 and above, undersaturation with respect to newberyite is induced (Boistelle and Abbona, 1983; Kontrec et al., 2005; Babić-Ivančić et al., 2006). Further, maintenance of neutral to alkaline conditions during struvite crystallization remains the simplest method of controlling struvite crystallization (Dastur, 2001; Adnan, 2002; Britton, 2002; Huang 2003; Fattah, 2004). In a solution initially containing newberyite and aqueous ammonia, pH plays a significant role in both the rate of ammonia removal and how much remains as equilibrium is approached.

Similar trends were observed with regard to the average ammonia removal rate for each combination of pH and temperature as illustrated in Figure 7. In all cases, ammonia removal occurred rapidly within the first hour. This indicates an enhanced rate of struvite formation that is driven by the high ammonium activity and, therefore, high  $S_s$  at the start of the test. Initial reaction rates were highest at pH 8 and 9. Further, the ammonia residual nears equilibrium in only three hours. For the batch tests without pH control, pH increased from approximately 5 to 6.6, due to the partial dissolution of newberyite, and gradually decreased as struvite formation begins to dominate. These conditions allowed for an ammonia removal of only 11% to 15% after 12 hours for the three temperatures. Ammonia removal was far greater in the cases where pH was maintained at 7 and above. At pH 7, the ammonia removal was boosted to between 71% and 79% by the end of the tests. The ranges of removal for pH 8 and 9 were slightly higher at 80% to 84% and 77% to 85% respectively. However, the final ammonia residuals for pH 7, 8 and 9 were statistically similar for 10° and 25° C, while a slight difference between batch tests with respect pH was exhibited for residuals at 35° C.

Overall, the data is in agreement with the results obtained by Sugiyama and colleagues (2005). They added newberyite to a 114 mg/L  $\text{NH}_4\text{-N}$  solution to provide a suspension Mg:N:P molar ratio of 1:1.1:1. In the present study, comparable ammonia removal efficiencies were obtained at pH 8, with a more concentrated solution. Interestingly, similar removals were observed at a far lower suspension N:P molar ratio, when compared to analogous tests by Novotny (2011) with an amorphous product of struvite thermal decomposition. This suggests that newberyite is a more efficient ammonia removal agent. At a newberyite dose of 1:1.1:1 Mg:N:P, it is apparent that 71% to 84% of ammonia can be removed from this simple solution by maintaining a pH between 7 and 8. However, the question remains: How much orthophosphate is released and, hence, lost during this process

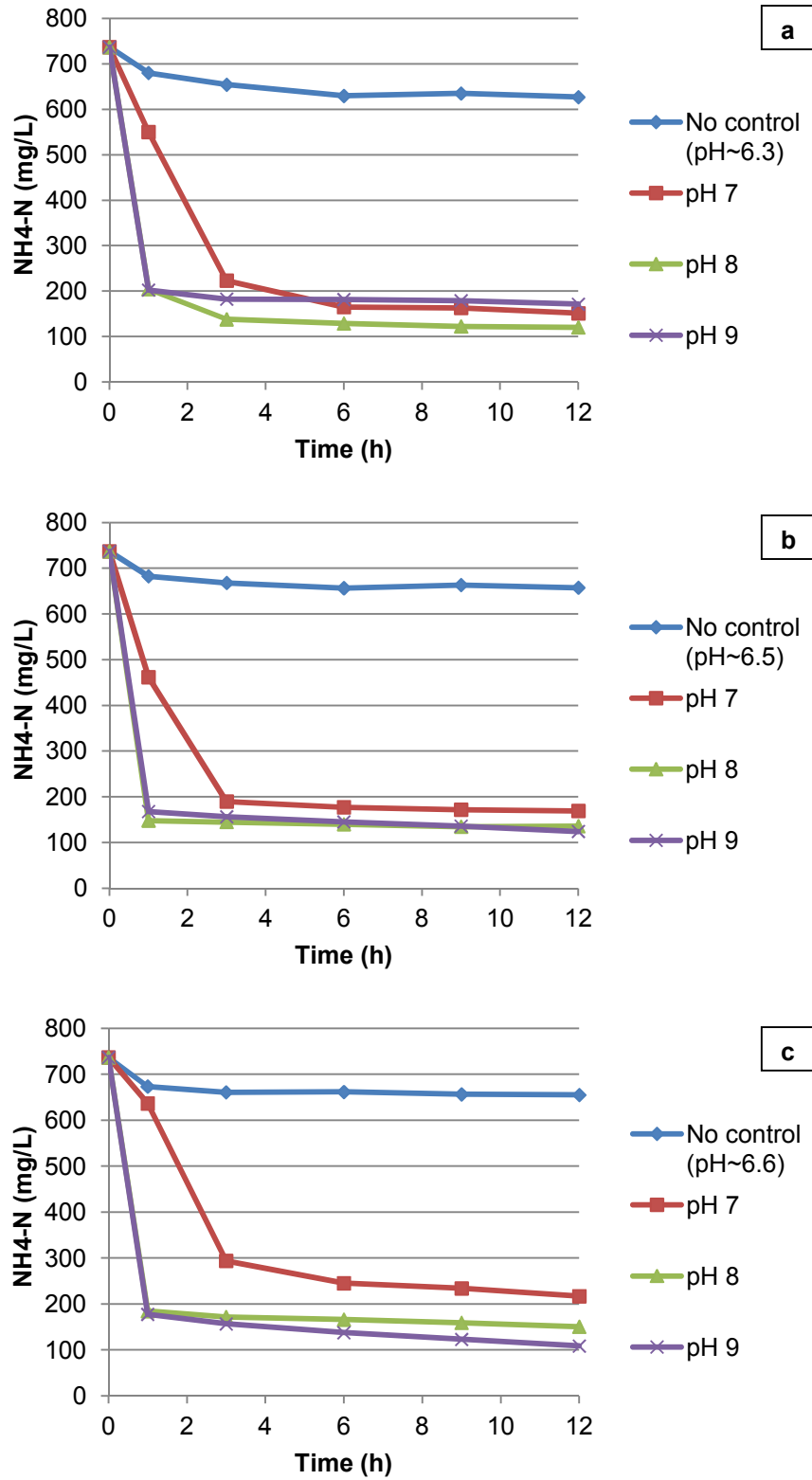


Figure 7 – NH<sub>4</sub>-N removed for various pH conditions at (a) 10°, (b) 25°, and (c) 35° C

### **6.2.2 pH effect on rate and extent of orthophosphate solubilization**

Orthophosphate residuals originate primarily from the dissolution of newberyite. On the contrary, higher supersaturation, with respect to struvite, results in lower orthophosphate residuals due to enhanced ammonia removals via struvite crystallization. The following section explores the effect of pH on orthophosphate solubilization.

Unless magnesium phosphates other than newberyite and struvite form during ammonia removal, the residual magnesium molar concentration is analogous to that of orthophosphate. As discussed in subsequent Section 6.2.5, no undesirable solid phases were detected in any of the samples analyzed by XRD. Figure 8 plots average orthophosphate residuals with time for various combinations of pH and temperature. Similarly to ammonia removal, orthophosphate solubilization rates are highest in the first hour. This indicates that newberyite dissolves rapidly during this time and this is probably enhanced by the maintenance of low  $S_N$  by simultaneous struvite formation. Orthophosphate concentration also appears to approach a state of equilibrium by 3 hours, especially when pH was controlled. The 12 hour orthophosphate residuals were highest in tests with no control of pH ranging from 199 to 352 mg/L  $PO_4$ -P. Residuals were significantly lower when pH was maintained above 7. This is expected to be due to the higher  $S_S$  induced at increased pH. After 12 hours, the orthophosphate concentration was significantly lower at pH 7 than with no pH control for all temperatures ranging from 115 to 119 mg/L. The lowest final residuals were measured at pH 8 and 9. Orthophosphate was in the range of 25 to 33 mg/L and 11 to 20 mg/L for pH 8 and 9 respectively. However, there was no significant difference between orthophosphate residuals at pH 8 and 9 for all cases.

The observed solubilization of orthophosphate confirms that a solid phase must first dissolve in order to transform into another, regardless of how chemically similar they are (Boistelle and Abbona, 1983; Kontrec et al., 2005; Babić-Ivančić et al., 2006; Novotny, 2011). It should also be noted that the residuals measured in the present study compare well to similar tests by Novotny (2011), in which considerably lower suspension N:P molar ratios were examined using thermally decomposed struvite pellets. Orthophosphate in the liquid phase, following ammonia removal constitutes a loss of the material that was added as newberyite. This is a concern because the effluent of the proposed ammonia recovery system must be returned to mainstream biological processes. If the effluent of this system is higher in orthophosphate than that in the influent, it

could make ammonia recovery less attractive, as the returned residual would increase phosphorus loading to secondary treatment operations. This also means more struvite will be consumed during thermal decomposition operations to make up for this loss. The orthophosphate residual originating from newberyite is accompanied by an equimolar magnesium residual. If these residuals are high enough, they may promote the formation of struvite scale with their return, which defeats one of the functions of struvite recovery. Nevertheless, the similarity between orthophosphate residuals at pH 8 and 9, suggests that a pH higher than 8 may not be necessary to maintain low orthophosphate residuals and this would represent a caustic savings. Further, a pH of 8 could provide high ammonia removal, while maintaining an orthophosphate concentration considerably lower than that of Annacis Island dewatering centrate.

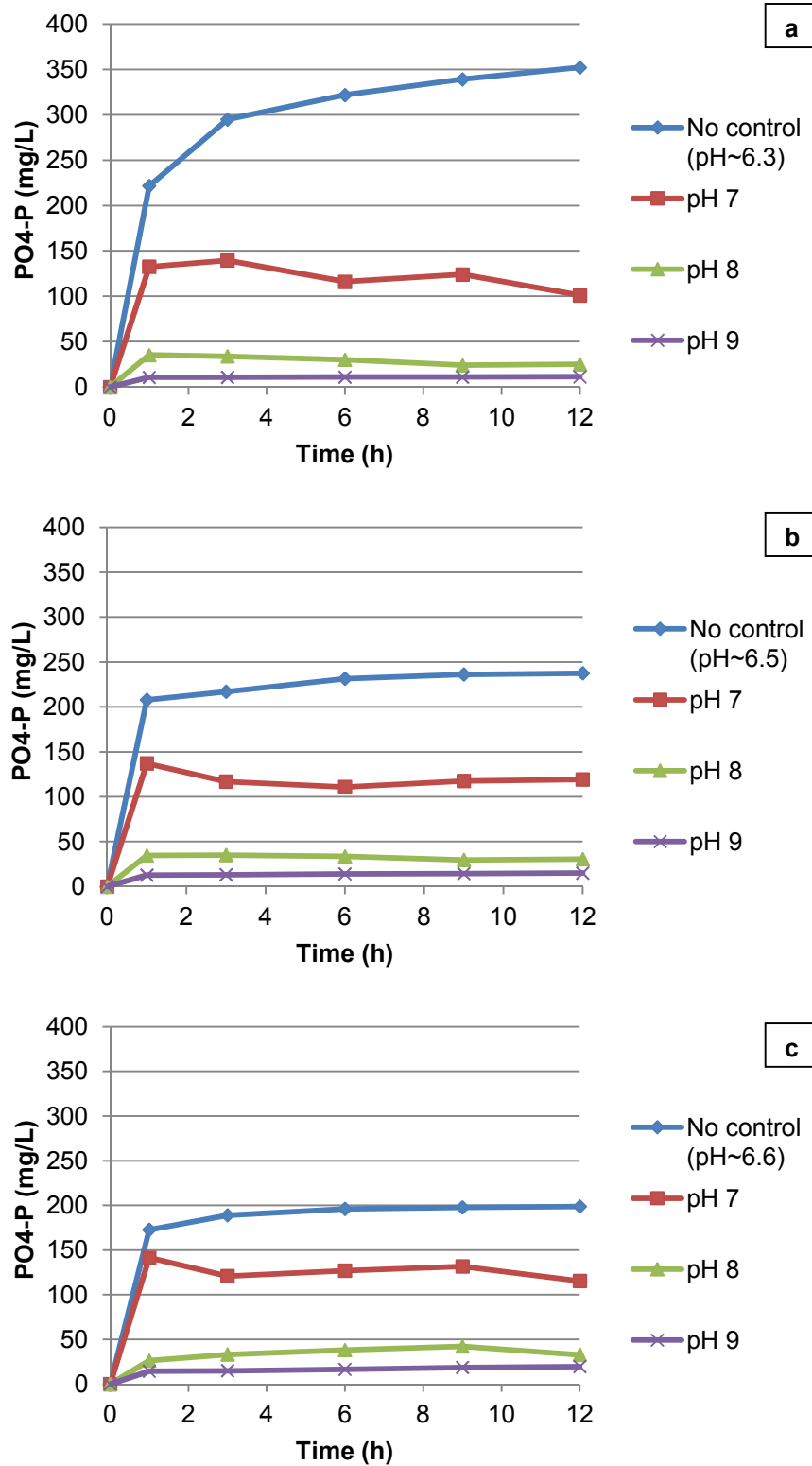


Figure 8 – Residual PO<sub>4</sub>-P for various pH conditions at (a) 10°, (b) 25°, and (c) 35° C

### **6.2.3 Temperature effect on rate and efficiency of ammonia removal**

Temperature affects many suspension characteristics including elemental activity, solid phase supersaturation, and solubility, as well as reaction kinetics. For instance, newberyite is more thermodynamically stable than struvite above 25° C if pH is below 6, while struvite is less soluble at lower temperatures (Boistelle and Abbona, 1983; Kontrec et al., 2005; Babić-Ivančić et al., 2006; Lobanov et al., 2013). Further, solid phase dissolution is enhanced at elevated temperatures due to the higher kinetic energy of water molecules. Temperature is expected to affect both the rate of ammonia utilization for struvite formation and near-equilibrium compositions.

Figure 9 compares average ammonia removals over time with respect to temperature. Contrary to expectations, temperature did not appear to affect the rate of ammonia utilization. At the end of the test period, the mean ammonia removal efficiencies at 10° C were highest in most cases. This is expected to be due to lower struvite solubility in these tests. However, there was no statistically significant difference between final ammonia residuals, with respect to temperature for all pH conditions.

Evidently, ammonia residual is less dependent on temperature than on pH. This suggests that fluctuations in wastewater temperature may not significantly affect ammonia removal efficiency. From a practical standpoint, the heat of biosolids digestate could be allocated to operations that would benefit from it prior to the ammonia recovery system to gain some process efficiency.

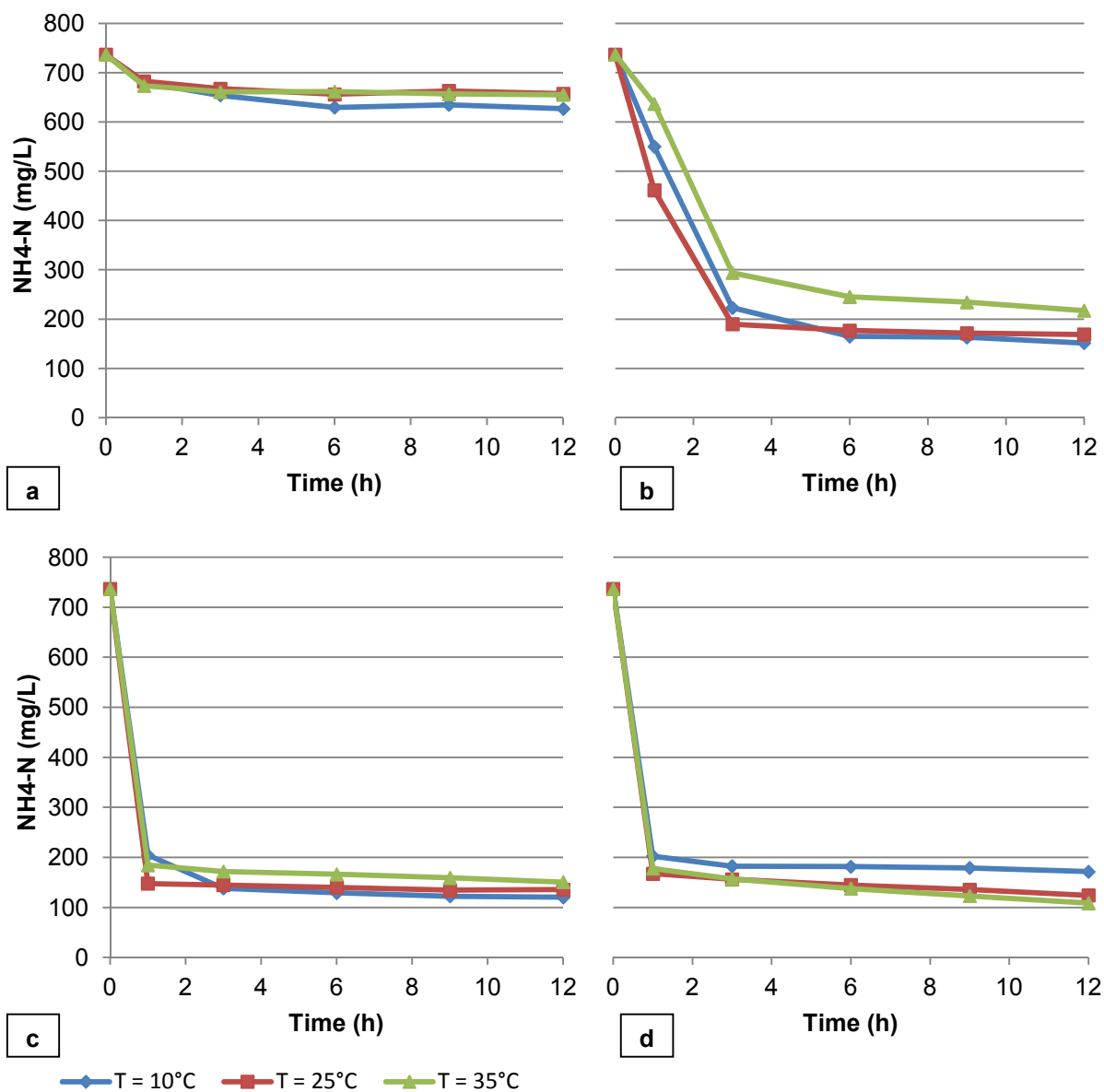


Figure 9 –  $\text{NH}_4\text{-N}$  removed for various temperatures for (a) no pH control, (b) pH 7, (c) pH 8, and (d) pH 9

#### **6.2.4 Temperature effect on rate and extent of orthophosphate solubilization**

Newberyite dissolution and struvite crystallization are separate mechanisms occurring simultaneously in this system. However, they are connected because as one reaction progresses, it affects the solution's supersaturation with respect to the coexisting solid phase. There is the potential for temperature to play a greater role in newberyite dissolution than it does in formation of struvite. This section examines the rates of orthophosphate solubilization and resulting residuals as affected by temperature.

Figure 10 illustrates the effect of temperature on average orthophosphate residuals for various pH conditions. Similarly to ammonia removal, the orthophosphate solubilization resulting from newberyite dissolution is not significantly affected by fluctuations in temperature between 10° C and 35° C at a pH of 7 and above. The exception is in tests with no pH control. There was a significant difference between final orthophosphate residuals for the three temperatures, despite ammonia removals that were statistically similar.

Struvite crystallization is enhanced at lower temperatures while newberyite dissolution is increased. These results reveal that wastewater cooling could provide better conversion efficiency between newberyite and struvite.

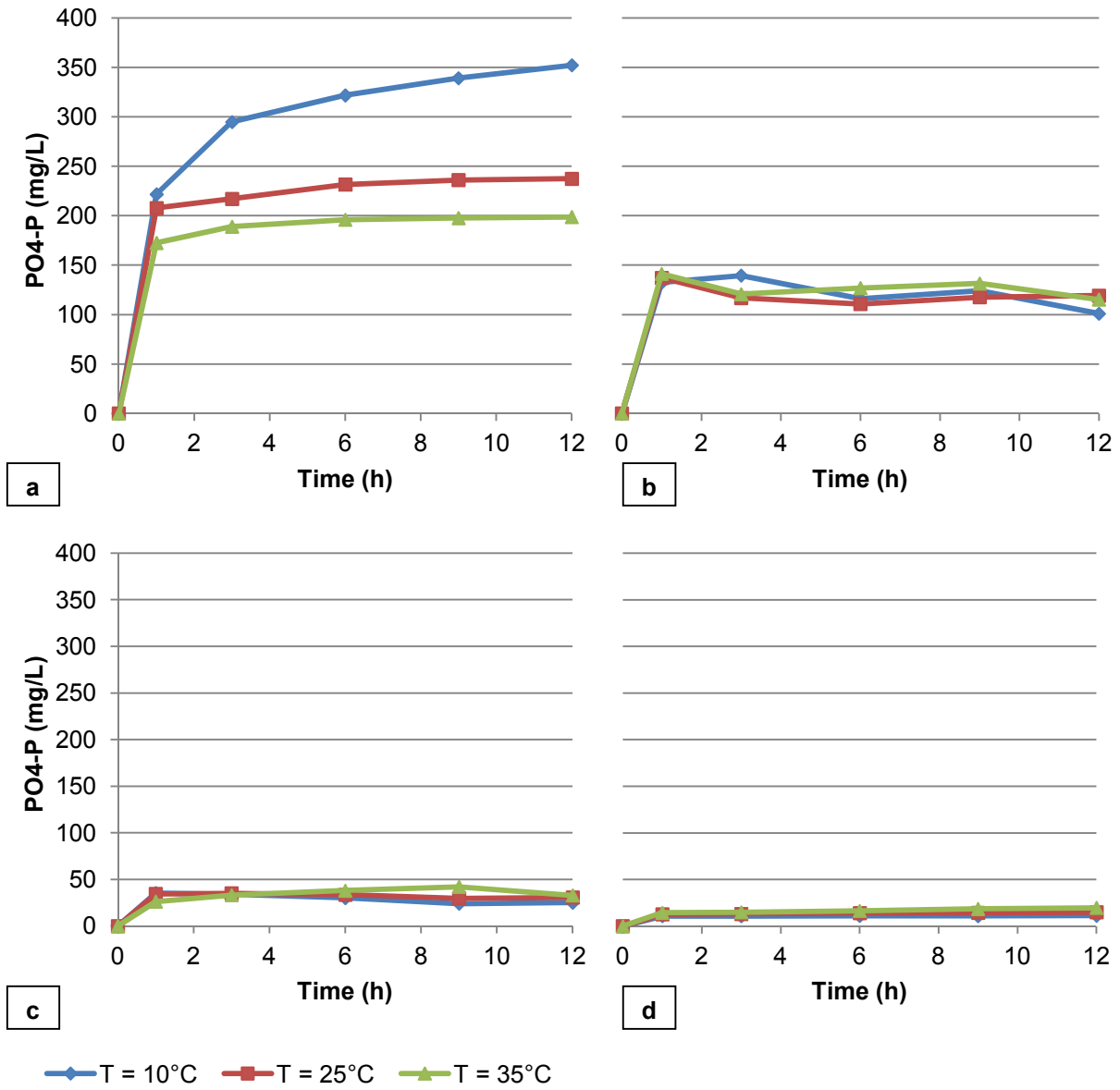


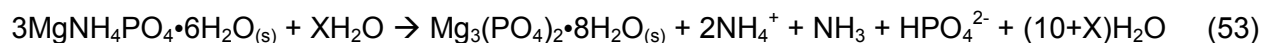
Figure 10 – Residual  $PO_4\text{-P}$  for various temperatures for (a) no pH control, (b) pH 7, (c) pH 8, and (d) pH 9

### 6.2.5 XRD analysis of solid phase mixtures

The parallel formation of compounds other than struvite and newberyite might reduce the amount of magnesium and orthophosphate available for ammonia removal. To search for potential contamination by these compounds, select samples of the solid mixture produced during ammonia-NH<sub>4</sub> batch tests were analyzed using XRD.

Bobbierite is known to form at high temperature and/or high pH (Taylor et al., 1963b; Königsberger and Königsberger, 2006; Lobanov et al., 2013). Therefore, 12 hour solid samples from pH 8 and 9 tests at 35°C were analyzed. Several other samples were examined, including one from each pH condition. No compounds other than newberyite or struvite were detected. Further, newberyite was detected in every sample even at a pH of 9. Nonetheless, struvite peaks were more well-pronounced for samples taken from systems at higher pH, while newberyite peaks get weaker as pH decreases. Hence, dominance of struvite peaks corresponds to increased struvite formation and, therefore, lower newberyite residuals (output graphs identifying solid phase XRD patterns for select samples can be found in Appendix C).

The transformation of newberyite and struvite into other solid phases is undesirable because they may contain no ammonium or have a Mg:P molar ratio more than 1:1. This is a concern with respect to the proposed ammonia recovery process. For instance, Eqn. 53 demonstrates the conversion of struvite to bobbierite.



In this case, ammonia removal is reduced because some of the magnesium and orthophosphate is used to form bobbierite rather than struvite. This also results in a higher orthophosphate residual because bobbierite formation requires three moles of magnesium for every two moles of orthophosphate. In the event that it is stable during the ammonia removal stage, bobbierite could potentially accumulate in the material that is harvested for thermal decomposition; if fresh struvite is not continuously added, the material's ammonia removal capacity will decrease after each subsequent cycle. Fortunately, the solid phase mixture produced in these systems was simply a mixture of struvite and residual newberyite.

### **6.2.6 Chemical composition of solid phase mixtures**

Although the XRD method employed could identify the crystalline compounds in solid phase samples, it is not capable of determining their composition with respect to newberyite and struvite content. The following section quantifies the extent of phase transformation from newberyite to struvite using results from elemental analyses of solid phase mixtures. Since newberyite contains no ammonium, N:P molar ratio essentially represents the molar fraction of struvite with respect to the total mixture of struvite and newberyite.

Figures 11 and 12 compare the N:P molar ratio for select solid samples at 1, 3 and 12 hour reaction times. The lowest struvite yield was found in the test with no pH control at 10° C. The sample was approximately 9% and 22% struvite after 1 and 3 hours respectively. Although the solid compositions are comparable among samples from the same pH, it appears that temperature plays a noticeable role in the first hour of struvite formation. For both pH 7 and 8, the fraction of struvite was slightly less in samples from 10° C tests, compared to that of 25° C. This may suggest that the effect of increased reaction rate may dominate over the effect of struvite's higher solubility early during the reaction. Further, struvite yields at pH 7 (34% and 42%) are considerably lower than that of pH 8 (78% and 92%) in 1 hour samples. The extent of conversion at pH 8 and 9 is comparable. However, equilibrium is approached after only 1 hour at pH 8 and 25° C. Therefore, it appears that these conditions may be near the optimum for rapid newberyite to struvite conversion. By 3 and 12 hours, pH 7, 8 and 9 samples are within 0.1 units of each other, with the exception of pH 7 at 35° C. This lower struvite yield is believed to be due to struvite's higher solubility at pH 7 at 35° C and corresponds with a lower ammonia removal efficiency.

The molar concentration of magnesium was often slightly lower than that of the orthophosphate in each of the samples, as reported in Appendix B. Considering no impurities were detected by XRD, this was deemed to be due to higher instrumental error with atomic adsorption, compared to flow injection analysis. For each of the selected samples for analysis, only one of the duplicate batch tests was examined. Therefore, error bars were not included for these figures. However, it is posited that, by providing a pH of 8 and moderate temperature, high newberyite-to-struvite conversion efficiency might be achieved, while limiting residuals.

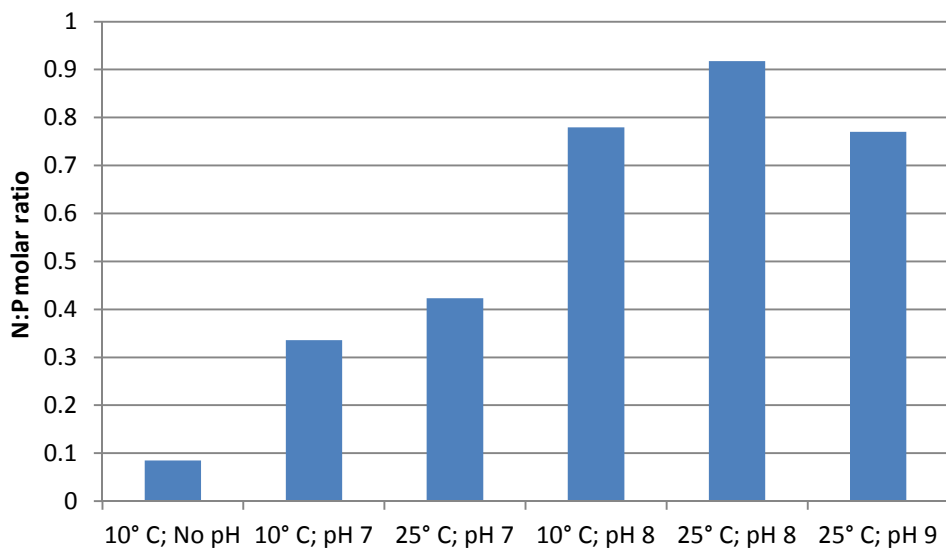


Figure 11 – N:P molar ratio of solid phase mixtures sampled at 1 h (No pH = no pH control)

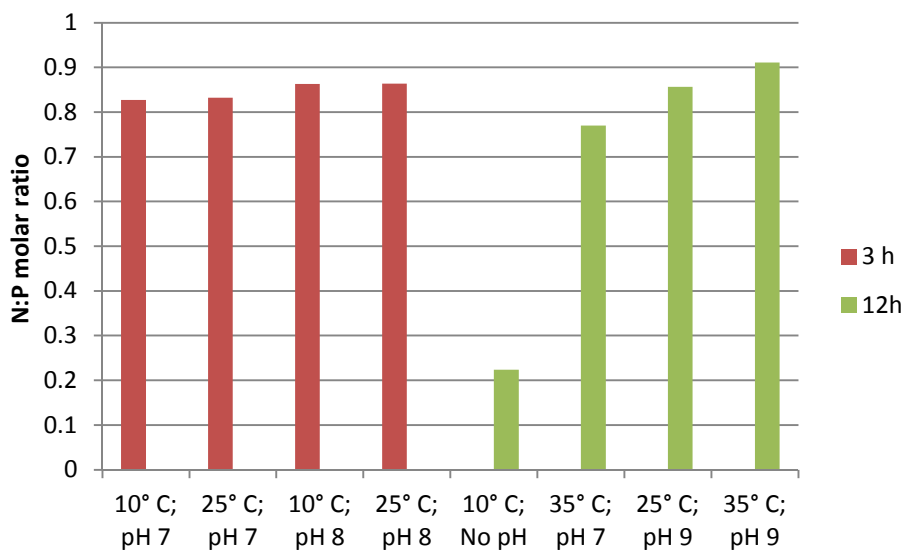


Figure 12 – N:P molar ratio of solid phase mixtures sampled at 3 and 12 h (No pH = no pH control)

### **6.2.7 Comparison of experimental results and model predictions**

Chemical equilibrium modelling can be a powerful tool for identifying the conditions required for struvite or ammonia recovery from wastewater and for predicting the characteristics of crystallizer effluent. The PHREEQC chemical equilibrium model allows the user to input the initial suspension composition and temperature and predicts the liquid and solid phase composition at equilibrium, as well as the caustic consumed when maintaining constant pH conditions. This study presented an opportunity to compare the liquid and solid compositions observed in 12 hour batch tests with model-predicted equilibria and, in the process, evaluate the model's accuracy.

As previously mentioned, newberyite and struvite were the only phases detected in solid samples. However, the model predicted that bobbierite would form in suspensions maintained at 35° C. Therefore, bobbierite was removed from the model. Following this exemption, the model predicted newberyite and/or struvite to exist in its place and generated residual ammonia and orthophosphate values that were closer to that found experimentally. Figure 13 and 14 compare average ammonia removals and orthophosphate residuals from 25° C batch tests to their corresponding equilibrium model outputs (raw modelling results for experiments and graphics not included in this section are provided in Appendix D).

For all of the tested conditions, the final ammonia residuals were remarkably similar to the equilibrium concentration estimated by the model. However, in several cases, the model-generated value was slightly lower. This is believed to be due to the fact that the suspensions may not have reached equilibrium by 12 hours. The orthophosphate concentrations were also similar to their model-generated counterparts with the exception of some of the tests with no pH control. The lack of correlation for these cases may be attributed to the discrepancy between the measured equilibrium pH and that predicted by the model.

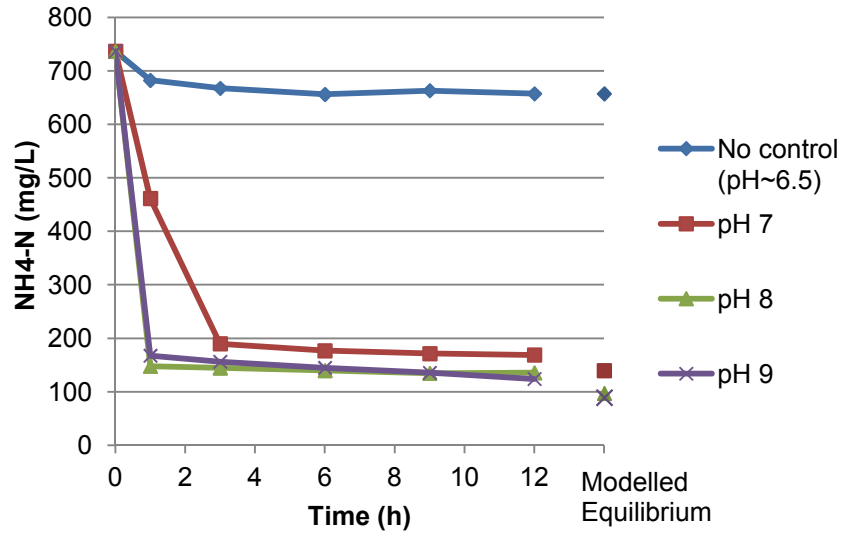


Figure 13 – Comparison of real and model-predicted NH<sub>4</sub>-N for 25° C

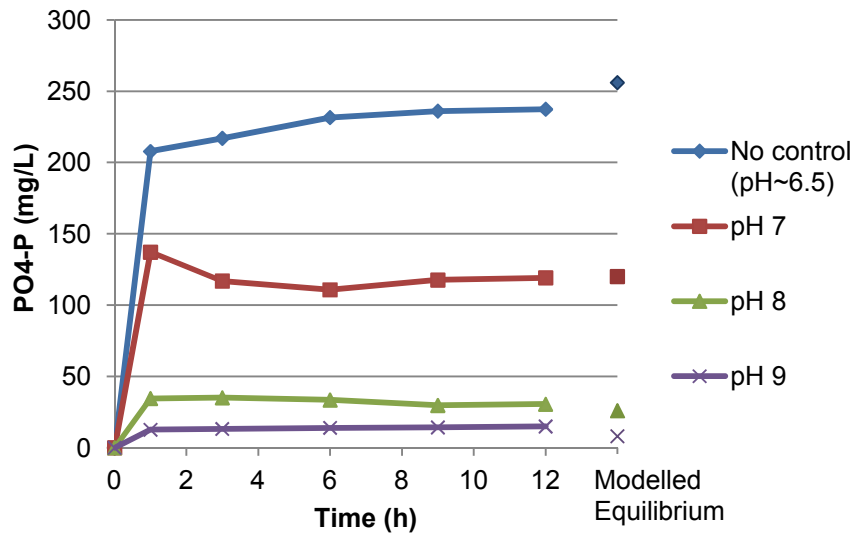
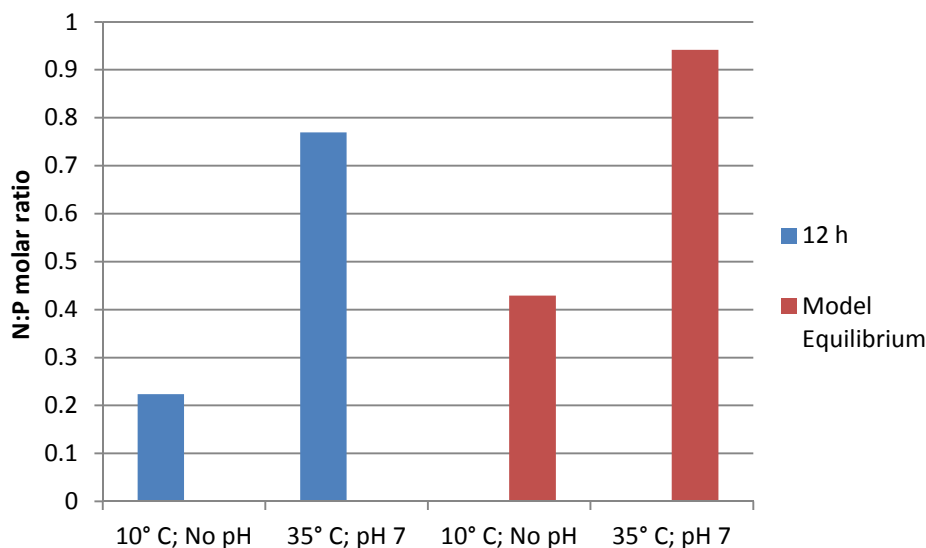


Figure 14 – Comparison of real and model-predicted PO<sub>4</sub>-P for 25° C

Figure 15 compares the N:P molar ratio of solid phase samples from two batch tests with that at equilibrium as predicted by the model. The model calculated struvite yields significantly higher than that which was observed in samples, even though ammonia removal rates suggest that

these systems are approaching equilibrium. Further, in several cases the model predicted complete transformation of newberyite into struvite, while corresponding samples showed that considerable newberyite remains even after 12 hours at conditions where struvite is highly insoluble.



**Figure 15 – Comparison of real and model-predicted N:P molar ratios of solid phase mixtures**

Discrepancy between model-predicted and experimental results is generally expected. Prediction of equilibrium states based on the laws of aqueous chemistry and thermodynamics is complicated by factors such as ionic activity, hydrodynamics, solid morphology, physical environment and atmospheric conditions. Further, the model does not take into consideration mechanisms such as crystal growth and agglomeration. Perhaps, the extent of transformation of newberyite into struvite is lower than that expected theoretically due to the entrapment of small newberyite fragments inside struvite crystals and agglomerates. This is referred to as crystal seeding. Although the model may not be able to predict the actual solid phase composition, it has proved itself valuable for identifying conditions where full conversion of newberyite to struvite cannot be achieved.

### **6.2.8 Initial rates of newberyite dissolution and struvite formation**

The previous sections examined the rates of newberyite dissolution and struvite formation in the scale of hours. Successful struvite crystallization pilot trials are characterized by an HRT of 3 to 10 mins (Huang, 2003; Fattah, 2004) which is a far shorter reaction time than the 1 to 3 hours required for synthetic newberyite to convert to struvite, in the presence of ammonium. Under the assumption that pelletized struvite could be produced from a mixture of solid and aqueous reagents, it would be valuable to know the time range in which struvite begins to form, given a Mg:N:P molar ratio of approximately 1:1.1:1.

From previous tests, the slowest reaction kinetics are expected at a temperature of 10° C, with no pH control. Figure 16 plots the variation of pH with time for synthetic newberyite in an ammonia solution with an initial concentration of 749 mg/L NH<sub>4</sub>-N. pH will vary as a result of the dissolution of newberyite and struvite formation. pH increases as newberyite dissolves due to the release of hydrogen phosphate ions (HPO<sub>4</sub><sup>2-</sup>) which consumes hydrogen to form dihydrogen phosphate (H<sub>2</sub>PO<sub>4</sub><sup>-</sup>). Struvite formation results in a decrease in pH due to the consumption of orthophosphate ions, which results in the release of hydrogen from hydrogen phosphate. Evidently, newberyite dissolution and struvite formation occur simultaneously under these conditions. pH increases to a maximum at 20 minutes, indicating that newberyite dissolution dominates for this period of time. A solid phase sample was collected at this time and XRD analysis showed that there are already well pronounced struvite peaks, which confirm the occurrence of a simultaneous newberyite dissolution-struvite formation mechanism. Following this point, pH decreased, suggesting that the rate of struvite formation is higher than that of newberyite dissolution.

A sample of the liquid phase was analyzed for 20 minutes time having a magnesium, NH<sub>4</sub>-N and PO<sub>4</sub>-P concentration of 81, 727 and 103 mg/L respectively. According to the ammonia concentration, minimal struvite formation has taken place suggesting that a maximum magnesium and orthophosphate concentration would be found at a time slightly under 20 minutes in this case. Therefore, struvite begins to form rapidly at some time between 0 and 20 minutes for the examined conditions. However, it is expected that struvite formation would initiate at an earlier time when caustic is added for pH control due to enhanced supersaturation

with respect to struvite. Further, the maximum magnesium and orthophosphate concentrations would be lower for these cases

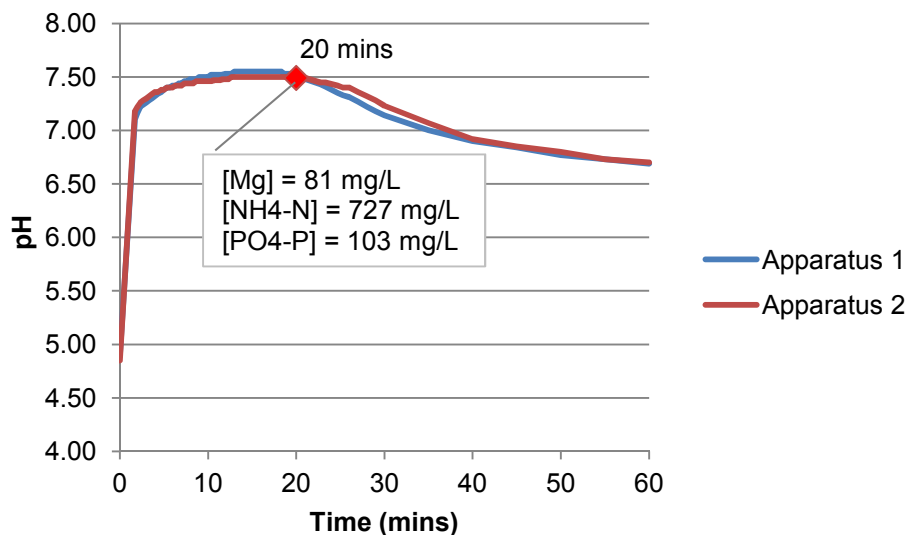


Figure 16 – pH vs time for no pH control at 10° C

### 6.3 Transformation of newberyite into struvite in ammonia solution:

#### Phase 2 – Suspension Mg:N:P molar ratio of 1:1.4:1

Adding newberyite in excess of ammonia is expected to increase  $S_S$  overall but may result in higher solubilization of magnesium and orthophosphate, which is undesirable from a wastewater treatment perspective. Alternatively, newberyite could be added in lower doses to provide a N:P molar ratio higher than 1. This excess ammonia would also result in a general increase in  $S_S$ . This stage of the study intends to answer the following questions:

- Will ammonia removal relative to available magnesium and orthophosphate be enhanced by increasing the N:P molar ratio above unity?
- Will this limit magnesium and orthophosphate residuals?

Table 11 outlines the average suspension characteristics immediately after newberyite is added to the ammonia solution. This can be considered time zero and Mg:N:P molar ratio represents the proportions of magnesium and orthophosphate contributed by newberyite and the ammonia initially in solution. Chemical analyses determined an initial Mg:P:N molar ratio of 1:1.4:1, indicating a 40% excess of ammonia relative to available magnesium and orthophosphate.

**Table 11 – Suspension characteristics at t = 0 h for Mg:N:P molar ratio 1:1.4:1 newberyite dose batch tests**

Reagents added as solid newberyite			Initial solution characteristics			Mg:N:P Molar Ratio
Newberyite added (g/L)	Mg (mM)	PO <sub>4</sub> -P (mM)	Mg (mM)	NH <sub>4</sub> -N (mM)	PO <sub>4</sub> -P (mM)	
7.0	37.3	37.3	0	52.6	0	1:1.4:1

### **6.3.1 Newberyite dose effect on rate and efficiency of ammonia removal**

Ammonia removal efficiency is reduced if you decrease newberyite dose, simply because there is less magnesium and orthophosphate available to form struvite. For instance, for each mole of magnesium and orthophosphate in the suspension there is approximately 1.4 moles of ammonium and, therefore, the maximum ammonia removal that can be achieved under these conditions is 71%. However, it is possible that ammonia removal efficiency relative to available magnesium and orthophosphate could be higher at reduced newberyite doses.

Figure 17 offers a complete account of average ammonia removals for the 12 batch tests at 1:1.4:1 Mg:N:P. The 12 hour removals ranged from 12% to 14% for no pH control and 60% to 68% for pH 7, 8 and 9. The 20% reduction in newberyite does not significantly affect the kinetics of ammonia removal. In all cases, ammonia concentration approaches equilibrium in 1 to 3 hours. Figure 18 compares the ammonia residuals for 1:1.1:1 and 1:1.4:1 Mg:N:P molar ratios. Evidently, ammonia residual does not vary much with newberyite dose when pH is not controlled. The ammonia removals for pH 7 to 9 at the 1:1.4:1 dose appear to be reduced by a common amount, compared to the 1:1.1:1 dose. On average, this reduction of newberyite dose results in a decrease in ammonia removal efficiency of about 15%. However, if removal is calculated relative to the maximum amount of ammonium that can be used to form struvite

based on the magnesium and orthophosphate available, 12 hour ammonia residuals for the 1:1.4:1 dose are comparable to that of 1:1.1:1. For instance, ammonia removals are 7% to 16% higher than the 1:1.1:1 dose when the percent removal for 1:1.4:1 is multiplied by the initial molar ratio of ammonia in solution to orthophosphate available (ie. 52.6 mM  $\text{NH}_4\text{-N}$ /37.3 mM  $\text{PO}_4\text{-P}$ ). This suggests that relative ammonia removal is slightly enhanced by reducing newberyite dose by about to 20%.

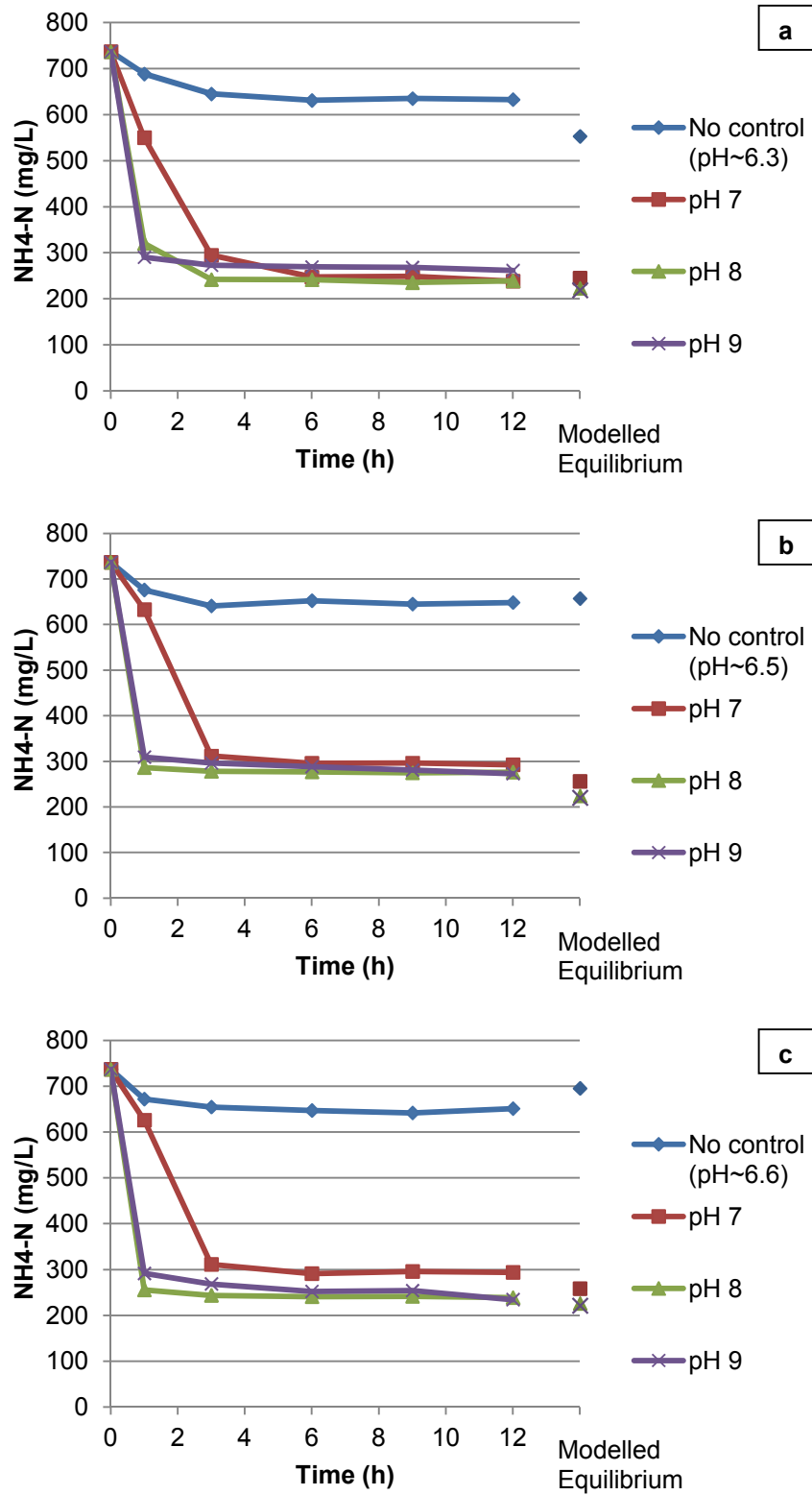


Figure 17 –  $\text{NH}_4\text{-N}$  removed for various pH conditions at (a) 10°, (b) 25°, and (c) 35° C

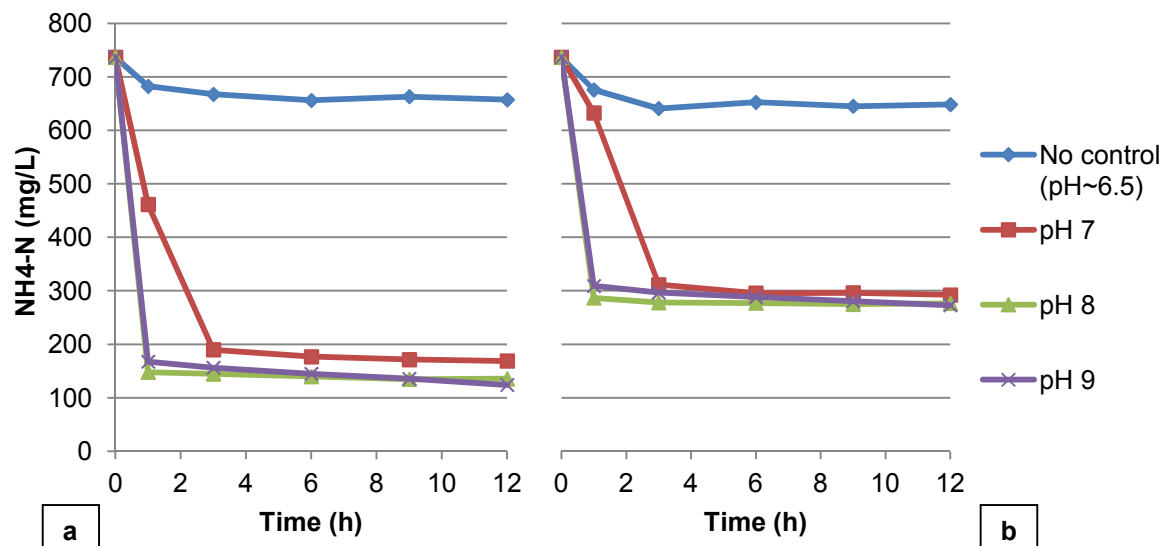


Figure 18 – NH<sub>4</sub>-N removed at 25° C for Mg:N:P molar ratio of (a) 1:1.1:1 and (b) 1:1.4:1

### 6.3.2 Newberyite dose effect on rate and extent of orthophosphate solubilization

By decreasing the newberyite dose, a general increase in  $S_s$  is expected due to the ammonia present in excess. Enhanced struvite formation corresponds to a reduction in magnesium and orthophosphate residual. This section intends to identify any reduction in orthophosphate solubilization that may result from decreasing newberyite dose by 20%.

Again, the molar concentration of orthophosphate is believed to be equivalent to that of magnesium. Figure 19 plots average orthophosphate residuals with time for the 12 batch tests at a Mg:N:P molar ratio of 1:1.4:1. The 12 hour PO<sub>4</sub>-P concentrations ranged from 196 to 307 mg/L for no pH control and 8 to 95 mg/L for pH 7, 8 and 9. Fig 20 compares the orthophosphate residuals for 1:1.1:1 and 1:1.4:1 Mg:N:P molar ratios at 25° C. A similar trend is observed between the 1:1.1:1 and 1:1.4:1 doses regarding the rate of orthophosphate solubilization. Again, orthophosphate appears to be approaching an equilibrium concentration after about 1 to 3 hours. Similarly to the ammonia residual, the 12 hour orthophosphate residual does not seem to be affected by a reduction in newberyite dose when pH is not controlled. For the cases with pH control, this residual does indeed appear to be slightly lower for the 1:1.4:1 dose compared

to that of the 1:1.1:1 dose for some cases. The discrepancies between mean 12 hour orthophosphate residuals, with respect to dose, are less than 25 mg/L PO<sub>4</sub>-P, with the exception of the tests at pH 7 and 35° C. In this case, the orthophosphate residual for the 1:1.4:1 dose was 78% lower than that of the 1:1.1:1 dose. This suggests that, theoretically, an ammonia removal efficiency of about 15% could be sacrificed for a reduction in orthophosphate residual if the treated wastewater maintains some heat of digestion.

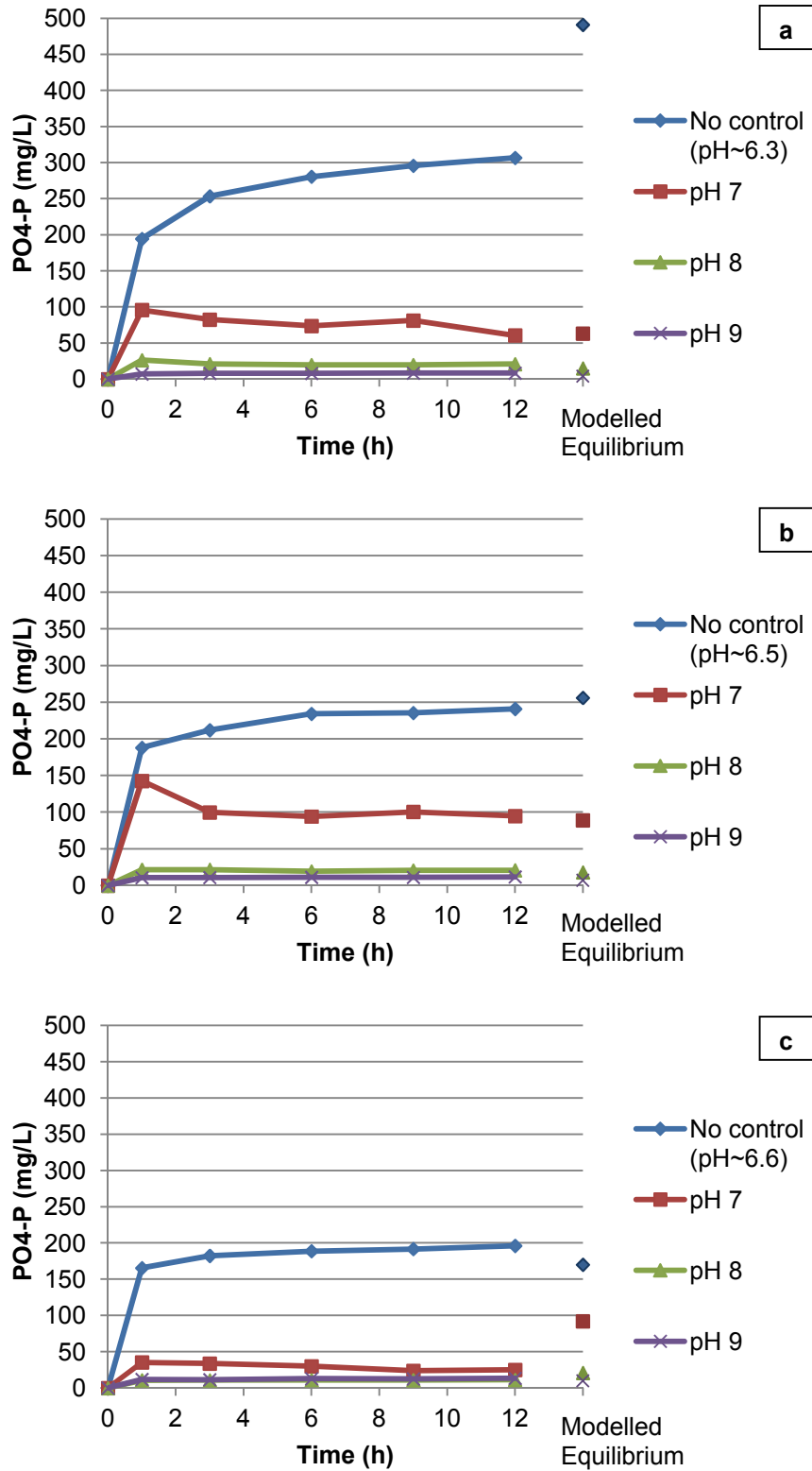


Figure 19 – Residual PO<sub>4</sub>-P for various pH conditions at (a) 10°, (b) 25°, and (c) 35° C

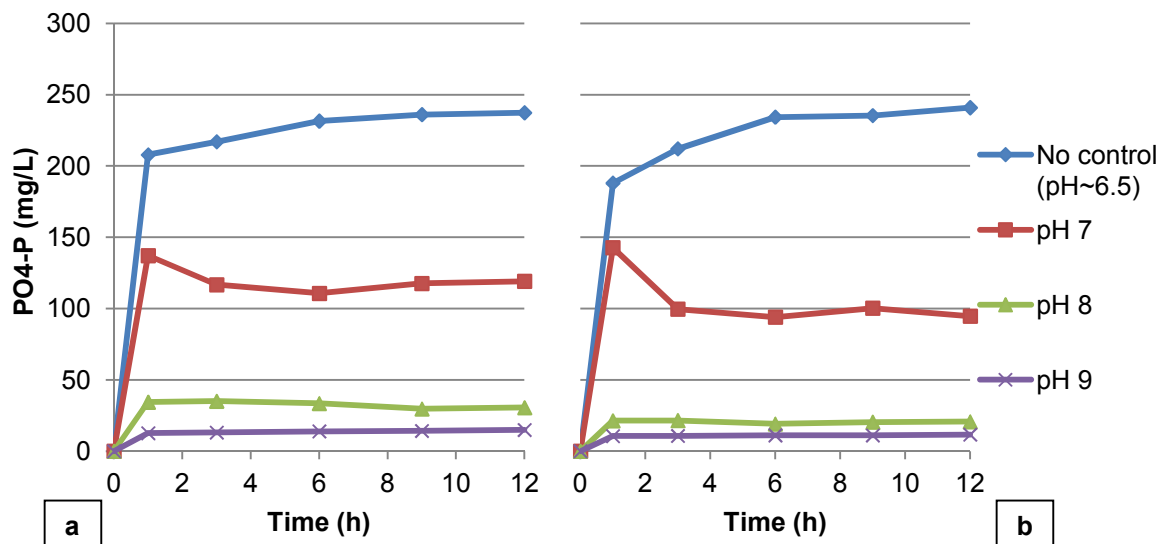
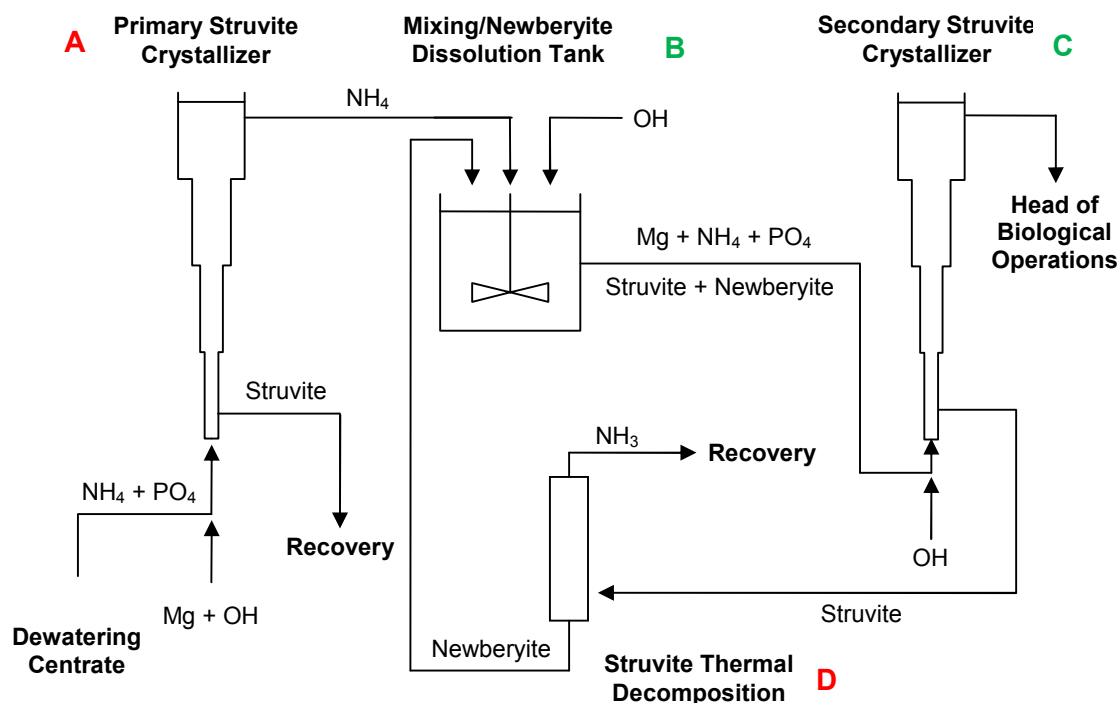


Figure 20 – PO<sub>4</sub>-P residual at 25° C for Mg:N:P molar ratio of (a) 1:1.1:1 and (b) 1:1.4:1

#### 6.4 Transformation of newberyite into struvite in synthetic crystallizer effluent

One objective of this study was to work towards the development of an ammonia recovery system by examining the reactions involved at conditions which might represent real wastewater streams. The effluent from a struvite crystallizer, treating a municipal post-digestion stream, was selected as one of the more promising feeds for ammonia removal using thermally decomposed struvite. Figure 21 is a schematic illustrating a potential process flow for combined recovery of struvite and ammonia from dewatering centrate. The outlined continuous or semi-continuous system is referred to as Reactor Configuration 1. This scenario involves four main operations consisting of struvite thermal decomposition (D) and primary (A) and secondary (C) struvite crystallization separated by a newberyite dissolution stage (B). Stage A could be considered a conventional struvite crystallizer, which harvests relatively large pellets such as that studied by Britton (2002), Huang (2003), and Fattah (2004) or that commissioned by Ostara Nutrient Recovery Technologies Inc. The still ammonia-rich crystallizer effluent is mixed with the newberyite yielded from thermal decomposition of struvite in Stage B. Caustic may be added in Stage B to allow for partial conversion of newberyite into struvite, which would, in turn, reduce the HRT required for secondary struvite crystallization. The suspension is mixed with caustic in

the injector of the secondary crystallizer, Stage C. The secondary crystallizer could potentially be a modified version of the conventional that would provide the HRT required for efficient reduction of newberyite and elemental residuals. Large pellets may not be necessary for the thermal decomposition stage; therefore, secondary crystallization might be characterized by shorter than conventional CRTs.



**Figure 21 – Reactor Configuration 1: Ammonia recovery from primary crystallizer effluent**

This section examines newberyite-to-struvite conversion as a method of removing ammonia from a solution representing the primary struvite crystallizer effluent that could be generated at the Annacis Island WWTP. Hence, the following batch tests simulated the reactions occurring in Stage B and C combined using synthetic newberyite and synthetic crystallizer effluent. A comparison of Annacis Island centrate and the synthetic crystallizer effluent is provided in Section 5.2. Further, Table 12 outlines the average suspension characteristics for time zero of these experiments. This solution is characterized to have relatively high ammonia, alkalinity and initial pH. From the previous tests, a pH range of 7 to 8 and a temperature range of 10° to 25° C were selected as near optimal experimental conditions. This selection is based on the assumption that a reduction in caustic use and, therefore, a decrease in chemical costs are

preferred over the small reduction in effluent magnesium and orthophosphate residuals that comes with operation at a pH above 8. Also, a suspension Mg:N:P molar ratio of 1:1:1 was chosen over lower newberyite doses to target even higher ammonia removal efficiencies at the expense of slightly higher orthophosphate residuals. The reaction time was limited to 4 hours, as previous tests demonstrated that equilibrium is nearly reached in 3 hours. This section works to answer the following questions:

- How is ammonia removal and orthophosphate residual affected by higher initial aqueous ammonia?
- How does a higher struvite harvest and higher initial pH and alkalinity impact caustic consumption?

**Table 12 – Suspension characteristics at t = 0 h for Mg:N:P molar ratio 1:1:1 newberyite dose in synthetic crystallizer effluent batch tests**

Reagents added as solid newberyite			Initial solution characteristics				Mg:N:P Molar Ratio
Newberyite added (g/L)	Mg (mM)	PO <sub>4</sub> -P (mM)	Mg (mM)	NH <sub>4</sub> -N (mM)	PO <sub>4</sub> -P (mM)	Alkalinity (mg/L as CaCO <sub>3</sub> )	
11.3	65.0	65.0	0.6	65.7	0.6	1470	1:1:1

#### **6.4.1 Ammonia removal**

As expected, average ammonia removal followed a familiar trend for synthetic newberyite in synthetic crystallizer effluent, as illustrated by Figure 22. Residual ammonia appears to be leveling out after a 3 hour reaction time. After 4 hours, mean ammonia removals ranged from 73% to 87%. Nevertheless, no statistical difference was found between the examined scenarios. These results also compare well to that observed for the ammonia solution treated at a Mg:N:P molar ratio of 1:1.1:1 (see Section 6.2.1). The changes to media composition, with respect to previous experiments, consist of the increase in ammonia from 740 to 920 mg/L NH<sub>4</sub>-N and the introduction of alkalinity. These additional constituents do not significantly affect performance with respect to ammonia removal.

With the presence of carbonates, the model predicted the formation of magnesite, alongside struvite, for this range of conditions. Magnesite and bobbierite become less soluble at high pH. To check for the existence of these phases, a 24 hour batch test was performed at room temperature and pH 9. Neither magnesite nor bobbierite were detected during XRD analysis of a solid sample from this test (the XRD output graph for this sample may be found in Appendix C). Therefore, entries for magnesite and bobbierite were excluded from the model phase input. Experimental and model results are compared in Figure 22. The model-generated ammonia residuals are considerably lower than that of the 4 hour batch tests. This discrepancy was expected as it may require days for these systems to reach chemical equilibrium. The reaction period was minimized to simulate a HRT that might be realistically achieved using continuous, side stream, unit processes. Yet, the model remains a powerful tool that can be used to estimate the completeness of newberyite-to-struvite conversion and, therefore, ammonia removal.

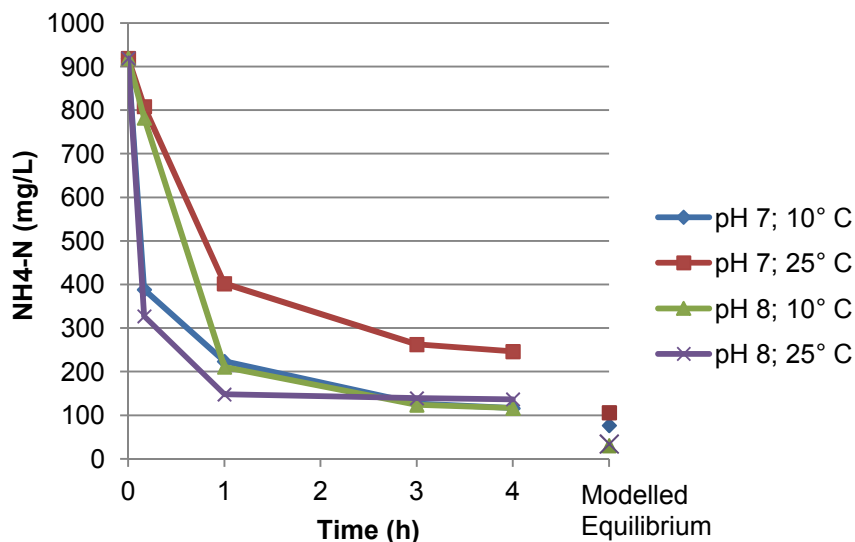


Figure 22 – Comparison of real and model-predicted  $\text{NH}_4\text{-N}$

#### 6.4.2 Orthophosphate residual

Figure 23 plots average orthophosphate concentration for the duration of transformation of newberyite into struvite in synthetic crystallizer effluent. The solubilization of orthophosphate

follows a similar pattern to that observed in previous experiments, with newberyite in ammonia solution. As discussed in Section 6.2.8, the orthophosphate peak observed at the 10 minute marks for some tests confirms the belief that a maximum magnesium and orthophosphate concentration exists minutes after the addition of newberyite due to its initial rapid dissolution. The 4 hour orthophosphate residuals are higher in pH 7 tests at 155 and 172 mg/L  $\text{PO}_4\text{-P}$  for 10° and 25° C respectively. Those of tests at pH 8 were significantly lower at around 50 mg/L  $\text{PO}_4\text{-P}$  due to increased supersaturation with respect to struvite. The 4 hour orthophosphate residuals are statistically comparable to that measured under similar conditions at the end of 12 hour tests with pure ammonia solution at a Mg:N:P molar ratio of 1:1.1:1. Since carbonates are not utilized to form magnesite, it appears that the presence of alkalinity in synthetic crystallizer effluent does not dramatically affect newberyite dissolution. However, the results for these conditions suggest that the use of newberyite as a source of magnesium and orthophosphate for secondary struvite crystallization may result in the release of at least 40% of the centrate orthophosphate previously removed by the primary struvite crystallizer. Nevertheless, this residual may perhaps be minimized with a small increase to caustic dose or by increasing the recycle ratio.

Figure 23 also compares measured orthophosphate residuals with outputs from the chemical equilibrium model. The 4 hour measurements compare well with model-generated residuals for all scenarios. Evidently, the model is more accurate in estimating orthophosphate residuals than it is in estimating ammonia removals for shorter reaction periods. This may be due to an equalizing effect by simultaneous newberyite dissolution and struvite formation. The solution is undersaturated with respect to newberyite, but supersaturated with respect to struvite for the entire reaction period. Yet, the orthophosphate residual appears to reach an equilibrium value before ammonia in several cases. Newberyite dissolution kinetics may limit the formation of struvite. For instance, aqueous orthophosphate is removed via struvite formation rapidly up until a point near its saturation. Thereafter, the orthophosphate released is utilized at a rate essentially determined by newberyite dissolution. Hence, the orthophosphate and magnesium concentrations can remain constant, while the ammonia concentration continues to decrease at low rates. The degree of phase saturation is discussed further in Section 6.4.4.

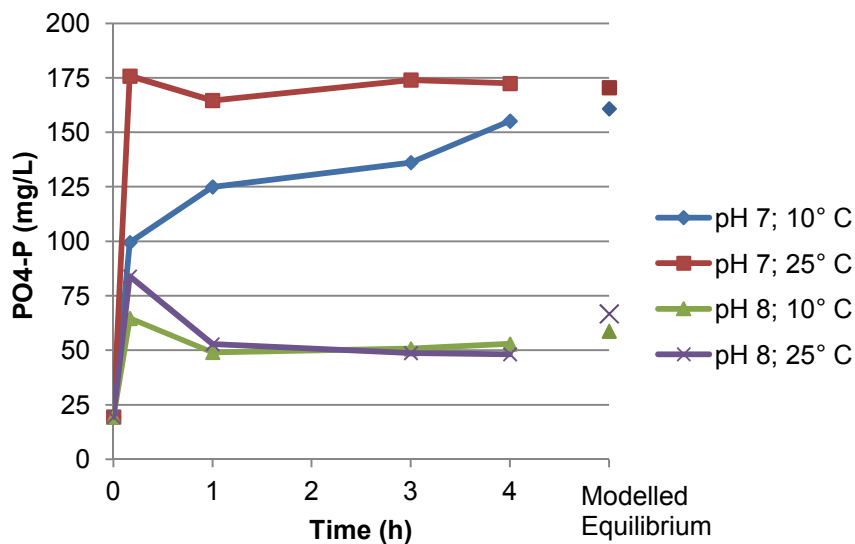


**Figure 23 – Comparison of real and model-predicted PO<sub>4</sub>-P**

### 6.4.3 Chemical composition of solid phase mixtures

The solid samples collected during 4 hour batch tests with synthetic newberyite and synthetic crystallizer effluent are assumed to contain only newberyite and struvite. Figure 24 compares the N:P molar ratios for solid phase samples at 1 and 4 hour reaction times. At the 1 hour sampling time, the lowest struvite yields were found with tests at pH 7 at 45% and 56%. The N:P molar ratios are higher for suspensions at pH 8 as a result of their higher overall  $S_s$ . Struvite makes up between 79% and 85% of the solid phase after an hour at pH 8. Evidently the system is near equilibrium after an hour at pH 8 and 25° C. Newberyite-to-struvite transformation progresses after this time for the other cases. The 4 hour struvite yields are 75%, 78%, and 91% for pH 7-25° C, pH 7-10° C, and pH 8-10° C respectively. Newberyite is more soluble while struvite is less soluble at lower temperatures and, therefore, struvite yields are slightly greater at 10° C compared to that of 25° C for the same pH. The solid phase is predicted to be greater than 98% struvite at equilibrium, according to model outputs. This suggests that newberyite theoretically continues to dissolve past 4 hours. However, it is possible that morphology plays a role in equilibrium of real solid-liquid systems. Struvite may potentially be forming as layers surrounding a newberyite seed, removing it from contact with the liquid phase and resulting in somewhat reduced conversion efficiencies.

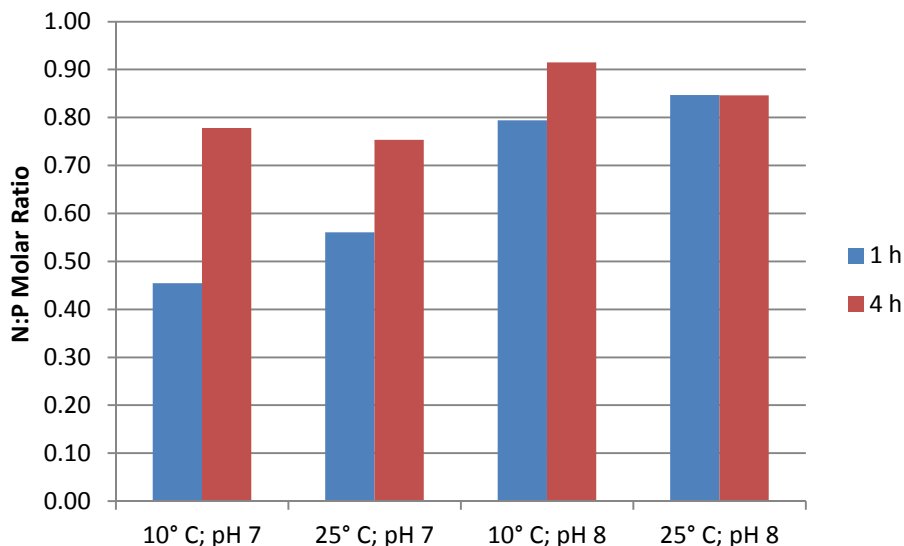


**Figure 24 – N:P molar ratio of solid phase sampled at 1 and 4 h**

#### **6.4.4 Newberyite and struvite supersaturation**

Ammonia, magnesium and orthophosphate concentrations vary with time as newberyite dissolves and struvite forms in synthetic crystallizer effluent. Therefore, supersaturation with respect to newberyite and struvite fluctuates accordingly. Since synthetic media was used in this study, the chemical equilibrium model was used to determine  $S_N$  and  $S_S$  based on liquid sample compositions, rather than constructing conditional supersaturation curves. Figures 25 and 26 present supersaturation ratios with time for pH 7 and 8 respectively. At time zero, solutions are undersaturated for both newberyite and struvite due to low initial magnesium and orthophosphate concentrations. Once newberyite is added, it begins to dissolve rapidly and saturation for both species increases with the solubilization of magnesium and orthophosphate. Due to the high initial ammonia concentration,  $S_S$  is the highest shortly after newberyite dissolution initiates and ammonia is removed through struvite formation. After an hour, struvite crystallization rates are significantly reduced and  $S_S$  decreases gradually towards equilibrium, while  $S_N$  remains somewhat constant. After 4 hours, newberyite has a slightly lower saturation for 10° C than it is for 25° C due to newberyite's higher stability at elevated temperatures. The opposite is the case for struvite, which is more soluble at higher temperature. Therefore,  $S_S$  is slightly higher for 25° C than it is for 10° C, as a result of higher magnesium, ammonia, and

orthophosphate residuals. Following an hour,  $S_S$  is comparable for both the tests at pH 7 and 8. At pH 7,  $S_S$  ranges from 1.21 to 1.43 and 1.11 to 1.30 for 1 hour and 4 hour samples respectively. 1 hour at pH 8 corresponds to a  $S_S$  between 1.36 and 1.61, while 4 hour values are between 1.26 and 1.39. Several studies suggested that supersaturation ratio is one of the primary control parameters with respect to performance of the UBC struvite crystallizer, with in-reactor  $S_S$  ranging from 1.0 to 2.2 (Dastur, 2001; Adnan, 2002; Britton, 2002; Huang, 2003; Fattah, 2004). Assuming pelletized struvite can be formed from a feed suspension containing both liquid and solid phases, it may be possible to recover ammonia using the conventional crystallizer by including a newberyite dissolution stage and by tailoring crystallizer parameters, such as recycle ratio, to attain supersaturations that proved successful for struvite pelletization.

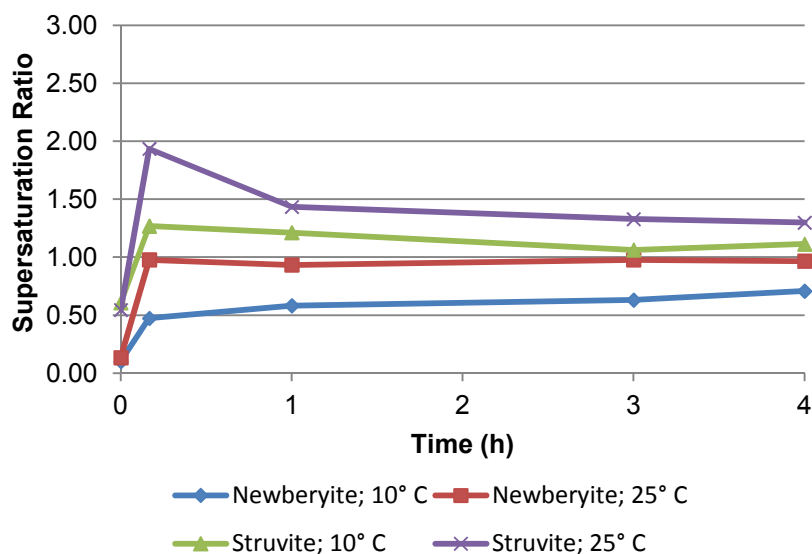
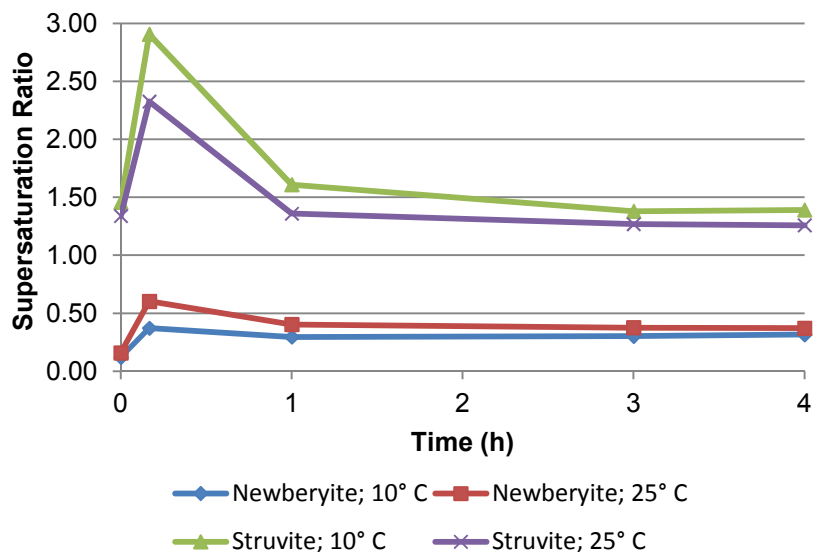
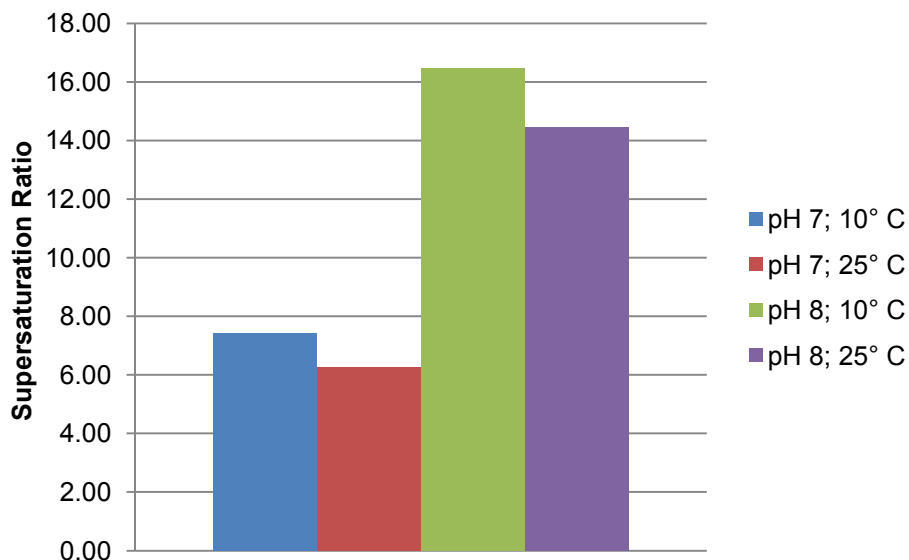


Figure 25 – Newberyite and struvite supersaturation ratio at pH 7



**Figure 26 – Newberyite and struvite supersaturation ratio at pH 8**

It should be noted that the addition of solid phase, rather than aqueous reagents, has an interesting effect on supersaturation with respect to struvite. If dissolved magnesium and orthophosphate were added at the same proportions to the ammonia-rich feed under similar conditions, the  $S_s$  immediately following addition would be considerably higher than that reported. Figure 27 shows the calculations for initial  $S_s$  following mixing of liquid reagents. These values for liquid reagent initial  $S_s$  are significantly higher than that measured after 10 minutes with newberyite in synthetic crystallizer effluent. Internal crystallizer recycle flow plays a role in maintaining the low struvite supersaturation ratios that promote struvite pelletization. Assuming crystallizer operation could be optimized to accommodate a feed suspension containing solid and aqueous reagents, recycle ratios are expected to be different, and perhaps lower than that with conventional liquid feed.



**Figure 27 – Theoretical struvite supersaturation ratio immediately after mixing of liquid reagents**

#### **6.4.5 Caustic consumption**

The amount of caustic consumed to achieve the previously discussed ammonia removals provides insight with regard to the operating costs involved with secondary struvite crystallization in primary crystallizer effluent. Figure 28 reports the cumulative mass of caustic as sodium hydroxide required to maintain a constant pH with time for newberyite in synthetic crystallizer effluent. The caustic required for these tests equates to about 1.3 to 2.1 kg of sodium hydroxide per cubic meter of synthetic feed treated. This range is nearly identical to that reported by Novotny (2011,) who observed similar ammonia removals from an ammonia solution using thermally decomposed struvite pellets. As expected, caustic consumption was higher to maintain a pH of 8 compared to that at pH 7. Further, temperature did not appear to have a dramatic effect on the caustic required to reach nearly steady state conditions. These results are generally slightly higher than under similar conditions explored with lower strength, pure-ammonia solutions. Model outputs were higher than that measured experimentally for caustic consumed in these systems. This is, in part due to the fact that these systems are not yet at true equilibrium at this time. Further, the discrepancy between these values is the result of differences between measured and model-generated initial pH of the synthetic crystallizer

effluent. Nevertheless, the model's ability to provide a rough estimate of caustic needs may prove helpful in planning future bench and pilot-scale studies on ammonia recovery.

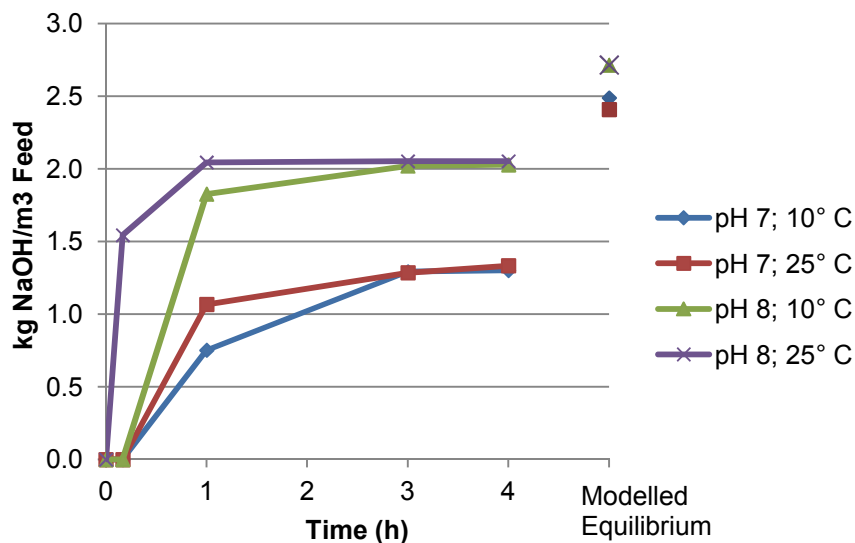


**Figure 28 – Comparison of real and model-predicted caustic consumption**

#### 6.4.6 Crystal morphology

Morphology is expected to play a role in the pelletization of struvite crystals. Nevertheless, how morphology factors in struvite agglomeration is not well documented. Images captured of solid phase samples using a microscope allow for the comparison of various experimental conditions, with respect to crystal morphology. The synthetic newberyite used in these experiments has a very distinctive crystal shape and habit compared to the struvite observed after 1 hour reactions with synthetic crystallizer effluent, as demonstrated by Figure 29. Newberyite crystals were characterized by tubular, rice-like rhombohedral structures. These were present as single crystals, X-shaped twinned crystals, star-shaped dendrites, and what appear to be rosette-like aggregates. In acknowledgement of literature reviewed during this study, this type of morphology has not yet been reported for newberyite. After 1 hour under the examined conditions, these structures have disappeared, leaving behind struvite crystals and small, relatively round shapes which could be the remains of dissolving rhombohedral newberyite crystals. If these small crystals are newberyite, it is possible that they are preserved as seeds for struvite crystal

growth; this could potentially result in reduced dissolution rates for a fraction of the newberyite added. This could, in part, explain the presence of residual newberyite after 12 hours under conditions where it should theoretically dissolve completely. Struvite crystals form with similar morphologies to newberyite; however, they were generally larger. Struvite crystals were characterized by orthorhombic platelets and star-shaped dendrites. In several cases, struvite crystals appear to be still growing after 1 hour, as suggested by protrusions of small crystal growths on the surfaces of well developed crystals; these probably grew at the beginning of tests, while newberyite was dissolving and supersaturation with respect to struvite was lower. The dendritic growth on larger crystals is likely the result of the following high supersaturation stage.

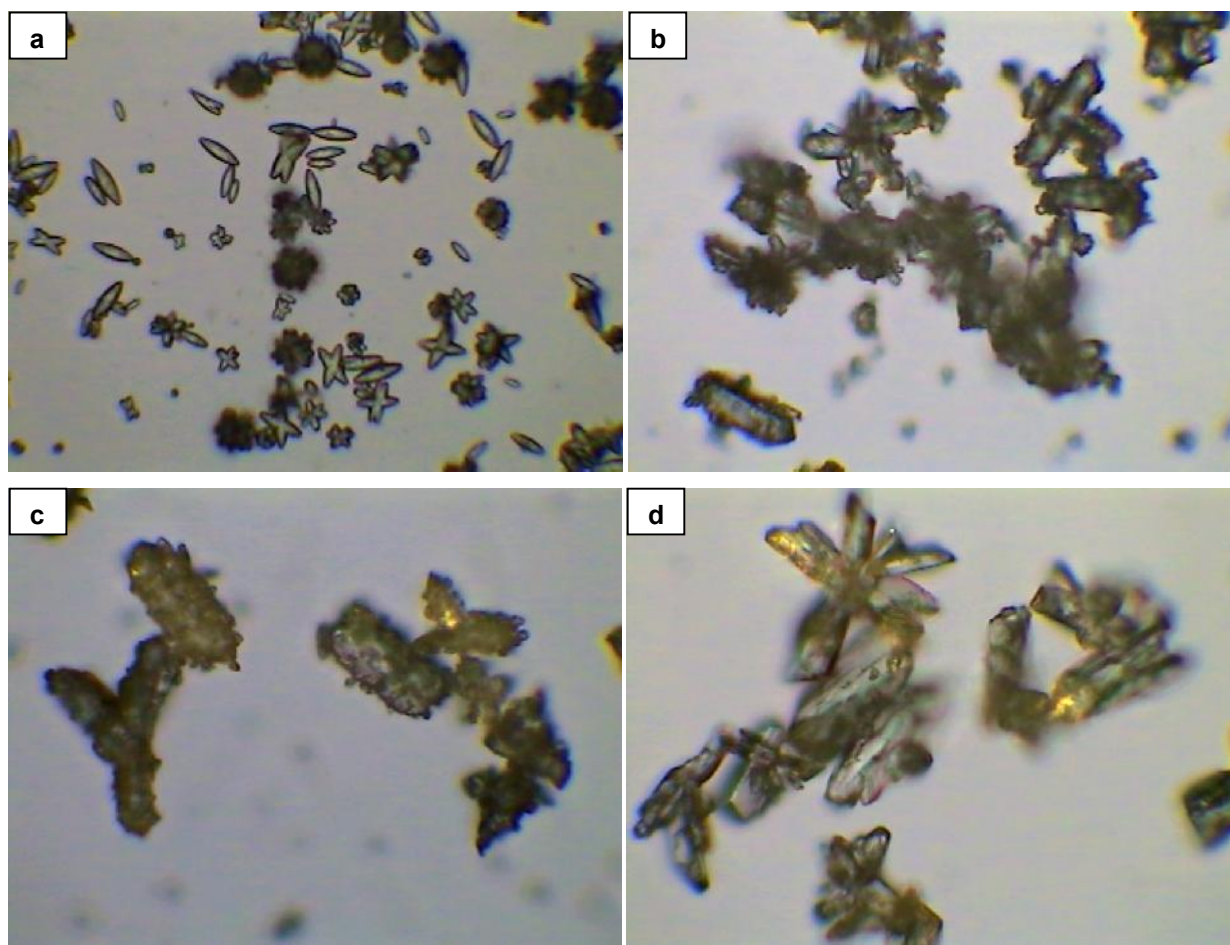


**Figure 29 – x40 magnified newberyite (a); 1 hour samples from pH 7-10° C (b), pH 7-25° C (c), and pH 8-25° C (d)**

Figure 30 compares the solid phase morphologies at a lower magnification for 4 hour samples from each test. Overall, orthorhombic platelets and dendrites were the dominant structure of struvite crystals. No striking difference was observed between crystals formed at pH 7 and 8 for each temperature. However, crystals at 25° C appear to be larger than that of 10° C. This difference in size may be explained by the fact that relatively larger crystals grow at lower supersaturation ratios. Further, supersaturation decreases with an increase in temperature due to enhanced struvite solubility.

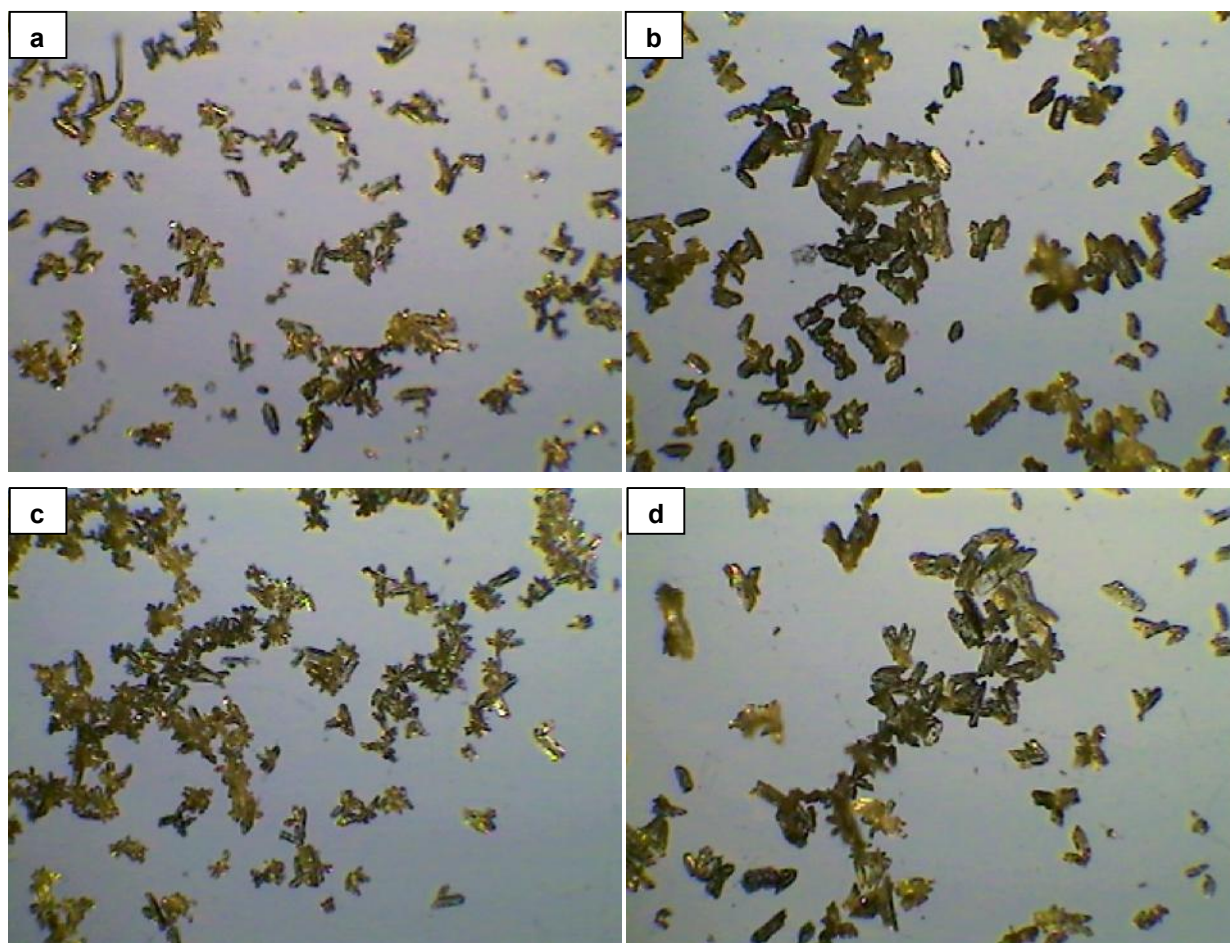


**Figure 30 – x10 magnified 4 hour samples from pH 7-10° C (a), pH 7-25° C (b), pH 8-10° C (c), and pH 8-25° C (d)**

The difference in struvite crystal size with temperature was also observed at higher magnifications, as illustrated by Figure 31. Struvite dendrites appear to be larger and to have

broader branches at 25° compared to 10° C. These struvite morphologies may be suitable for agglomeration into pellets. The core of struvite pellets have been shown to contain primarily agglomerated platelet and dendrite structures in previous struvite pelletization studies (Huang, 2003; Fattah, 2004)

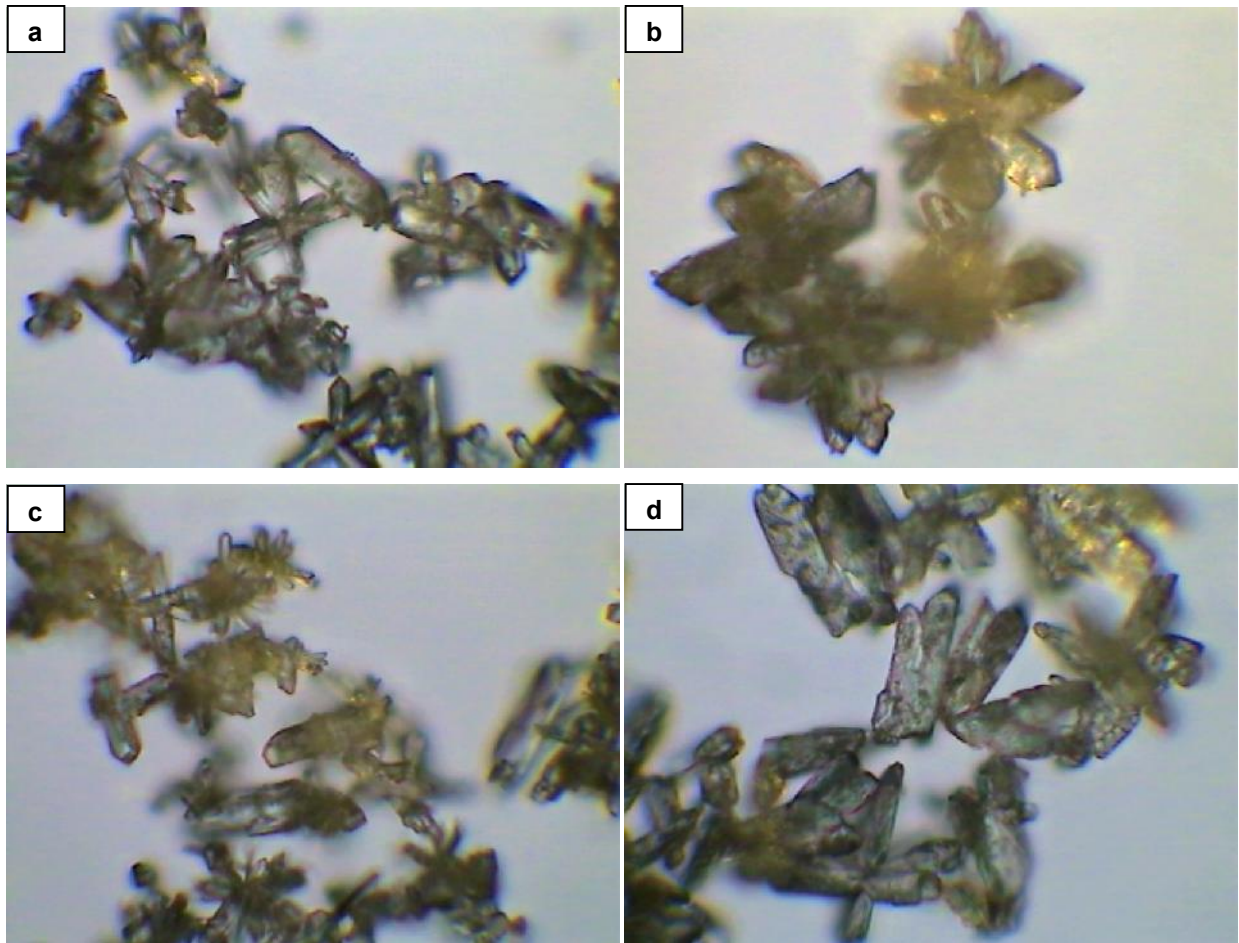


**Figure 31 – x40 magnified 4 hour samples from pH 7-10° C (a), pH 7-25° C (b), pH 8-10° C (c), and pH 8-25° C (d)**

### **6.5 Transformation of newberyite into struvite in synthetic centrate**

Ammonia and struvite could potentially be recovered using a reactor configuration that employs a single struvite crystallizer. Hence, raw dewatering centrate is also a suitable feed for ammonia removal using thermally decomposed struvite. Figure 32 provides an overview of Reactor

Configuration 2, a potential continuous or semi-continuous system for this purpose. This scenario consists of three main unit processes, including a conventional struvite crystallizer (Stage E), a newberyite dosing tank (Stage B), and a struvite thermal decomposition reactor (Stage D). Stage E could potentially be a commercially available struvite crystallizer repurposed to produce struvite pellets suitable for both subsequent thermal decomposition and use as a fertilizer. Assuming the centrate initially contains ammonia in excess of orthophosphate, a portion of struvite produced is recovered as a source of revenue, while the remaining portion is recycled for ammonia removal. Similarly to Reactor Configuration 1, this may require the adoption of nonconventional HRTs to reduce undesirable residuals. Essentially, Reactor Configuration 2 involves upgrading existing technology to include Stages B and D, which would allow for the recycling of a portion of the struvite produced; this would provide the magnesium and orthophosphate required to recover the excess ammonia contained in the centrate.

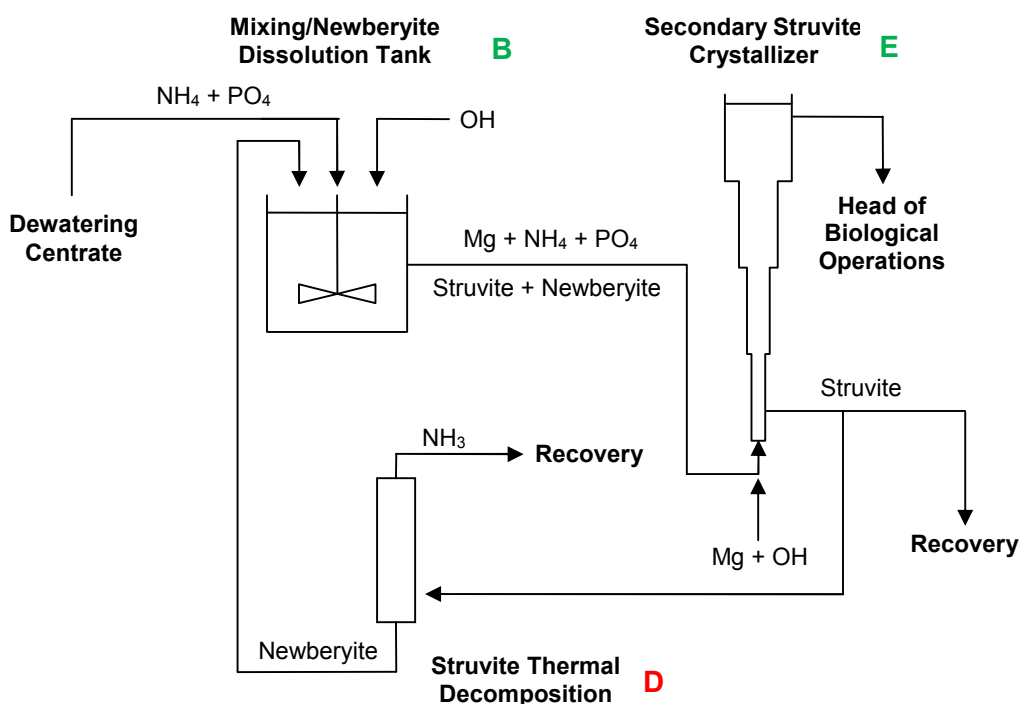


**Figure 32 – Reactor Configuration 2: Ammonia recovery from dewatering centrate**

This section investigated the potential removal of ammonia from a solution simulating dewatering centrate from Annacis Island WWTP. Hence, the following batch tests represent the combined reactions occurring in Stage B and E. A comparison of Annacis Island centrate and

the synthetic centrate is provided in Section 5.2. The synthetic centrate is distinguished from synthetic crystallizer effluent by containing significantly higher initial orthophosphate, as well as magnesium chloride, which would be supplied alongside newberyite to bring the suspension Mg:N:P molar ratio to 1:1:1. Table 13 outlines the average suspension characteristics for time zero of these experiments. The conditions examined were the same as that of the experiments with synthetic crystallizer effluent, in order to identify any advantages or drawbacks of Reactor Configuration 2 compared to 1. This stage of the study intends to answer the following questions:

- How is ammonia removal and orthophosphate residual affected by higher initial aqueous magnesium and orthophosphate?
- How does the presence of these aqueous reagents impact caustic consumption?

**Table 13 – Suspension characteristics at t = 0 h for Mg:N:P molar ratio 1:1.05:1 newberyite dose in synthetic centrate batch tests**

Reagents added as solid newberyite			Initial solution characteristics				Mg:N:P Molar Ratio
Newberyite added (g/L)	Mg (mM)	PO <sub>4</sub> -P (mM)	Mg (mM)	NH <sub>4</sub> -N (mM)	PO <sub>4</sub> -P (mM)	Alkalinity (mg/L as CaCO <sub>3</sub> )	
11.7	63.5	63.5	4.8	72.0	4.7	1475	1:1.05:1

### 6.5.1 Ammonia removal

Ammonia removal from synthetic centrate followed a similar trend to that of synthetic crystallizer effluent, as shown in Figure 33. Again, residual ammonia appears to be approaching an equilibrium value after 1 to 3 hours. By 4 hours, ammonia removals are within 71% to 83%. However, there was no significant difference between experimental results. Further, these ammonia removals are comparable to that observed with synthetic crystallizer effluent (see Section 6.4). It appears that the presence of high initial aqueous orthophosphate and magnesium (added in liquid form at the same time as newberyite) did not dramatically affect the ammonia removal efficiency, compared to cases where magnesium and orthophosphate are initially present as newberyite.

Similarly to the synthetic crystallizer effluent, the chemical equilibrium model indicated that magnesite would form in small amounts during each of the synthetic centrate batch tests. However, patterns for magnesite and bobbierite did not appear during XRD analysis of solid phase samples and, therefore, these phases were not included with model inputs (the XRD output graphs for these tests may be found in Appendix C). As illustrated in Figure 33, the model-generated ammonia residuals are considerably lower than that of the 4 hour batch tests. Again, the discrepancy between theoretical and experimental ammonia residuals is believed to be due to the non-equilibrium state of the suspensions after 4 hours and, potentially, entrapment of newberyite residuals by struvite.

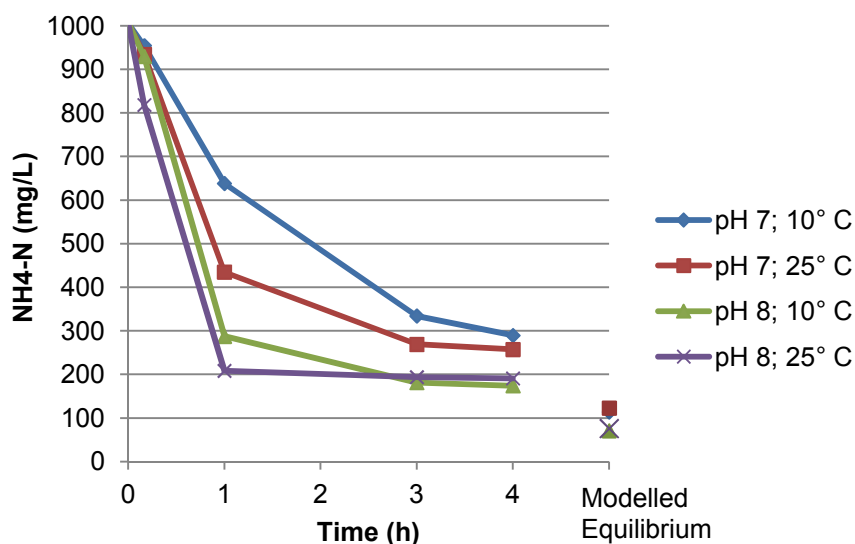


Figure 33 – Comparison of real and model-predicted  $\text{NH}_4\text{-N}$

### 6.5.2 Online ammonium residual monitoring

The apparatus used for batch tests limited the frequency of sample collection and, therefore, reduced the resolution of observed trends, especially for reactions occurring immediately after the addition of reagents. To verify that no distinct inflection points occur on plots between 10 minute and 1 hour reaction times, ammonium activity was measured in “real time” using an ammonium selective electrode. Solution conductivity was logged simultaneously and measured values were used to estimate ionic strength with time from a calibration curve. Another

calibration curve was constructed correlating ionic strength with model-generated ammonium activity coefficient. With measured ammonium activities and attributed coefficients, ammonia concentration was plotted with time. Figure 34 compares probe and sample measured values for two synthetic centrate batch tests. It should be noted that the probe used was sensitive to changes in positioning and hydrodynamics, resulting from routine sample collection. Hence, abrupt changes to offsets and a general lack of trend smoothness were occasionally observed with online data.

Background ionic strength varies with the release and uptake of elemental components. Therefore, offsets may also have been caused by discrepancies between estimated and real ionic strength. Nevertheless, the probe-measured data followed a similar trend to that observed in collected samples. This data confirmed that no rapid drops in ammonium were experienced between 10 minute and 1 hour sampling times and that the lines fitted to sample measurements represent the examined reactions remarkably well.

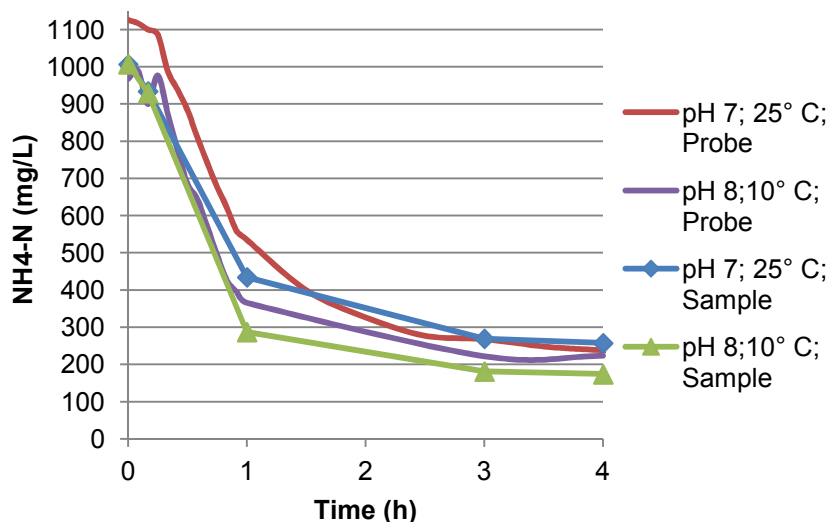
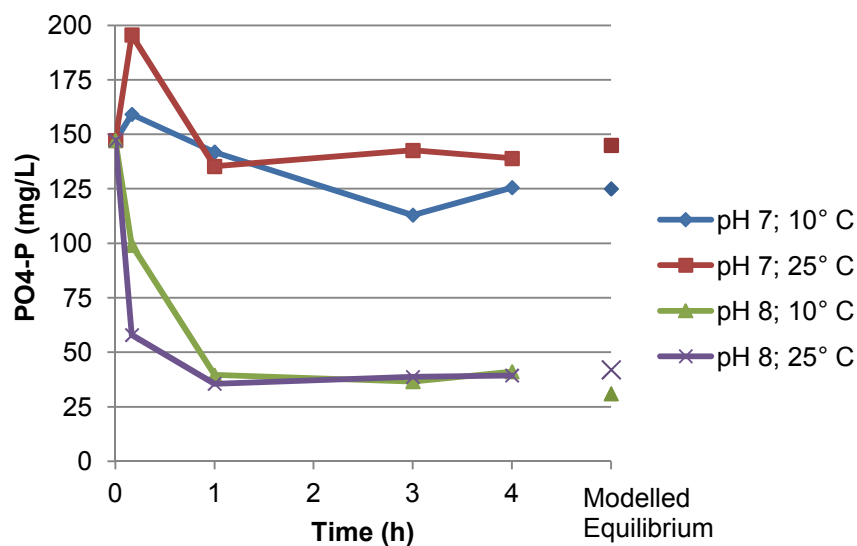


Figure 34 – Comparison of probe and sample measured NH<sub>4</sub>-N

### **6.5.3 Orthophosphate residual**

Magnesium and orthophosphate molar concentrations were assumed to be similar for the duration of batch tests containing newberyite and synthetic centrate, as suggested by the absence of magnesite or bobbierite patterns on XRD output graphs (see Appendix C). Figure 35 plots average orthophosphate residuals over time for newberyite in synthetic centrate. Residual orthophosphate follows a similar trend to that of synthetic crystallizer effluent. The highest final orthophosphate residuals were 126 and 139 mg/L PO<sub>4</sub>-P for tests at pH 7. At pH 8, 4 hour residuals were around 40 mg/L PO<sub>4</sub>-P. Further, no statistical difference was observed between these measurements and that of synthetic crystallizer effluent. This suggests that the initial presence of high aqueous magnesium and orthophosphate does not significantly affect equilibrium residuals compared to cases where these reagents originate exclusively from newberyite. Further, as a simulation of a single struvite crystallizer process using newberyite as a supplemental reagent, these results suggest that a simultaneous 73% orthophosphate and 83% ammonia removal could be possible.

Figure 35 also provides a comparison of measured orthophosphate residuals and model-generated values. These data sets are remarkably similar, despite the expected difference in considered reaction time. However, magnesium and orthophosphate residuals were predicted to be lower in synthetic centrate than crystallizer effluent. This is likely due to the synthetic centrate tests' slightly higher N:P molar ratio.



**Figure 35 – Comparison of real and model-predicted PO<sub>4</sub>-P**

#### **6.5.4 Chemical composition of solid phase mixtures**

According to XRD analyses (see Appendix C), solid samples from synthetic centrate are expected to contain only newberyite and struvite. Figure 36 compares the N:P molar ratios measured for the solid phase at 1 and 4 hour reaction times. After 1 hour, struvite yields ranged from 35% to 61% and 71% to 80% for pH 7 and pH 8 respectively. The 4 hour measurements were higher at around 80% for all cases. The model predicted the solid component of these suspensions to be 100% struvite at equilibrium, with the exception of pH 7-25° C (which is expected to contain residual newberyite at 4%). Again, this suggests incomplete reactions and potentially newberyite entrapment within struvite crystals.

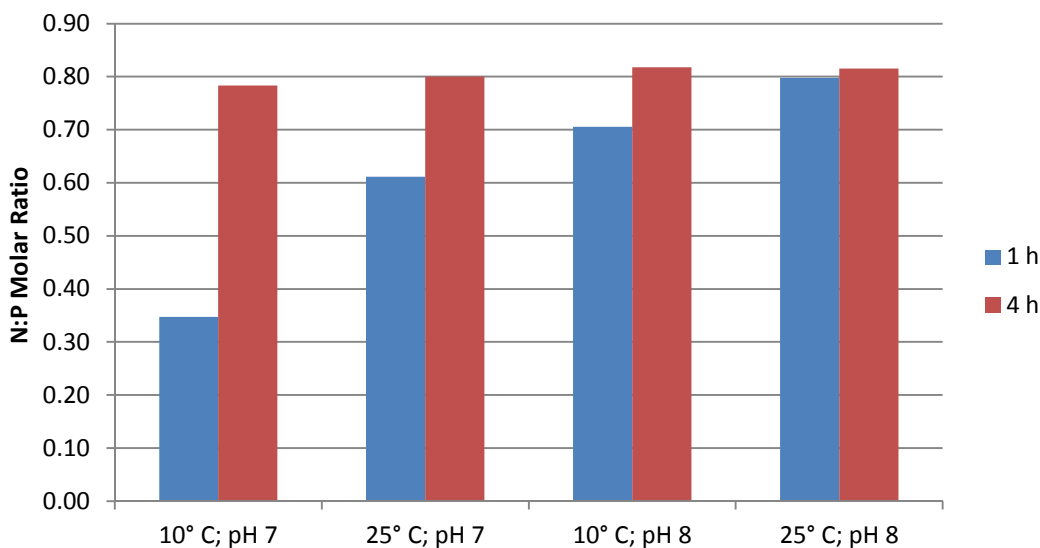


**Figure 36 – N:P molar ratio of solid phase sampled at 1 and 4 h**

### **6.5.5 Newberyite and struvite supersaturation**

With measured values for aqueous magnesium, ammonia and orthophosphate, the supersaturation with respect to newberyite and struvite in synthetic centrate was estimated using the chemical equilibrium model. Figures 37 and 38 illustrate  $S_N$  and  $S_S$  with time for pH 7 and pH 8 batch tests. Initially, newberyite and struvite are very undersaturated in the absence of magnesium. 10 minutes after dosing the synthetic centrate with newberyite and supplemental magnesium,  $S_S$  ranges from 2.15 to 4.40. These values are generally higher than that of similar tests with synthetic crystallizer effluent due to higher initial dissolved magnesium and orthophosphate. However, supersaturation ratios in synthetic crystallizer effluent and centrate are comparable after 1 hour.  $S_S$  appears to level out soon after this time, approaching more normal ratios between 1.19 and 1.47 after 4 hours. With the assumption that struvite crystals will agglomerate, these supersaturation ratios with respect to struvite are within a preferable range for struvite pelletization after an hours' time; thus, there is the potential for combined struvite and ammonia recovery from dewatering centrate using newberyite as an additional source of magnesium and orthophosphate.

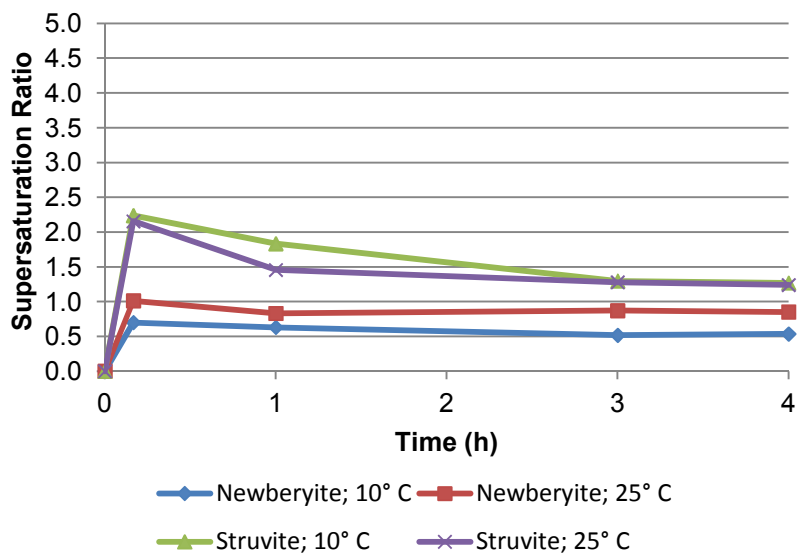


Figure 37 – Newberyite and struvite supersaturation ratio at pH 7

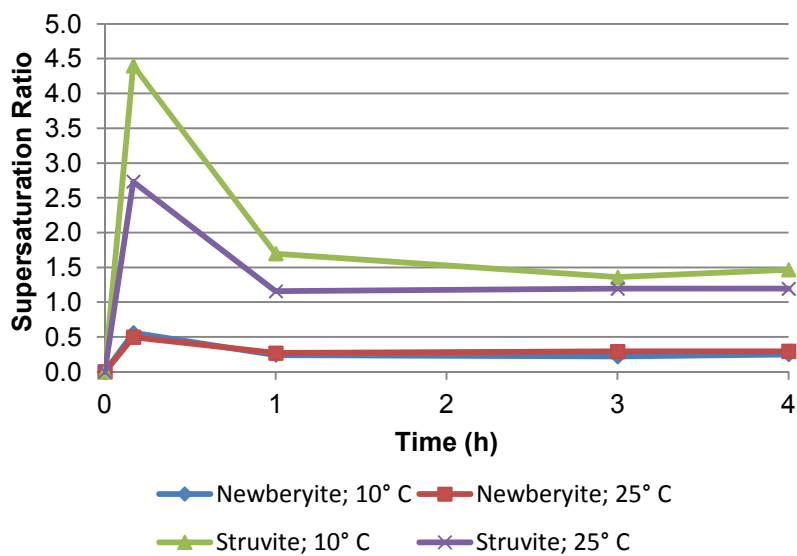


Figure 38 – Newberyite and struvite supersaturation ratio at pH 8

### 6.5.6 Caustic consumption

The mass of caustic provided to promote combined ammonia and phosphorous removals represents a major component of the Reactor Configuration 2 operating costs. Figure 39 plots the cumulative mass of sodium hydroxide consumed with time for the synthetic centrate batch tests. Around 1.6 kg was required to maintain a pH of 7, while a total mass of 2.1 kg was used to maintain a pH 8. Interestingly, the amount of caustic consumed for simultaneous orthophosphate and ammonia removal from synthetic centrate is about the same as that used to remove only the ammonia from synthetic crystallizer effluent. This is promising from a practical perspective, as it suggests that combined phosphorus and nitrogen recovery could potentially be achieved with a single crystallizer, at a caustic expense similar to that required to remove the ammonia alone.

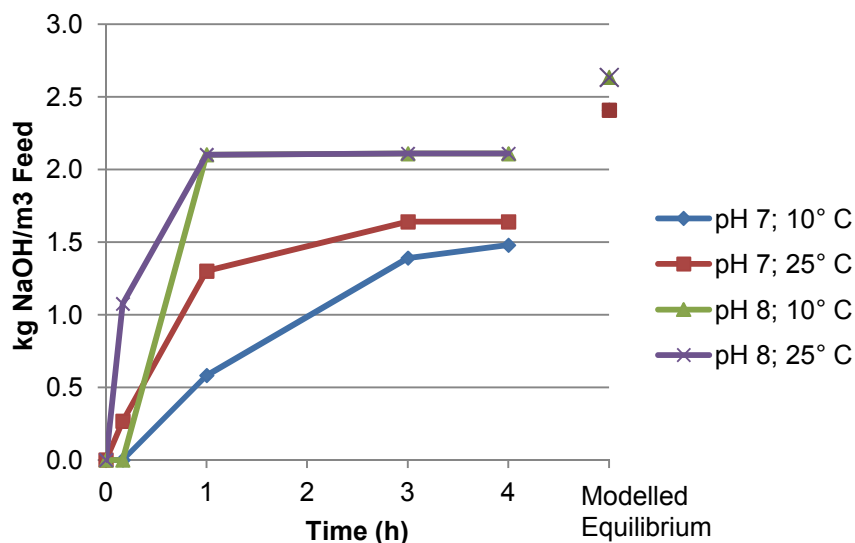
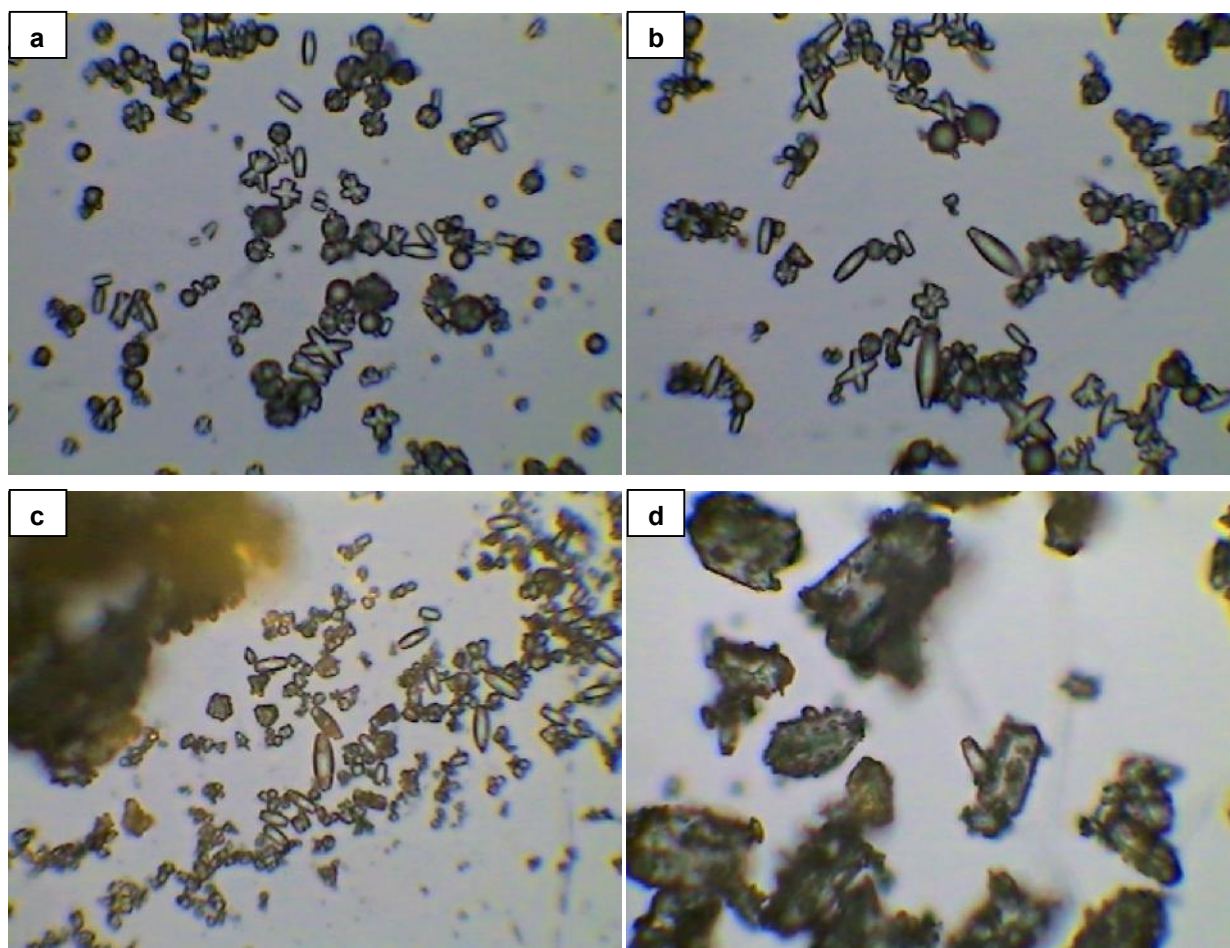


Figure 39 – Comparison of real and model-predicted caustic consumption

### 6.5.7 Crystal morphology

Examining solid phase samples using a microscope allowed for the identification of residual newberyite, as well as the study of variations in struvite crystal morphology across experimental

conditions. Figure 40 compares raw newberyite crystals with the solid phase after an hour in synthetic centrate at pH 7. The tubular or rice-shaped newberyite crystals were identified in a sample from the pH 7-10° C test. However, only struvite platelets and dendrites were observed at 25° C. The residual newberyite, at the lower temperature of 10° C, is likely caused by reduced kinetics of newberyite dissolution. Similarly to pH 7 tests with synthetic crystallizer effluent, small protrusions on struvite platelet surfaces were also observed after 1 hour at pH 7 in synthetic centrate; these are believed to be young struvite crystals that grow into dendrite branches or are separated from the surface through attrition.



**Figure 40 – x40 magnified synthetic newberyite batches (a and b); 1 hour samples from pH 7-10° C (c), and pH 7-25° C (d)**

Figures 41 and 42 show two different magnifications for images of solid phases after 4 hour reaction times. In all cases, only orthorhombic platelets and dendrites characteristic of struvite are apparent. These are similar to those grown in synthetic crystallizer effluent and resemble that observed in the core of struvite pellets produced by a UBC struvite crystallizer (Huang, 2003; Fattah, 2004). However, crystal size did not vary with temperature in the manner that it did in the crystallizer effluent. Rather, crystal length, relative to width, increases from pH 7 to 8. This is typical of struvite, as it is known to form long, needle-shaped crystals at higher supersaturation ratios (Abbona et al., 1985).

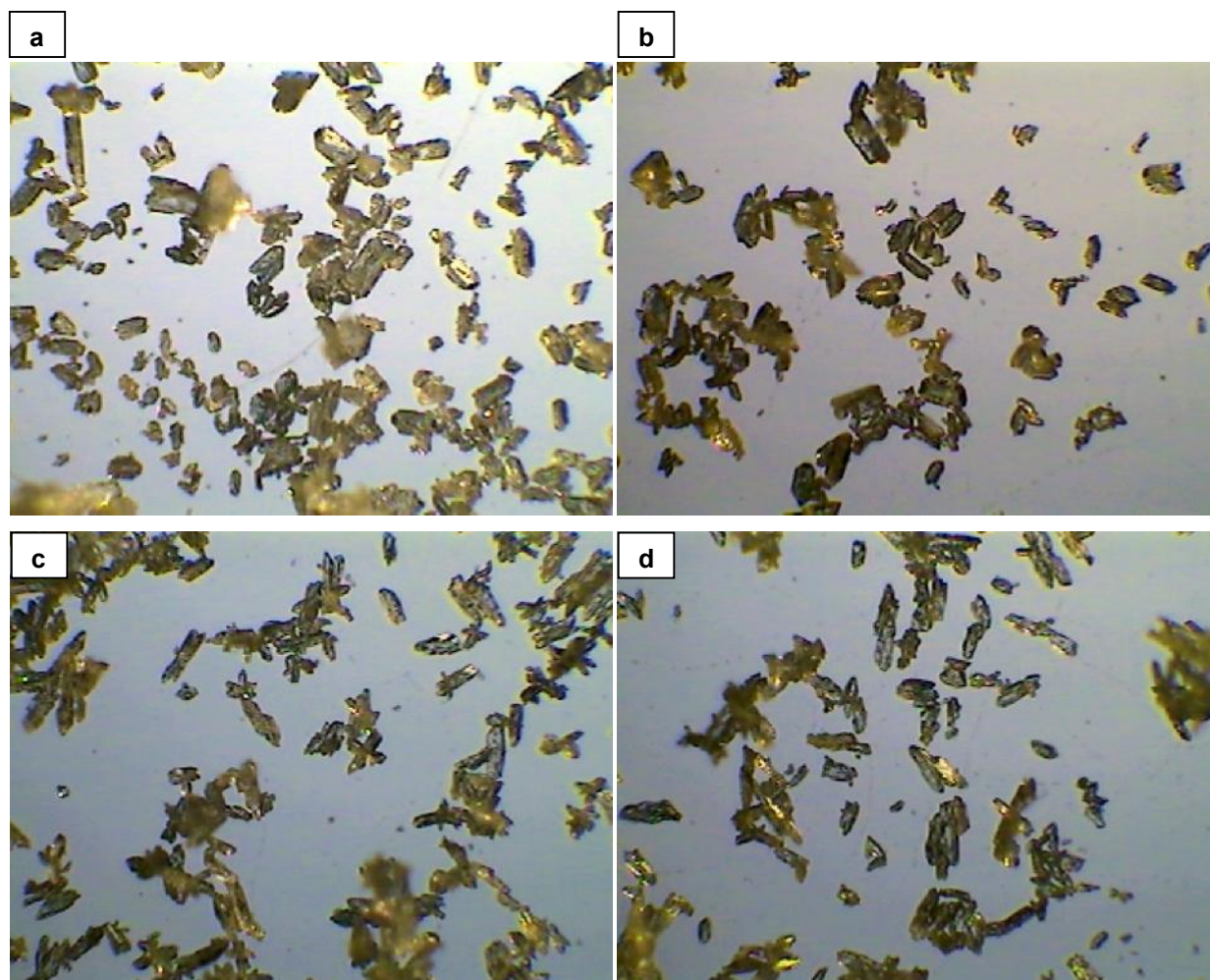


**Figure 41 – x10 magnified 4 hour samples from pH 7-10° C (a), pH 7-25° C (b), pH 8-10° C (c), and pH 8-25° C (d)**

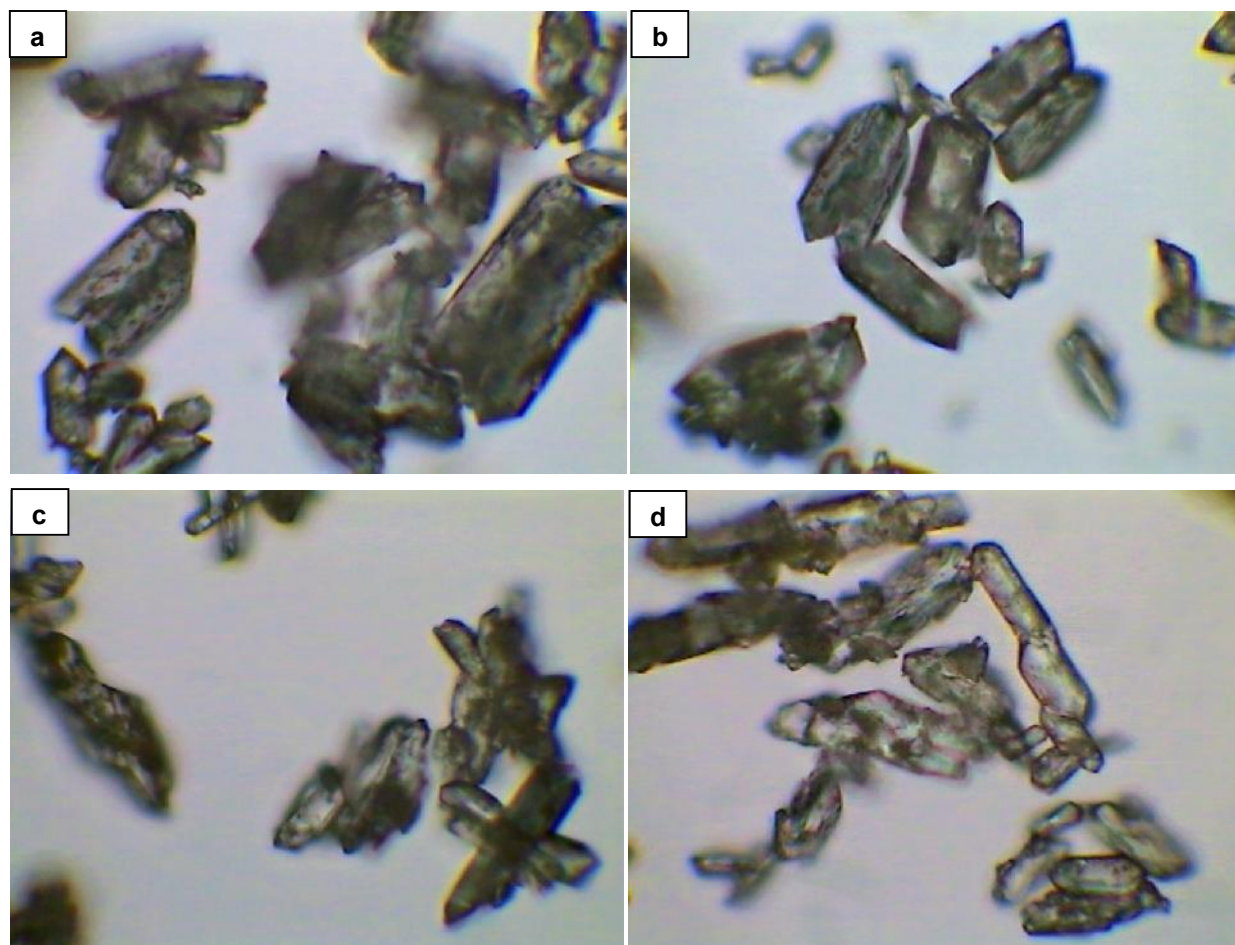


Figure 42 – x40 magnified 4 hour samples from pH 7-10° C (a), pH 7-25° C (b), pH 8-10° C (c), and pH 8-25° C (d)

## CHAPTER 7: CONCLUSIONS

Based on knowledge gained from experimental and model-generated results regarding ammonia recovery from synthetic wastewaters using newberyite, the following conclusions are made:

- pH control by caustic addition is the dominant factor over temperature, with respect to ammonia removal and orthophosphate solubilization resulting from simultaneous newberyite dissolution and struvite crystallization.
- All of the explored systems approached equilibrium between 1 and 3 hours reaction time.
- Maintenance of a pH of 7 and above provides ammonia removal efficiencies between 77% and 87%, given a newberyite dose providing a suspension Mg:N:P molar ratio of approximately 1:1:1. At a pH below 7, considerable orthophosphate residuals result from newberyite dissolution; however, residuals may be reduced to as low as 10 mg/L PO<sub>4</sub>-P at pH 9.
- A decrease in newberyite dose generally allows for only slight reductions in orthophosphate residual.
- No bobbierite or magnesite was formed during newberyite-to-struvite conversion even at pH 9 and 35° C. The solid phase mixture produced contains residual newberyite regardless of pH and reaction time. This suggests that, unless it is pre-dissolved, some residual could remain in struvite pellets. Nevertheless, newberyite-to-struvite conversions as high as 92% were achieved.
- Conditions approaching the optimum were suggested as follows, based on ammonia removal, orthophosphate and newberyite residual, and caustic consumption:
  - pH 7 – 8
  - 10° – 25° C
  - Newberyite dose providing suspension Mg:N:P molar ratio of 1:1:1

- The proposed secondary crystallization process (Reactor Configuration 1) using newberyite to treat primary crystallizer effluent may result in considerable solubilization of orthophosphate
- The proposed single stage crystallization process (Reactor Configuration 2) using newberyite to treat centrate may provide simultaneous ammonia and orthophosphate removals as high as 83% and 73% respectively, with a caustic consumption similar to that of secondary crystallization
- For these configurations,  $S_S$  was between 1.9 and 4.4 after 10 minutes but between 1.2 and 1.8 after 1 hour suggesting that a pretreated newberyite-struvite suspension may have potential as a feed for a UBC struvite crystallizer
- The observed and model-generated liquid phase compositions were comparable. Predicted solid phase compositions were significantly different than that produced in batch tests, but the model proved to be an excellent tool for identifying conditions where newberyite is still stable and for estimating caustic consumption
- An unreported newberyite morphology was revealed: rice-shaped, elongated rhombohedrals

## CHAPTER 8: RECOMMENDATIONS

The following research tasks are recommended for the development of ammonia recovery via the struvite formation-thermal decomposition cycle:

- Perform pilot studies for the optimization of thermally decomposed struvite composition and quality
- Using this study's model, explore ammonia removal and orthophosphate solubilization for newberyite and  $\text{MgCl}_2$  combination doses providing N:P ratios below 1 and Mg:P ratios above 1
- Perform batch tests using combinations of real thermally decomposed struvite with synthetic and real wastewaters and delineate the effect of pellet size on newberyite dissolution
- Evaluate caustic consumption and struvite quality in two pilot studies using UBC struvite crystallizers with:
  1. An acidic feed containing ammonia, orthophosphate, and dissolved newberyite
  2. A caustic-enhanced feed containing a suspension of ammonia, orthophosphate, and newberyite and struvite fines
- Perform bench-scale studies to better understand the fundamentals of struvite crystal agglomeration and pelletization in FBRs for the development of next generation reactor designs

---

## REFERENCES

- Abbona, F., & Boistelle, R. (1985). Nucleation of struvite ( $\text{MgNH}_4\text{PO}_4 \cdot 6\text{H}_2\text{O}$ ) single crystals and aggregates. *Crystal Res. Technol.*, 20(2), 133–40.
- Abdelrazig, B., & Sharp, J. (1988). Phase changes on heating ammonium magnesium phosphate hydrates. *Thermochim. acta*, 129, 197–215.
- Adnan, A. (2002). Pilot-scale study of phosphorus recovery through struvite crystallization.
- Aiking, H. (2011). Future protein supply. *Trends Food Sci. Tech.*, 22, 112–20.
- Allar, A. D., & Beler-Baykal, B. (2013). Phosphorus recovery from source separated human urine upon processing with clinoptilolite. *Proceedings of the WEF/IWA Conference: Nutrient Removal and Recovery*.
- Andrade, A., & Schuiling, R. D. (2001). The chemistry of struvite crystallization. *Mineral Journ.*, 23(5), 37–46.
- APHA, AWWA, WEF (2012). *Standard Methods for the Examination of Water and Wastewater*, 22<sup>nd</sup> Edition. *American Public Health Association, Washington, D.C.*
- Babić-Ivančić, V., Kontrec, J., Brečević, L., & Kralj, D. (2002). Precipitation Diagrams of Struvite and Dissolution Kinetics of Different Struvite Morphologies. *Croat. Chem. Acta*, 75(1), 89–106.
- Babić-Ivančić, V., Kontrec, J., Brečević, L., & Kralj, D. (2006). Kinetics of struvite to newberyite transformation in the precipitation system  $\text{MgCl}_2\text{--NH}_4\text{H}_2\text{PO}_4\text{--NaOH--H}_2\text{O}$ . *Water Res.*, 40(18), 3447–3455.
- Başakçıldan-Kabakci, S., İpekoğlu, A. N., & Talinli, I. (2007). Recovery of Ammonia from Human Urine by Stripping and Absorption. *Environ. Eng. Sci.*, 24(5), 615–24.

- Belser-Baykal, B., Allar, a D., & Bayram, S. (2011). Nitrogen recovery from source-separated human urine using clinoptilolite and preliminary results of its use as fertilizer. *Water Sci. Technol.*, 63(4), 811–7.
- Bénezeth, P., Saldi, G. D., Dandurand, J.-L., & Schott, J. (2011). Experimental determination of the solubility product of magnesite at 50 to 200°C. *Chem. Geol.*, 286(1-2), 21–31.
- Berthouex, P. Mac, & Brown, L. C. (2002). *Statistics for Environmental Engineers (Second Edition)*. Boca Raton, Florida: Lewis Publishers.
- Bhuiyan, M. I. H., Mavinic, D. S., & Beckie, R. D. (2007). A solubility and thermodynamic study of struvite. *Environ. Technol.*, 28(9), 1015–26.
- Bhuiyan, M. I. H., Mavinic, D. S., & Koch, F. A. (2008). Thermal decomposition of struvite and its phase transition. *Chemosphere*, 70(8), 1347–56.
- Boistelle, R., Abbona, F., Madsen, H. E. L., & Massimo, S. (1983). On the transformation of struvite into newberyite in aqueous systems. *Phys. Chem. Minerals*, 9(5), 216–222.
- Britton, A. T. (2002). Pilot-scale struvite recovery trials from a full-scale anaerobic digester supernatant at the City of Penticton Advanced Wastewater Treatment Plant.
- Britton, A., Prasad, R., Baizer, B., Cabbage, L. (2009). Pilot testing and economic evaluation of struvite recovery from dewatering centrate at HRSD's Nansemond WWTP. In *Proceedings of the International Conference on Nutrient Recovery from Wastewater Streams* (pp. 193–202).
- Christensen, C. H., Johannessen, T., Sørensen, R. Z., & Nørskov, J. K. (2006). Towards an ammonia-mediated hydrogen economy? *Catal.Today*, 111, 140–44.
- Cilona, A., Nilsson, S., Malpei, F., & Levlin, E. (2009). Gas transfer membrane for ammonia removal of condensed flue gas.

Cohen, L. H., & Ribbe, P. H. (1966). Magnesium phosphate mineral replacement at Mono Lake, California. *Am. Mineral.*, 51, 1755–1765.

Le Corre, K. S., Valsami-Jones, E., Hobbs, P., & Parsons, S. A. (2009). Phosphorus recovery from wastewater by struvite crystallization: A Review. *Crit. Rev. Env. Sci. Technol.*, 39(6), 433–77.

Dastur, M. B. (2001). Investigation into the factors affecting controlled struvite crystallization at the bench-scale.

Elmøe, T. D., Sørensen, R. Z., Quaade, U., Christensen, C. H., Nørskov, J. K., & Johannessen, T. (2006). A high-density ammonia storage/delivery system based on  $Mg(NH_3)_6Cl_2$  for – in vehicles. *Chem. Eng. Sci.*, 61, 2618–25.

Elston, J. T., & Karmarkar, D. (2003). Aqueous ammonia stripping technology for SCR applications. In *Proceedings of the Electric Power Conference*.

Environment Canada. (2001). Priority Substances List Assessment Report: Ammonia in the Aquatic Environment.

Erisman, J. W., Sutton, M. A., Galloway, J., Klimont, Z., & Winiwarter, W. (2008). How a century of ammonia synthesis changed the world. *Nature Geosci.*, 1(10), 636–9.

Evans, T. D., & Thompson, A. (2009). Recovering ammonium fertiliser – an alternative to blowing it away. In *Proceedings of the 14th European Biosolids & Organic Resources Conference*.

Fassbender, A. G. (2001). ThermoEnergy Ammonia Recovery Process for municipal and agricultural wastes. *ScientificWorldJournal*, 1(S2), 908–13.

Fattah, K. P. (2004). Pilot scale struvite recovery potential from centrate at Lulu Island Wastewater Treatment Plant.

Franke, J., & Mersmann, A. (1995). The influence of the operational conditions on the precipitation process. *Chem. Eng. Sci.*, 50(11), 1737–53.

Frost, R. L., Weier, M. L., & Erickson, K. L. (2004). Thermal decomposition of struvite – Implications for the decomposition of kidney stones. *J. Therm. Anal. Calorim.*, 76, 1025–1033.

Fux, C., & Siegrist, H. (2004). Nitrogen removal from sludge digester liquids by nitrification/denitrification or partial nitritation/anammox: environmental and economical considerations. *Water Sci. Technol.*, 50(10), 19–26.

He, S., Zhang, Y., Yang, M., Du, W., & Harada, H. (2007). Repeated use of MAP decomposition residues for the removal of high ammonium concentration from landfill leachate. *Chemosphere*, 66(11), 2233–2238.

Hedström, A. (2006). Reactive filter materials for ammonium and phosphorus sorption in small scale wastewater treatment.

Hejze, T., Besenhard, J. O., Kordesch, K., Cifrain, M., & Aronsson, R. R. (2008). Current status of combined systems using alkaline fuel cells and ammonia as a hydrogen carrier. *J. Power Sources*, 176, 490–93.

Huang, H. (2003). Pilot-scale phosphorus recovery from anaerobic digester supernatant.

Huang, H. M., Xiao, X. M., & Yan, B. (2009). Recycle use of magnesium ammonium phosphate to remove ammonium nitrogen from rare-earth wastewater. *Water Sci. Technol.*, 59(6), 1093–1099.

Huang, H., Xu, C., & Zhang, W. (2011). Removal of nutrients from piggery wastewater using struvite precipitation and pyrogenation technology. *Bioresour. Technol.*, 102(3), 2523–2528.

Huang, H. M., Song, Q. W., & Xu, C. L. (2011). The Mechanism and influence factors of struvite precipitation for the removal of ammonium nitrogen. *Adv. Mater. Res.*, 189-193, 2613–20.

Jaffer, Y., Clark, T. a, Pearce, P., & Parsons, S. a. (2002). Potential phosphorus recovery by struvite formation. *Water Res.*, 36(7), 1834–42.

Kessler, K. (2010). Analysis of Nitrogen Loading Reductions for Wastewater Treatment Facilities and Non-Point Sources in the Great Bay Estuary Watershed - Appendix E : Capital and Operation/Maintenance Costs Associated with Nitrogen Removal at 18 Municipal Wastewater Treatment Facilities Discharging to the Great Bay Estuary.

Kiehl, S., & Hardt, H. (1933). The dissociation pressures of magnesium ammonium phosphate hexahydrate and some related substances. VII. *J. Am. Chem. Soc.*, 55(2), 605–618.

Königsberger, E., & Königsberger, L. (2006). *Biom mineralization – Medical Aspects of Solubility*. West Sussex: John Wiley & Sons, Ltd.

Kontrec, J., Babić-Ivančić, V., & Brečević, L. (2005). Formation and morphology of struvite and newberyite in aqueous solutions at 25 and 37 degrees C. *Coll. antropol.*, 29(1), 289–94.

Koutsoukos, P. G., Kofina, A. N., & Kanellopoulou, D. G. (2007). Solubility of salts in water: Key issue for crystal growth and dissolution processes. *Pure Appl. Chem.*, 79(5), 825–850.

Kurtulus, G., & Tas, A. C. (2011). Transformations of neat and heated struvite ( $\text{MgNH}_4\text{PO}_4 \cdot 6\text{H}_2\text{O}$ ). *Mater Lett*, 65(19-20), 2883–2886.

Lan, R., Irvine, J. T. S., & Tao, S. (2012). Ammonia and related chemicals as potential indirect hydrogen storage materials. *Int. J. Hydrogen Energ.*, 37, 1482–94.

Liu, Y., Kumar, S., Kwag, J.-H., & Ra, C. (2013). Magnesium ammonium phosphate formation, recovery and its application as valuable resources: A review. *J. Chem. Technol. Biotechnol.*, 88, 181–89.

Lobanov, S., Koch, F. A., & Mavinic, D. S. (2013). The implication of aqueous equilibrium modelling to evaluate the potential for nutrient recovery from wastewater streams. In Proceedings of the WEF/IWA Conference: Nutrient Removal and Recovery.

Maggio, G., & Cacciola, G. (2012). When will oil, natural gas, and coal peak? *Fuel*, 98, 111–23.

Maxwell, G. R. (2004). *Synthetic Nitrogen Products: A Practical Guide to the Products and Processes*. New York: Kluwer Academic/Plenum Publishers.

Mohr, S. H., & Evans, G. M. (2011). Long term forecasting of natural gas production. *Energy Policy*, 39, 5550–60.

Münch, E. V., & Barr, K. (2001). Controlled struvite crystallisation for removing phosphorus from anaerobic digester sidestreams. *Water Res.*, 35(1), 151–9.

Novotny, C. (2011). Ammonia removal and recovery using heated struvite as an adsorbent.

Ohlinger, K. N., Young, T. M., & Schroeder, E. D. (1998). Predicting struvite formation in digestion. *Water Res.*, 32(12).

Ohlinger, K. N., Young, T. M., & Schroeder, E. D. (1999). Kinetics effects on preferential struvite accumulation in wastewater. *J. Environ. Eng.*, 125(8), 730–737.

Orentlicher, M. (2012). Overview of nitrogen removal technologies and application/use of associated end products. In Proceedings of: Got Manure? Enhancing Environmental and Economic Sustainability Conference.

Ostara Nutrient Recovery Technologies Inc. (2007). Ostara Nutrient Recovery Technologies Inc.: Edmonton reveals world's first industrial scale sewage treatment facility to recycle nutrients into environmentally-safe commercial fertilizer. Retrieved April 29, 2013, from <http://www.ostara.com/news/news-releases/2007/ostara-nutrient-recovery-technologies-inc-edmonton-reveals-worlds-first-indu>

Ostara Nutrient Recovery Technologies Inc. (2011). Utility plans expansion of phosphorus recovery system. Retrieved May 1, 2013, from <http://www.ostara.com/content/utility-plans-expansion-phosphorus-recovery-system>

Paulik, F., & Paulik, J. (1975a). TG and EGA investigations of the decomposition of magnesium ammonium phosphate hexahydrate by means of the derivatograph under conventional and quasi-isothermal-quasi-isobaric conditions. *J. Therm. Anal.*, 8, 557–566.

Paulik, J., & Paulik, F. (1975b). TG and EGA investigations of the decomposition of some metal ammonium phosphate monohydrates by means of the derivatograph under conventional and quasi-isothermal-quasi-isobaric conditions. *J. Therm. Anal.*, 8, 567–576.

Pokrovsky, O. S., Schott, J., & Thomas, F. (1999). Processes at the magnesium-bearing carbonates/solution interface . I. A surface speciation model for magnesite. *Geochim. Cosmochim. Acta*, 63(6), 863–880.

Randall, D. J., & Tsui, T. K. N. (2002). Ammonia toxicity in fish. *Mar. Pollut. Bull.*, 45(1-12), 17–23.

Reiter, A. J., & Kong, S.-C. (2011). Combustion and emissions characteristics of compression-ignition engine using dual ammonia-diesel fuel. *Fuel*, 90, 87–97.

Ribbe, P. (1969). The decomposition of struvite: further evidence. *Mineral. Mag.*, 37(286), 290–291.

Shand, M. A. (2006). *The Chemistry and Technology of Magnesia*. Hoboken: John Wiley & Sons, Ltd.

Söhnel, O., & Garside, J. (1992). *Precipitation: Basic Principles and Industrial Applications*. Oxford: Butterworth-Heinemann.

Stefanowicz, T., Napieralska-Zagozda, S., & Osittska, M. (1992). Ammonia removal from waste solutions by precipitation of  $MgNH_4PO_4 \cdot 6H_2O$ . Ammonia removal and recovery with recycling of regenerate. *Resour., Conserv. Recycling*, 6, 339–345.

Smil, V. (2001). *Enriching the Earth: Fritz Haber, Carl Bosch and the Transformation of World Food Production*.

Sugiyama, S., Yokoyama, M., Ishizuka, H., Sotowa, K.-I., Tomida, T., & Shigemoto, N. (2005). Removal of aqueous ammonium with magnesium phosphates obtained from the ammonium-elimination of magnesium ammonium phosphate. *J. Colloid Interface Sci.*, 292(1), 133–8.

Sugiyama, S., Yokoyama, M., Fujii, M., Seyama, K., & Sotowa, K.-I. (2007). Recycling of thin-layer of magnesium hydrogen phosphate for removal and recovery of aqueous ammonium. *J. Chem. Eng. Jpn.*, 40, 198–201.

Taylor, A. W., Frazier, A. W., & Gurney, E. L. (1963a). Solubility products of magnesium ammonium and magnesium potassium phosphates. *Trans. Faraday Soc.*, 1580–1584.

Taylor, A. W., Frazier, A. W., Gurney, E. L., & Smith, J. P. (1963b). Solubility products of di- and trimagnesium phosphates and the dissociation of magnesium phosphate solutions. *Trans. Faraday Soc.*, 59, 1585.

Tchobanoglous, G., Burton, F. L., & Stensel, H. D. (2003). *Wastewater engineering: treatment and reuse*. Metcalf & Eddy, Inc. New York: McGraw-Hill.

ThermoEnergy Corporation. (2007). *Ammonia Recovery Process: Cost benefits to the operation of a typical wastewater treatment plant*.

Türker, M., & Celen, I. (2007). Removal of ammonia as struvite from anaerobic digester effluents and recycling of magnesium and phosphate. *Bioresour. Technol.*, 98(8), 1529–1534.

Ulbricht, M., Schneider, J., Stasiak, M., & Sengupta, A. (2013). Ammonia recovery from industrial wastewater by TransMembraneChemiSorption. *Chem. Ing. Tech.*, 85(8), 1259–62.

USDA ERS. (2013). Fertilizer use and price. Retrieved from <http://www.ers.usda.gov/data-products/fertilizer-use-and-price.aspx#26727>

USEPA. (2008). Municipal Nutrient Removal Technologies Reference Document: Volume 1 - Technical Report.

USGS. (2013). PHREEQC (Version 3) - A Computer Program for Speciation, Batch-Reaction, One-Dimensional Transport, and Inverse Geochemical Calculations: In database file, "Inl.dat." Retrieved from [http://wwwbrr.cr.usgs.gov/projects/GWC\\_coupled/phreeqc/](http://wwwbrr.cr.usgs.gov/projects/GWC_coupled/phreeqc/)

Verbeeck, R. M. H., De Bruyne, P. A. M., Driessens, F. C. M., & Verbeek, F. (1984). Solubility of magnesium hydrogen phosphate trihydrate and ion-pair formation in the system  $Mg(OH)_2$ - $H_3PO_4$ - $H_2O$  at 25° C. *Inorg. Chem.*, 23(13), 1922–1926.

WERF. (2010). Nutrient recovery: State of the knowledge.

Whitaker, A. (1968). The decomposition of struvite. *Mineral. Mag.*, (1966), 820–824.

Wood, S., & Cowie, A. (2004). A review of greenhouse gas emission factors for fertiliser production. IEA Bioenergy Task, 38.

Yin, S. F., Xu, B. Q., Zhou, X. P., & Au, C. T. (2004). A mini-review on ammonia decomposition catalysts for on-site generation of hydrogen for fuel cell applications. *Appl. Catal., A*, 277, 1–9.

Zamfirescu, C., & Dincer, I. (2008). Using ammonia as a sustainable fuel. *J. Power Sources*, 185, 459–65.

Zamfirescu, C., & Dincer, I. (2009). Ammonia as a green fuel and hydrogen source for vehicular applications. *Fuel Process. Technol.*, 90, 729–37.

Zhang, S., Yao, C., Feng, X., & Yang, M. (2004). Repeated use of  $MgNH_4PO_4 \cdot 6H_2O$  residues for ammonia removal by acid dipping. *Desalination*, 170(1), 27–32.

Zhang, T., Ding, L., Ren, H., & Xiong, X. (2009). Ammonium nitrogen removal from coking wastewater by chemical precipitation recycle technology. *Water Res.*, 43(20), 5209–5215.

## APPENDIX A: INSTRUMENT OPERATIONAL SETTINGS

**Table A.1 – Settings for magnesium analysis using flame atomic absorption spectrophotometer**

Parameter	Setting
Mode	Absorbance
Measurement Mode	Integration
Flame Type	Air/C <sub>2</sub> H <sub>2</sub>
Lamp Current	4.0 mA
Wavelength	202.6 nm
Calibration Range	0-250 mg/L

**Table A.2 – Settings for ammonia and orthophosphate analysis using flow injection analysis**

Parameter	NH <sub>4</sub> -N	PO <sub>4</sub> -P
Method	4500-NH <sub>3</sub> H <sup>1</sup>	4500-P G <sup>1</sup>
Temperature	63° C	63° C
Calibration Range	0-50 mg/L	0-25 mg/L

1. APHA, AWWA, WEF (2012). Standard Methods for the Examination of Water and Wastewater, 22<sup>nd</sup> Edition. *American Public Health Association, Washington, D.C.*

## APPENDIX B: LIQUID AND SOLID SAMPLE COMPOSITIONS

The following tables report the mean of triplicate analyses of liquid and solid phase samples. Initial synthetic wastewater volumes were 500 mL and the 2 M sodium hydroxide titrant measurements represent cumulative consumption. Solid analyses are presented as Mg:N:P molar ratios with respect to orthophosphate concentration.

**Table B.1 – Liquid sample analyses for Mg:N:P molar ratio 1:1.1:1, no pH control, 10° C**

Sample Time (h)	NH <sub>4</sub> -N (mg/L)		PO <sub>4</sub> -P (mg/L)		Mg (mg/L)		pH		NaOH (mL)	
	R1	R2	R1	R2	R1	R2	R1	R2	R1	R2
0	737	737	0	0	0	0	4.72	6.11	0	0
1	683	677	220	223	163	163	6.52	6.57	0	0
3	645	663	291	299	212	215	6.33	6.39	0	0
6	633	626	320	324	229	229	6.20	6.25	0	0
9	637	632	341	338	239	239	6.17	6.22	0	0
12	622	631	355	349	254	241	6.15	6.20	0	0

**Table B.2 – Liquid sample analyses for Mg:N:P molar ratio 1:1.1:1, pH 7, 10° C**

Sample Time (h)	NH <sub>4</sub> -N (mg/L)		PO <sub>4</sub> -P (mg/L)		pH		NaOH (mL)	
	R1	R2	R1	R2	R1	R2	R1	R2
0	737	737	0	0	4.99	4.55	0	0
1	538	562	129	136	7.01	7.03	3.7	3.3
3	219	227	139	140	7.03	7.05	8.2	8.1
6	150	180	96	136	7.11	7.10	9.2	8.7
9	150	176	107	141	7.00	6.98	9.2	8.7
12	137	166	83	119	7.14	7.01	9.3	8.8

**Table B.3 – Liquid sample analyses for Mg:N:P molar ratio 1:1.1:1, pH 8, 10° C**

Sample Time (h)	NH <sub>4</sub> -N (mg/L)		PO <sub>4</sub> -P (mg/L)		pH		NaOH (mL)	
	R1	R2	R1	R2	R1	R2	R1	R2
0	737	737	0	0	5.37	5.39	0	0
1	196	213	26	45	8.11	8.03	9.4	8.9
3	139	137	33	34	8.11	8.01	10.6	10.1
6	129	129	31	29	8.20	8.07	10.8	10.3
9	122	123	22	26	8.47	8.26	10.4	10.3
12	120	120	23	28	8.30	8.16	10.4	10.3

**Table B.4 – Liquid sample analyses for Mg:N:P molar ratio 1:1.1:1, pH 9, 10° C**

Sample Time (h)	NH <sub>4</sub> -N (mg/L)		PO <sub>4</sub> -P (mg/L)		pH		NaOH (mL)	
	R1	R2	R1	R2	R1	R2	R1	R2
0	737	737	0	0	4.73	5.07	0	0
1	194	211	11	10	9.13	9.13	10.2	10.4
3	176	190	11	11	9.36	9.41	10.4	10.4
6	178	186	10	11	9.16	9.23	10.5	10.4
9	174	185	11	11	9.16	9.27	10.5	10.4
12	164	179	12	11	9.06	9.20	10.5	10.4

**Table B.5 – Liquid sample analyses for Mg:N:P molar ratio 1:1.1:1, no pH control, 25° C**

Sample Time (h)	NH <sub>4</sub> -N (mg/L)		PO <sub>4</sub> -P (mg/L)		pH		NaOH (mL)	
	R1	R2	R1	R2	R1	R2	R1	R2
0	737	737	0	0	4.88	4.55	0	0
1	643	682	203	212	6.62	6.66	0	0
3	650	668	221	213	6.50	6.47	0	0
6	655	657	234	229	6.45	6.38	0	0
9	652	663	238	234	6.44	6.35	0	0
12	645	657	239	236	6.42	6.35	0	0

**Table B.6 – Liquid sample analyses for Mg:N:P molar ratio 1:1.1:1, pH 7, 25° C**

Sample Time (h)	NH <sub>4</sub> -N (mg/L)		PO <sub>4</sub> -P (mg/L)		pH		NaOH (mL)	
	R1	R2	R1	R2	R1	R2	R1	R2
0	737	737	0	0	5.17	5.20	0	0
1	435	488	136	138	6.99	6.99	4.7	3.9
3	179	201	116	118	7.02	7.09	8.8	8.8
6	167	187	110	112	7.02	7.00	9.0	9.1
9	163	180	116	119	7.01	6.98	9.0	9.1
12	159	179	117	122	7.01	7.08	9.0	9.2

**Table B.7 – Liquid sample analyses for Mg:N:P molar ratio 1:1.1:1, pH 8, 25° C**

Sample Time (h)	NH <sub>4</sub> -N (mg/L)		PO <sub>4</sub> -P (mg/L)		pH		NaOH (mL)	
	R1	R2	R1	R2	R1	R2	R1	R2
0	737	737	0	0	5.49	5.03	0	0
1	148	148	39	30	8.06	8.13	10.3	10.6
3	144	146	31	39	8.15	7.95	10.3	10.6
6	143	137	27	40	8.32	8.35	10.6	10.9
9	135	134	30	30	8.20	8.23	10.7	10.9
12	135	136	29	32	8.23	8.17	10.7	10.9

**Table B.8 – Liquid sample analyses for Mg:N:P molar ratio 1:1.1:1, pH 9, 25° C**

Sample Time (h)	NH <sub>4</sub> -N (mg/L)		PO <sub>4</sub> -P (mg/L)		Mg (mg/L)		pH		NaOH (mL)	
	R1	R2	R1	R2	R1	R2	R1	R2	R1	R2
0	737	737	0	0	0	0	5.07	4.56	0	0
1	166	169	14	12	6	5	9.28	9.81	11.4	12.2
3	155	158	14	12	7	5	9.31	9.78	11.4	12.2
6	145	145	14	14	7	6	9.27	9.69	11.4	12.2
9	136	135	15	13	8	6	9.22	9.65	11.4	12.2
12	125	123	16	14	8	7	9.18	9.60	11.4	12.2

**Table B.9 – Liquid sample analyses for Mg:N:P molar ratio 1:1.1:1, no pH control, 35° C**

Sample Time (h)	NH <sub>4</sub> -N (mg/L)		PO <sub>4</sub> -P (mg/L)		pH		NaOH (mL)	
	R1	R2	R1	R2	R1	R2	R1	R2
0	737	737	0	0	5.06	4.92	0	0
1	672	675	173	172	6.67	6.67	0	0
3	660	662	190	188	6.54	6.52	0	0
6	663	660	196	196	6.50	6.51	0	0
9	653	660	197	199	6.51	6.53	0	0
12	652	658	198	199	6.49	6.52	0	0

**Table B.10 – Liquid sample analyses for Mg:N:P molar ratio 1:1.1:1, pH 7, 35° C**

Sample Time (h)	NH <sub>4</sub> -N (mg/L)		PO <sub>4</sub> -P (mg/L)		pH		NaOH (mL)	
	R1	R2	R1	R2	R1	R2	R1	R2
0	737	737	0	0	4.99	4.87	0	0
1	637	637	141	142	7.02	7.09	1.1	1.2
3	288	300	119	122	7.10	7.12	6.6	6.6
6	238	252	126	128	6.96	6.98	7.2	7.2
9	228	241	130	133	6.97	6.98	7.3	7.3
12	212	222	116	114	7.07	7.10	7.5	7.5

**Table B.11 – Liquid sample analyses for Mg:N:P molar ratio 1:1.1:1, pH 8, 35° C**

Sample Time (h)	NH <sub>4</sub> -N (mg/L)		PO <sub>4</sub> -P (mg/L)		pH		NaOH (mL)	
	R1	R2	R1	R2	R1	R2	R1	R2
0	737	737	0	0	4.65	4.73	0	0
1	176	193	30	22	8.11	8.15	10.2	10.1
3	170	174	37	30	8.03	8.22	10.2	10.1
6	163	170	41	35	7.98	8.10	10.2	10.1
9	158	161	44	41	7.92	7.98	10.3	10.1
12	147	154	30	35	8.24	8.08	10.4	10.2

**Table B.12 – Liquid sample analyses for Mg:N:P molar ratio 1:1.1:1, pH 9, 35° C**

Sample Time (h)	NH <sub>4</sub> -N (mg/L)		PO <sub>4</sub> -P (mg/L)		pH		NaOH (mL)	
	R1	R2	R1	R2	R1	R2	R1	R2
0	737	737	0	0	4.85	4.97	0	0
1	179	176	16	13	9.19	9.62	11.7	12.4
3	160	154	16	14	9.15	9.54	11.7	12.4
6	139	137	17	16	9.04	9.47	11.7	12.4
9	124	123	20	17	8.92	9.40	11.7	12.4
12	109	108	21	18	8.95	9.30	11.8	12.4

**Table B.13 – Solid sample analyses for Mg:N:P molar ratio 1:1.1:1, Reactor 2**

Temperature	pH	Sample Time (h)	Solid Molar Ratio		
			Mg:	NH <sub>4</sub>	:PO <sub>4</sub>
10° C	No control	1	0.976	0.085	1
		12	0.975	0.223	1
	7	1	0.942	0.336	1
		3	0.971	0.827	1
	8	1	0.942	0.779	1
		3	0.942	0.863	1
25° C	7	1	0.953	0.423	1
		3	0.946	0.832	1
	8	1	0.939	0.917	1
		3	0.939	0.864	1
	9	1	0.954	0.770	1
		12	0.986	0.856	1
35° C	7	12	0.991	0.770	1
	9	12	0.990	0.911	1

**Table B.14 – Liquid sample analyses for Mg:N:P molar ratio 1:1.4:1, no pH control, 10° C**

Sample Time (h)	NH <sub>4</sub> -N (mg/L)		PO <sub>4</sub> -P (mg/L)		pH		NaOH (mL)	
	R1	R2	R1	R2	R1	R2	R1	R2
0	737	737	0	0	5.30	5.26	0	0
1	685	692	192	197	6.52	6.48	0	0
3	640	650	252	255	6.33	6.29	0	0
6	618	643	276	285	6.26	6.21	0	0
9	635	635	296	296	6.19	6.15	0	0
12	630	635	307	307	6.14	6.12	0	0

**Table B.15 – Liquid sample analyses for Mg:N:P molar ratio 1:1.4:1, pH 7, 10° C**

Sample Time (h)	NH4-N (mg/L)		PO4-P (mg/L)		pH		NaOH (mL)	
	R1	R2	R1	R2	R1	R2	R1	R2
0	737	737	0	0	4.76	4.89	0	0
1	538	562	94	98	7.13	7.19	2.4	2.8
3	300	290	83	82	7.10	7.11	6.4	6.8
6	251	244	73	74	7.13	7.02	7.1	7.4
9	254	243	82	81	6.86	6.87	7.1	7.4
12	244	233	63	58	7.10	7.16	7.3	7.6

**Table B.16 – Liquid sample analyses for Mg:N:P molar ratio 1:1.4:1, pH 8, 10° C**

Sample Time (h)	NH4-N (mg/L)		PO4-P (mg/L)		pH		NaOH (mL)	
	R1	R2	R1	R2	R1	R2	R1	R2
0	737	737	0	0	4.52	4.68	0	0
1	312	330	22	30	8.15	8.12	7.0	6.7
3	244	240	20	22	7.98	7.99	7.9	8.0
6	246	237	22	18	7.99	8.36	7.9	8.1
9	240	231	21	19	7.91	8.16	7.9	8.1
12	241	237	22	20	7.97	8.14	8.0	8.1

**Table B.17 – Liquid sample analyses for Mg:N:P molar ratio 1:1.4:1, pH 9, 10° C**

Sample Time (h)	NH4-N (mg/L)		PO4-P (mg/L)		pH		NaOH (mL)	
	R1	R2	R1	R2	R1	R2	R1	R2
0	737	737	0	0	4.68	4.96	0	0
1	303	279	7	9	9.21	9.14	8.8	8.4
3	282	264	8	9	9.26	9.10	8.9	8.4
6	275	264	7	9	9.25	9.11	8.9	8.5
9	278	259	8	9	9.22	9.03	8.9	8.5
12	268	256	8	9	9.20	9.04	8.9	8.5

**Table B.18 – Liquid sample analyses for Mg:N:P molar ratio 1:1.4:1, no pH control, 25° C**

Sample Time (h)	NH <sub>4</sub> -N (mg/L)		PO <sub>4</sub> -P (mg/L)		pH		NaOH (mL)	
	R1	R2	R1	R2	R1	R2	R1	R2
0	737	737	0	0	4.92	4.98	0	0
1	673	678	189	187	6.66	6.71	0	0
3	640	642	214	210	6.47	6.51	0	0
6	652	653	235	234	6.40	6.42	0	0
9	645	645	236	235	6.36	6.38	0	0
12	643	653	241	241	6.34	6.36	0	0

**Table B.19 – Liquid sample analyses for Mg:N:P molar ratio 1:1.4:1, pH 7, 25° C**

Sample Time (h)	NH <sub>4</sub> -N (mg/L)		PO <sub>4</sub> -P (mg/L)		pH		NaOH (mL)	
	R1	R2	R1	R2	R1	R2	R1	R2
0	737	737	0	0	5.23	5.32	0	0
1	630	635	147	139	6.99	7.07	1.8	2.1
3	320	303	102	98	6.96	7.00	6.0	6.5
6	301	291	92	94	7.08	6.99	6.4	6.5
9	298	294	98	103	6.94	6.92	6.4	6.5
12	295	290	95	94	6.98	6.98	6.4	6.6

**Table B.20 – Liquid sample analyses for Mg:N:P molar ratio 1:1.4:1, pH 8, 25° C**

Sample Time (h)	NH <sub>4</sub> -N (mg/L)		PO <sub>4</sub> -P (mg/L)		pH		NaOH (mL)	
	R1	R2	R1	R2	R1	R2	R1	R2
0	737	737	0	0	4.94	4.86	0	0
1	287	286	23	20	8.00	8.15	7.9	8.2
3	282	275	23	20	8.09	8.16	8.1	8.2
6	277	278	17	21	8.28	8.10	8.2	8.2
9	277	273	17	24	8.26	8.05	8.2	8.2
12	277	276	18	24	8.25	8.03	8.2	8.2

**Table B.21 – Liquid sample analyses for Mg:N:P molar ratio 1:1.4:1, pH 9, 25° C**

Sample Time (h)	NH <sub>4</sub> -N (mg/L)		PO <sub>4</sub> -P (mg/L)		pH		NaOH (mL)	
	R1	R2	R1	R2	R1	R2	R1	R2
0	737	737	0	0	5.70	4.76	0	0
1	316	303	10	11	9.12	9.02	9.6	9.4
3	300	293	10	11	9.12	8.99	9.6	9.4
6	293	284	9	12	9.13	9.01	9.8	9.6
9	285	276	10	12	9.17	8.99	9.9	9.6
12	277	269	11	12	9.11	8.97	9.9	9.6

**Table B.22 – Liquid sample analyses for Mg:N:P molar ratio 1:1.4:1, no pH control, 35° C**

Sample Time (h)	NH <sub>4</sub> -N (mg/L)		PO <sub>4</sub> -P (mg/L)		pH		NaOH (mL)	
	R1	R2	R1	R2	R1	R2	R1	R2
0	737	737	0	0	5.00	4.90	0	0
1	670	673	166	166	6.74	6.76	0	0
3	658	650	183	182	6.55	6.52	0	0
6	652	642	192	185	6.53	6.49	0	0
9	643	640	192	191	6.49	6.48	0	0
12	652	650	196	197	6.48	6.47	0	0

**Table B.23 – Liquid sample analyses for Mg:N:P molar ratio 1:1.4:1, pH 7, 35° C**

Sample Time (h)	NH <sub>4</sub> -N (mg/L)		PO <sub>4</sub> -P (mg/L)		pH		NaOH (mL)	
	R1	R2	R1	R2	R1	R2	R1	R2
0	737	737	0	0	5.03	4.39	0	0
1	605	647	26	45	7.05	7.14	1.4	1.0
3	304	318	33	34	7.05	7.05	6.2	5.9
6	287	295	31	29	7.09	7.04	6.4	6.3
9	292	300	22	26	7.08	7.01	6.4	6.3
12	291	296	23	28	7.15	7.08	6.4	6.3

**Table B.24 – Liquid sample analyses for Mg:N:P molar ratio 1:1.4:1, pH 8, 35° C**

Sample Time (h)	NH4-N (mg/L)		PO4-P (mg/L)		pH		NaOH (mL)	
	R1	R2	R1	R2	R1	R2	R1	R2
0	737	737	0	0	5.01	4.93	0	0
1	253	259	11	10	8.09	8.28	8.6	8.9
3	243	245	11	11	8.08	8.30	8.7	8.9
6	234	248	11	11	8.15	8.22	8.9	8.9
9	233	250	11	11	8.09	8.20	9.0	8.9
12	232	245	12	11	8.06	8.17	9.0	8.9

**Table B.25 – Liquid sample analyses for Mg:N:P molar ratio 1:1.4:1, pH 9, 35° C**

Sample Time (h)	NH4-N (mg/L)		PO4-P (mg/L)		Mg (mg/L)		pH		NaOH (mL)	
	R1	R2	R1	R2	R1	R2	R1	R2	R1	R2
0	737	737	0	0	0	0	5.02	4.93	0	0
1	307	276	11	13	7	9	9.09	8.80	10.4	10.1
3	277	260	11	12	8	9	9.08	9.06	10.5	10.6
6	260	244	12	14	8	9	9.07	9.01	10.6	10.6
9	255	253	13	13	9	9	9.04	8.99	10.6	10.6
12	231	238	13	14	9	9	8.99	8.99	10.6	10.6

**Table B.26 – Solid sample analyses for Mg:N:P molar ratio 1:1.4:1, Reactor 2**

Temperature	pH	Sample Time (h)	Solid Molar Ratio		
			Mg:	NH4	:PO4
10° C	9	12	0.975	0.774	1
35° C	9	12	0.963	0.841	1

**Table B.27 – Liquid sample analyses for Mg:N:P molar ratio 1:1:1 in synthetic crystallizer effluent, pH 7, 10° C**

Sample Time (h)	NH <sub>4</sub> -N (mg/L)		PO <sub>4</sub> -P (mg/L)		Mg (mg/L)		pH		NaOH (mL)	
	R1	R2	R1	R2	R1	R2	R1	R2	R1	R2
0	919	919	19	19	16	16	8.35	8.37	0	0
0.17	382	395	96	103	71	77	7.28	7.12	0	0
1	232	215	118	132	88	98	7.00	7.00	4.5	4.8
3	133	121	136	137	101	102	7.00	7.00	8.0	8.0
4	122	110	153	157	115	117	6.98	6.98	8.1	8.0

**Table B.28 – Liquid sample analyses for Mg:N:P molar ratio 1:1:1 in synthetic crystallizer effluent, pH 8, 10° C**

Sample Time (h)	NH <sub>4</sub> -N (mg/L)		PO <sub>4</sub> -P (mg/L)		Mg (mg/L)		pH		NaOH (mL)	
	R1	R2	R1	R2	R1	R2	R1	R2	R1	R2
0	919	919	19	19	16	16	8.35	8.41	0	0
0.17	783	782	62	67	47	52	8.00	8.00	0	0
1	217	205	46	53	31	36	8.00	8.00	11.5	11.1
3	132	116	49	53	32	36	7.99	7.97	12.7	12.3
4	124	109	49	57	33	38	7.99	8.02	12.7	12.4

**Table B.29 – Liquid sample analyses for Mg:N:P molar ratio 1:1:1 in synthetic crystallizer effluent, pH 7, 25° C**

Sample Time (h)	NH <sub>4</sub> -N (mg/L)		PO <sub>4</sub> -P (mg/L)		Mg (mg/L)		pH		NaOH (mL)	
	R1	R2	R1	R2	R1	R2	R1	R2	R1	R2
0	919	919	19	19	16	16	8.09	8.05	0	0
0.17	799	818	191	161	137	119	7.03	7.45	0	0
1	423	381	170	160	122	116	7.00	7.00	5.9	7.3
3	279	247	184	164	130	118	6.98	7.04	7.3	8.6
4	263	230	181	164	129	117	7.01	7.03	7.9	8.6

**Table B.30 – Liquid sample analyses for Mg:N:P molar ratio 1:1:1 in synthetic crystallizer effluent, pH 8, 25° C**

Sample Time (h)	NH4-N (mg/L)		PO4-P (mg/L)		Mg (mg/L)		pH		NaOH (mL)	
	R1	R2	R1	R2	R1	R2	R1	R2	R1	R2
0	919	919	19	19	16	16	8.07	8.09	0	0
0.17	356	299	85	82	62	59	8.00	8.00	9.0	10.1
1	150	146	54	52	37	36	8.04	8.07	12.5	12.8
3	141	137	46	51	32	35	8.11	8.04	12.6	12.8
4	138	136	46	50	32	36	8.12	8.03	12.6	12.8

**Table B.31 – Solid sample analyses for Mg:N:P molar ratio 1:1:1 in synthetic crystallizer effluent, Reactor 1**

Temperature	pH	Sample Time (h)	Solid Molar Ratio		
			Mg:	NH4	:PO4
10° C	7	1	1.012	0.455	1
		4	1.004	0.778	1
	8	1	1.008	0.794	1
		4	1.024	0.915	1
25° C	7	1	1.003	0.560	1
		4	1.005	0.754	1
	8	1	1.020	0.847	1
		4	0.994	0.846	1

**Table B.32 – Liquid sample analyses for Mg:N:P molar ratio 1:1.05:1 in synthetic centrate, pH 7, 10° C**

Sample Time (h)	NH4-N (mg/L)		PO4-P (mg/L)		Mg (mg/L)		pH		NaOH (mL)	
	R1	R2	R1	R2	R1	R2	R1	R2	R1	R2
0	1007	1007	147	147	0	0	7.89	7.85	0	0
0.17	946	963	143	175	92	123	7.00	7.00	0	0
1	591	685	132	152	89	106	7.00	6.99	3.0	4.2
3	304	364	125	101	93	75	7.00	7.03	9.2	9.2
4	271	308	142	109	89	81	7.00	7.04	9.3	9.3

**Table B.33 – Liquid sample analyses for Mg:N:P molar ratio 1:1.05:1 in synthetic centrate, pH 8, 10° C**

Sample Time (h)	NH4-N (mg/L)		PO4-P (mg/L)		Mg (mg/L)		pH		NaOH (mL)	
	R1	R2	R1	R2	R1	R2	R1	R2	R1	R2
0	1008	1008	147	147	0	0	7.56	7.51	0	0
0.17	918	941	106	93	81	85	8.00	8.00	0	0
1	277	298	47	32	34	21	8.09	8.11	12.8	13.2
3	169	194	40	33	27	19	8.06	8.22	12.9	13.2
4	164	185	46	36	32	23	7.91	8.12	12.9	13.2

**Table B.34 – NH<sub>4</sub> probe readings for Mg:N:P molar ratio 1:1.05:1 in synthetic centrate, pH 8, 10° C**

Time (h)	Conductivity Reading	Ionic Strength (mol/L)	Activity Coefficient, $\gamma$	Probe {NH4-N} (mg/L)	[NH4-N] (mg/L)
0.00	18.9	0.0979	0.757	732	967
0.08	18.5	0.0958	0.758	751	990
0.17	18.2	0.0942	0.760	684	900
0.25	18.7	0.0969	0.758	740	977
0.33	18.5	0.0958	0.758	664	875
0.42	18.2	0.0942	0.760	589	775
0.50	17.9	0.0927	0.761	522	686
0.58	17.5	0.0906	0.763	492	645
0.67	17.2	0.0891	0.765	436	570
0.75	17.1	0.0886	0.765	378	494
0.83	16.8	0.0870	0.767	326	425
0.92	16.6	0.0860	0.768	303	395
1.00	16.5	0.0855	0.768	281	366
3.00	16.2	0.0840	0.770	171	222
4.00	16.2	0.0840	0.770	172	224

**Table B.35 – Liquid sample analyses for Mg:N:P molar ratio 1:1.05:1 in synthetic centrate, pH 7, 25° C**

Sample Time (h)	NH4-N (mg/L)		PO4-P (mg/L)		Mg (mg/L)		pH		NaOH (mL)	
	R1	R2	R1	R2	R1	R2	R1	R2	R1	R2
0	1007	1007	147	147	0	0	7.58	7.57	0	0
0.17	929	940	197	194	128	134	7.00	7.00	1.5	1.8
1	439	430	133	138	118	98	7.02	7.02	7.5	8.6
3	271	268	143	143	87	102	6.99	7.12	10.1	10.2
4	261	254	141	137	85	97	7.00	7.12	10.1	10.2

**Table B.36 – NH<sub>4</sub> probe readings for Mg:N:P molar ratio 1:1.05:1 in synthetic centrate, pH 7, 25° C**

Time (h)	Conductivity Reading	Ionic Strength (mol/L)	Activity Coefficient, $\gamma$	Probe {NH4-N} (mg/L)	[NH4-N] (mg/L)
0.00	18.4	0.1015	0.750	844	1126
0.08	18.3	0.1009	0.750	838	1117
0.17	17.8	0.0980	0.753	828	1100
0.25	17.8	0.0980	0.753	818	1087
0.33	17.7	0.0974	0.753	745	989
0.42	17.4	0.0957	0.755	708	938
0.50	17.2	0.0945	0.756	668	884
0.58	17.0	0.0934	0.757	613	810
0.67	16.8	0.0922	0.758	562	742
0.75	16.5	0.0905	0.759	514	677
0.83	16.4	0.0900	0.760	471	620
0.92	16.2	0.0888	0.761	424	557
1.00	16.2	0.0888	0.761	407	535
1.50	15.7	0.0861	0.764	305	399
2.00	15.3	0.0839	0.766	250	326
2.50	15.3	0.0839	0.766	212	277
3.00	15.3	0.0839	0.766	205	268
3.50	15.1	0.0828	0.767	190	248
3.75	14.9	0.0817	0.768	186	242
5.00	14.5	0.0795	0.770	170	221

**Table B.37 – Liquid sample analyses for Mg:N:P molar ratio 1:1.05:1 in synthetic centrate, pH 8, 25° C**

Sample Time (h)	NH4-N (mg/L)		PO4-P (mg/L)		Mg (mg/L)		pH		NaOH (mL)	
	R1	R2	R1	R2	R1	R2	R1	R2	R1	R2
0	1008	1008	147	147	0	0	7.51	7.38	0	0
0.17	812	825	65	51	65	55	8.00	8.00	7.7	5.6
1	210	207	39	32	25	21	8.05	8.12	12.8	13.2
3	198	189	38	39	25	26	8.07	8.03	12.9	13.2
4	194	188	38	40	25	26	8.07	8.03	12.9	13.2

**Table B.38 – Solid sample analyses for Mg:N:P molar ratio 1:1.05:1 in synthetic centrate**

Temperature	pH	Reactor	Sample Time (h)	Solid Molar Ratio		
				Mg:	NH4	:PO4
10° C	7	1	1	0.929	0.405	1
			4	0.960	0.813	1
		1	0.964	0.289	1	
	8	2	4	0.948	0.753	1
			1	0.952	0.706	1
		4	0.948	0.818	1	
25° C	7	1	1	0.956	0.642	1
			4	0.945	0.808	1
		1	0.954	0.581	1	
	8	2	4	0.950	0.792	1
			1	0.949	0.798	1
		4	0.967	0.815	1	

## **APPENDIX C: RESULTS OF XRD ANALYSIS OF SOLID SAMPLES**

The following figures are output graphs from XRD analyses of select solid samples. Samples were screened for patterns representing various magnesium salts of interest. However, only newberyite and struvite were detected. Note that the graph legend varies for each figure.

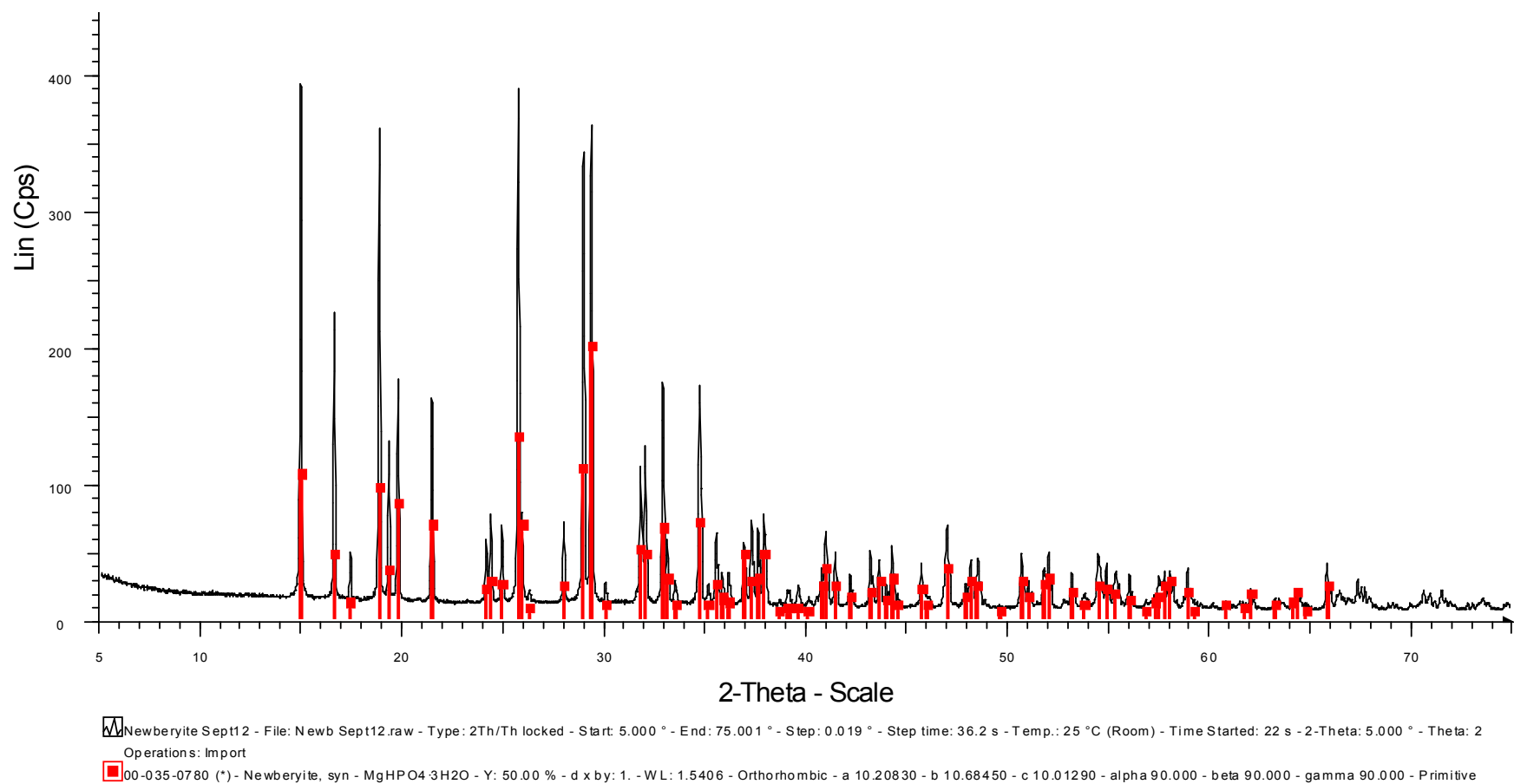


Figure C.1– Synthetic newberyite prepared September 12<sup>th</sup>, 2012

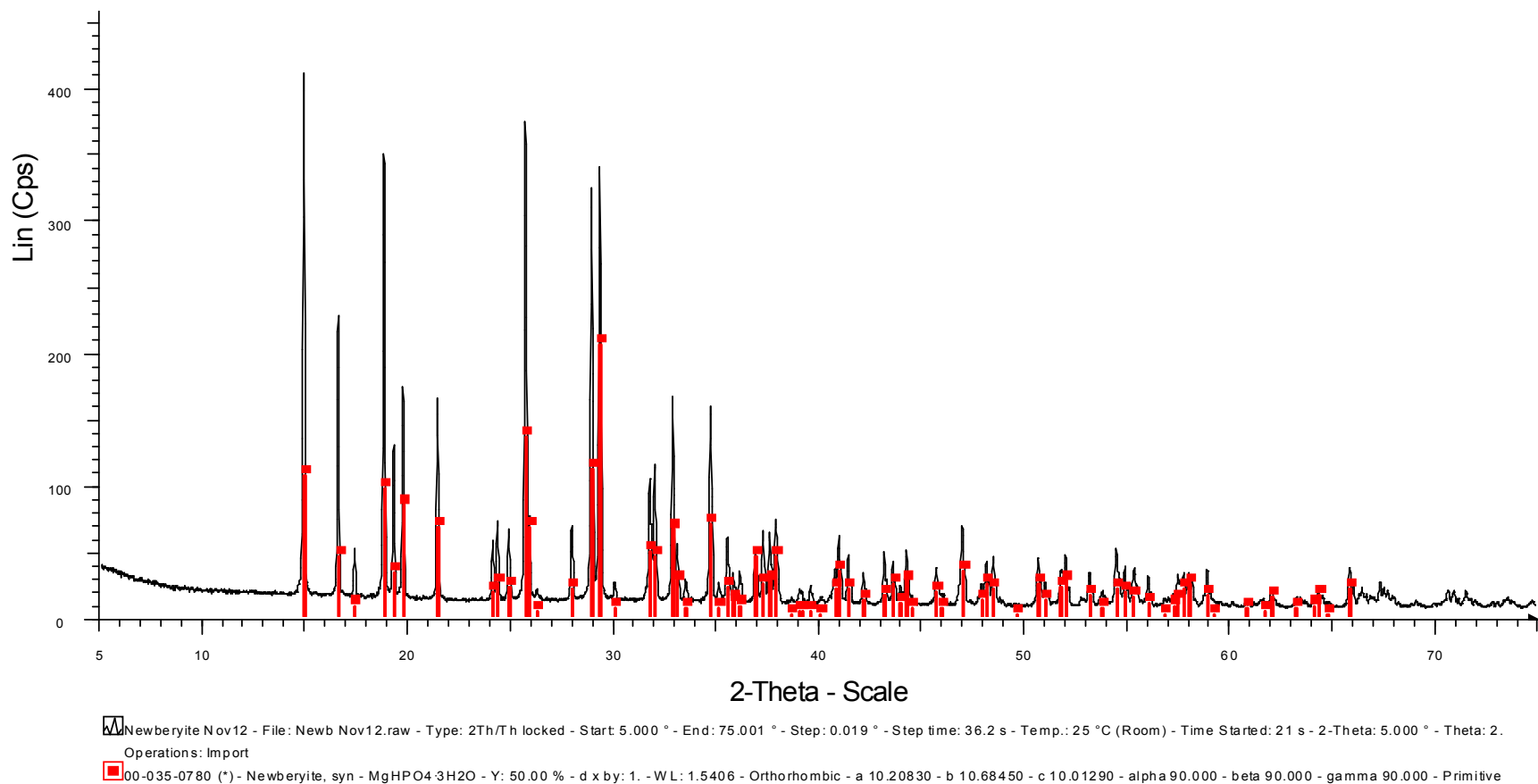


Figure C.2 – Synthetic newberyite prepared November 12<sup>th</sup>, 2012

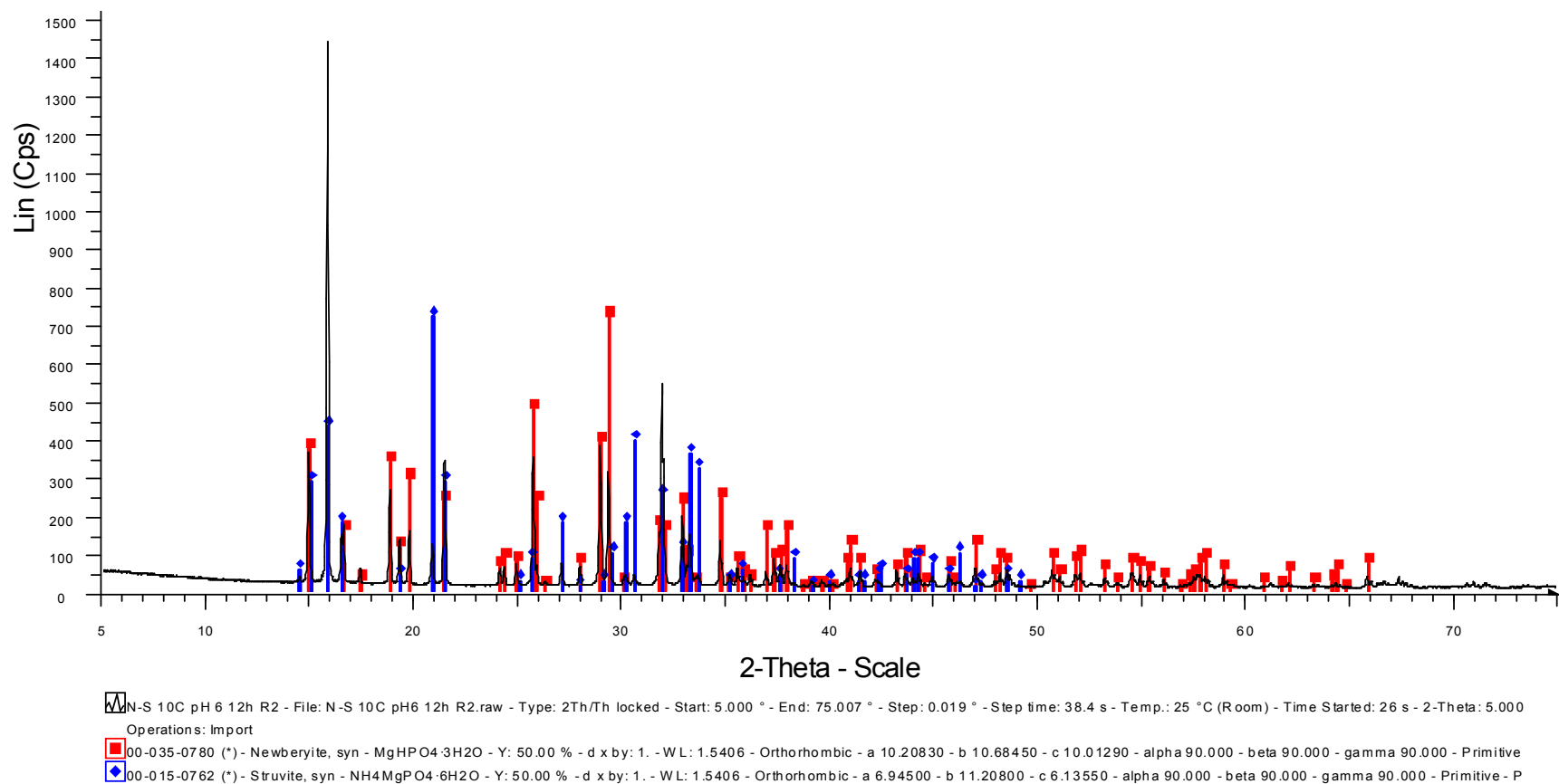


Figure C.3 – XRD output for Mg:N:P molar ratio 1:1.1:1, no pH control, 10° C, 12 h

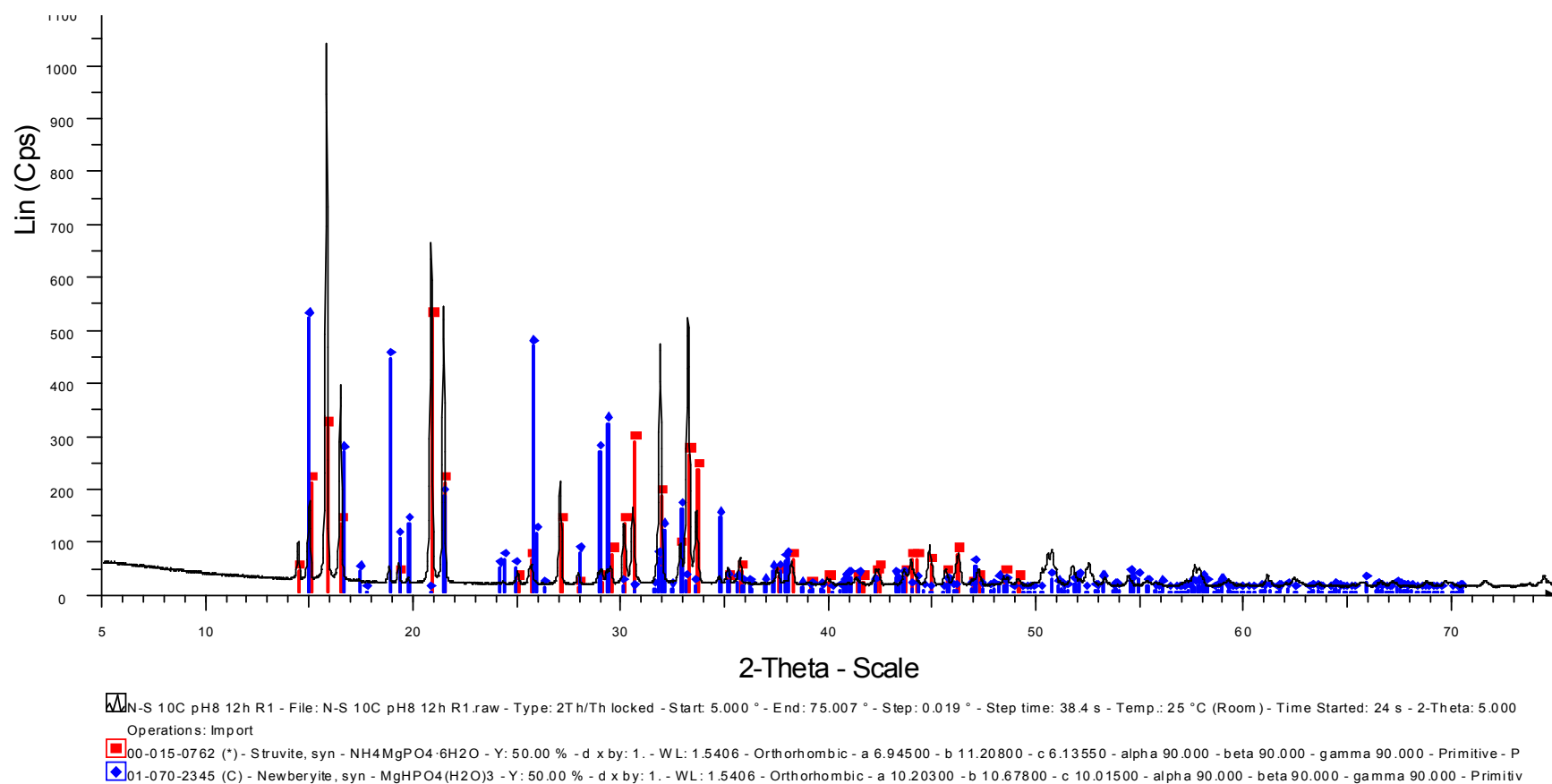


Figure C.4 – XRD output for Mg:N:P molar ratio 1:1.1:1, pH 8, 10° C, 12 h

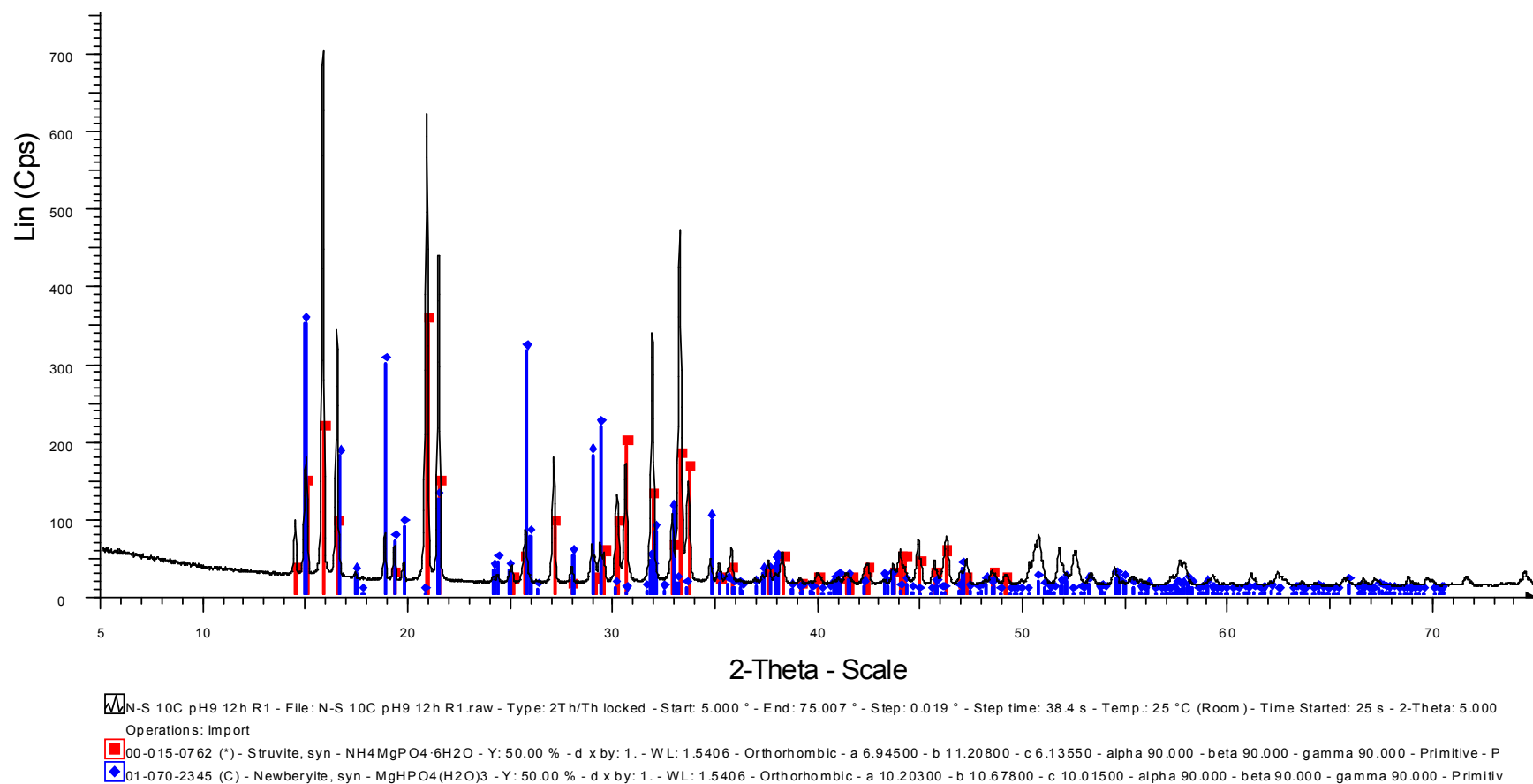


Figure C.5 – XRD output for Mg:N:P molar ratio 1:1.1:1, pH 9, 10° C, 12 h

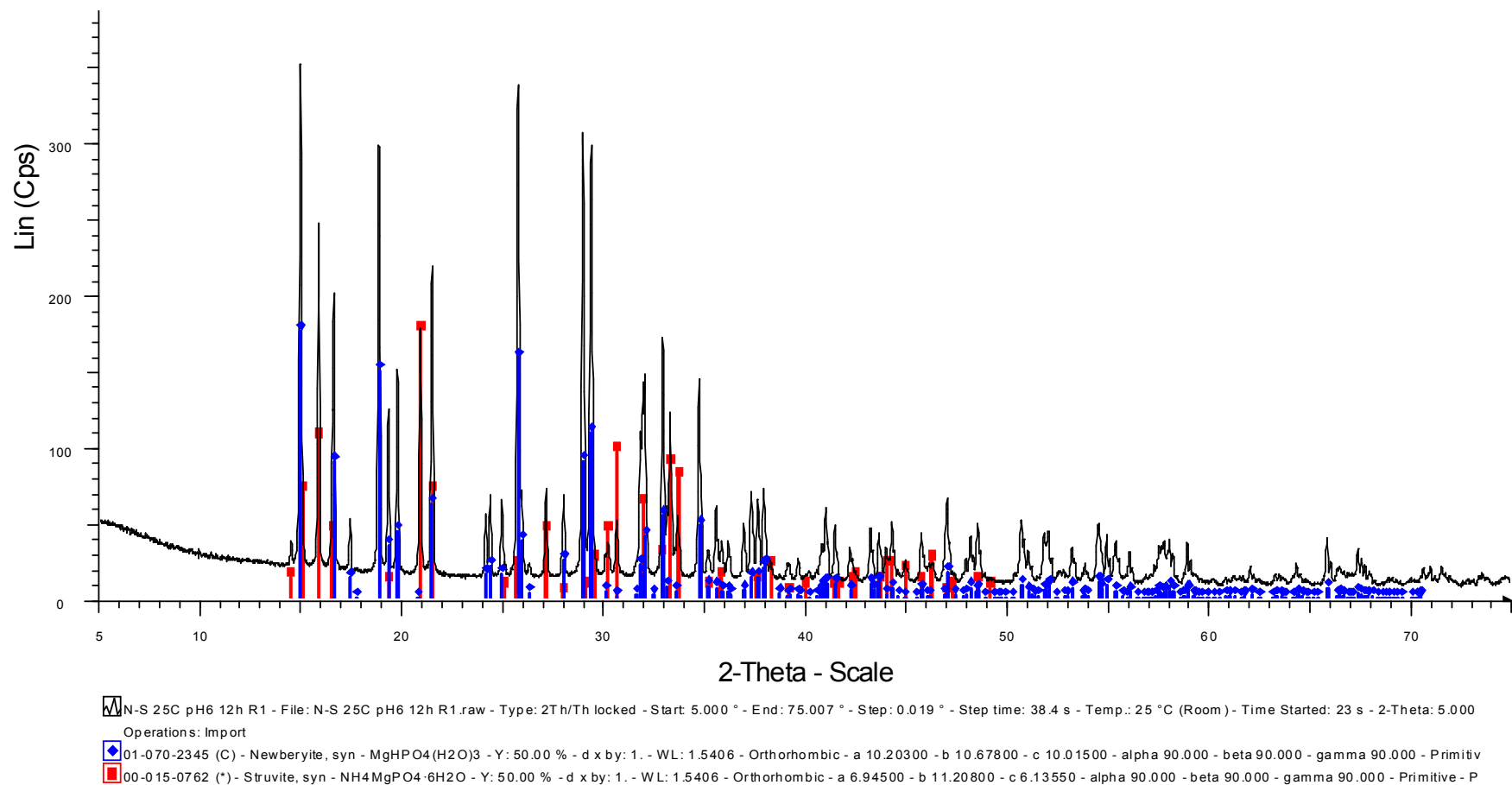


Figure C.6 – XRD output for Mg:N:P molar ratio 1:1.1:1, no pH control, 25° C, 12 h

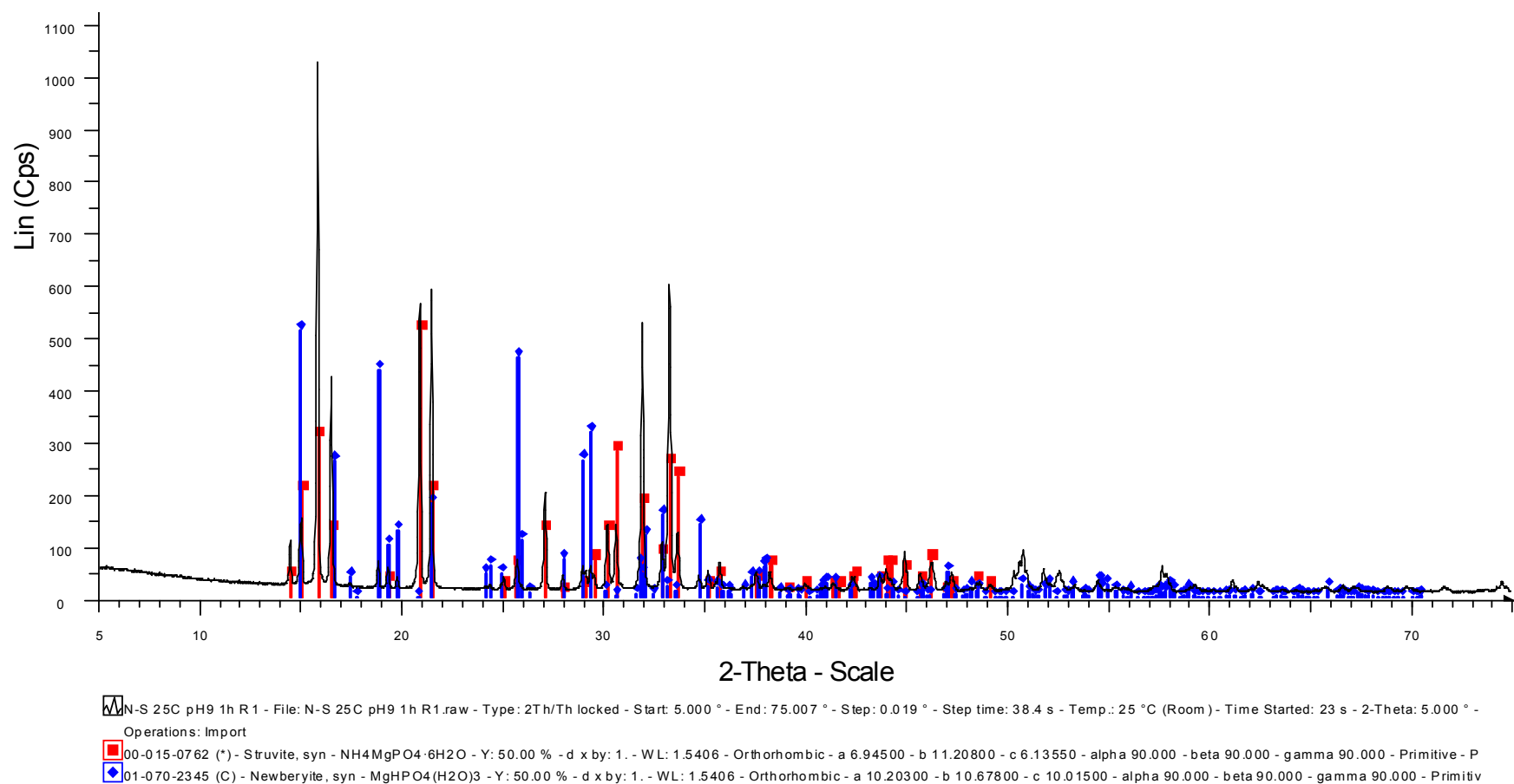


Figure C.7 – XRD output for Mg:N:P molar ratio 1:1.1:1, pH 9, 25° C, 1 h

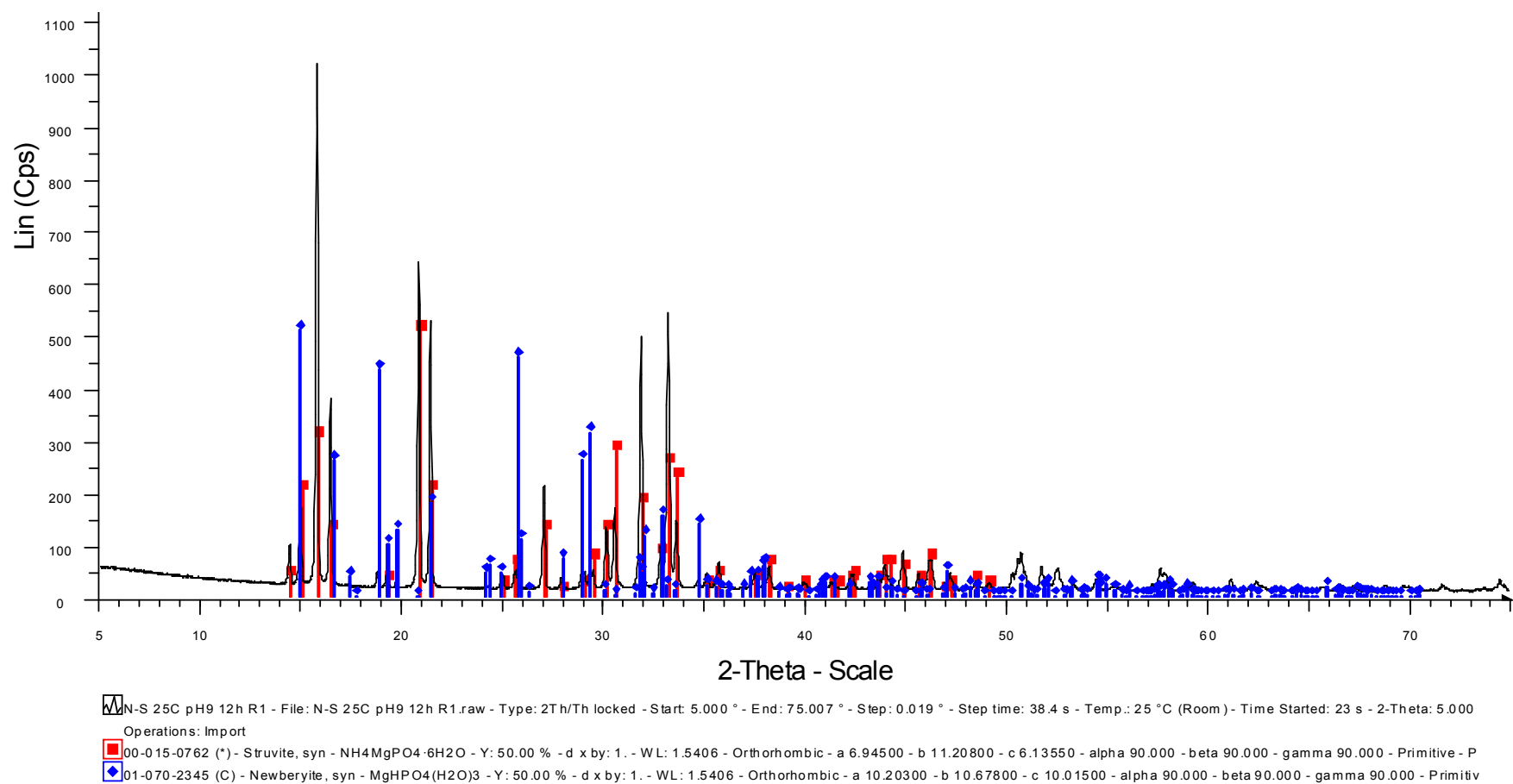


Figure C.8 – XRD output for Mg:N:P molar ratio 1:1.1:1, pH 9, 25° C, 12 h

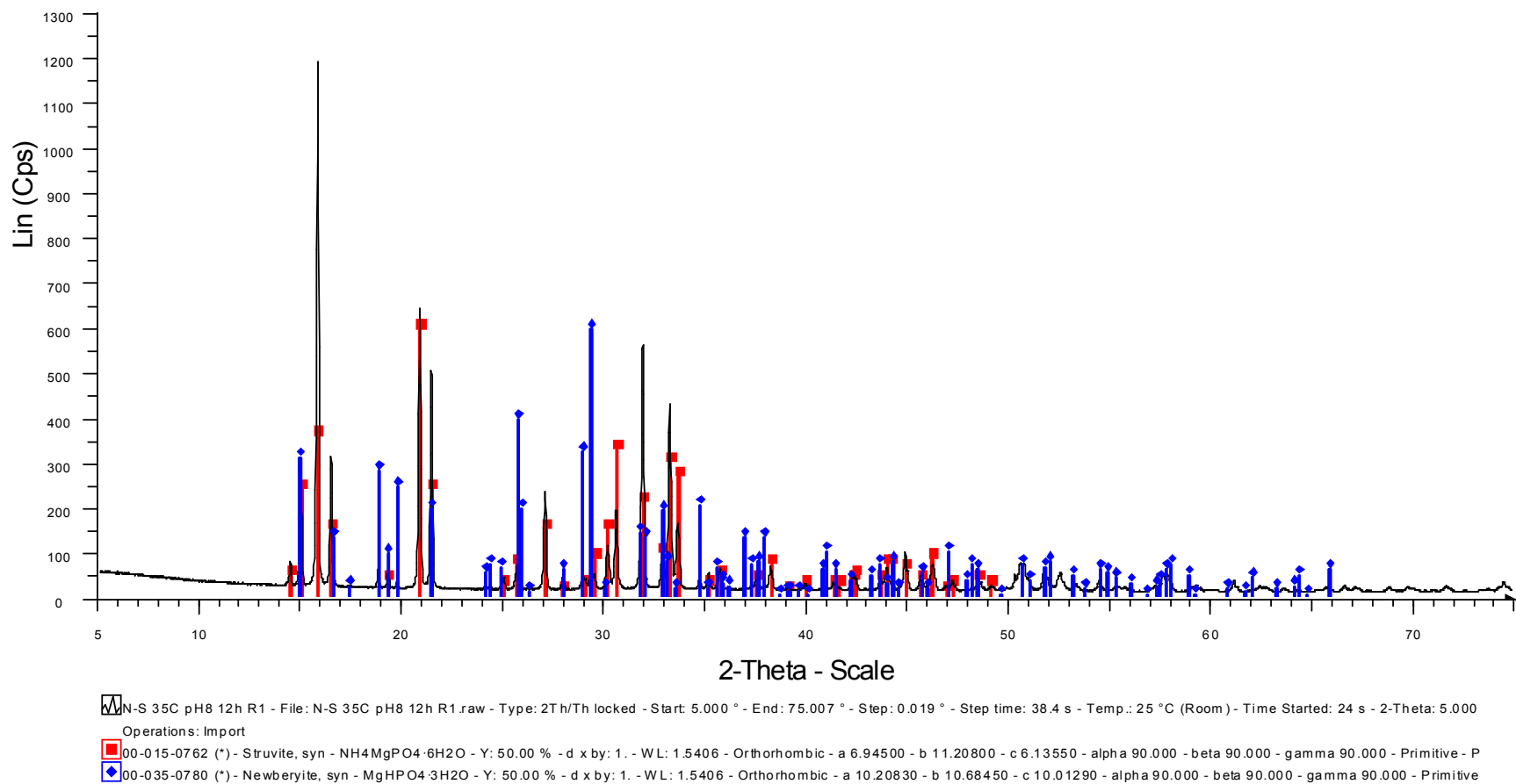


Figure C.9 – XRD output for Mg:N:P molar ratio 1:1.1:1, pH 8, 35° C, 12 h

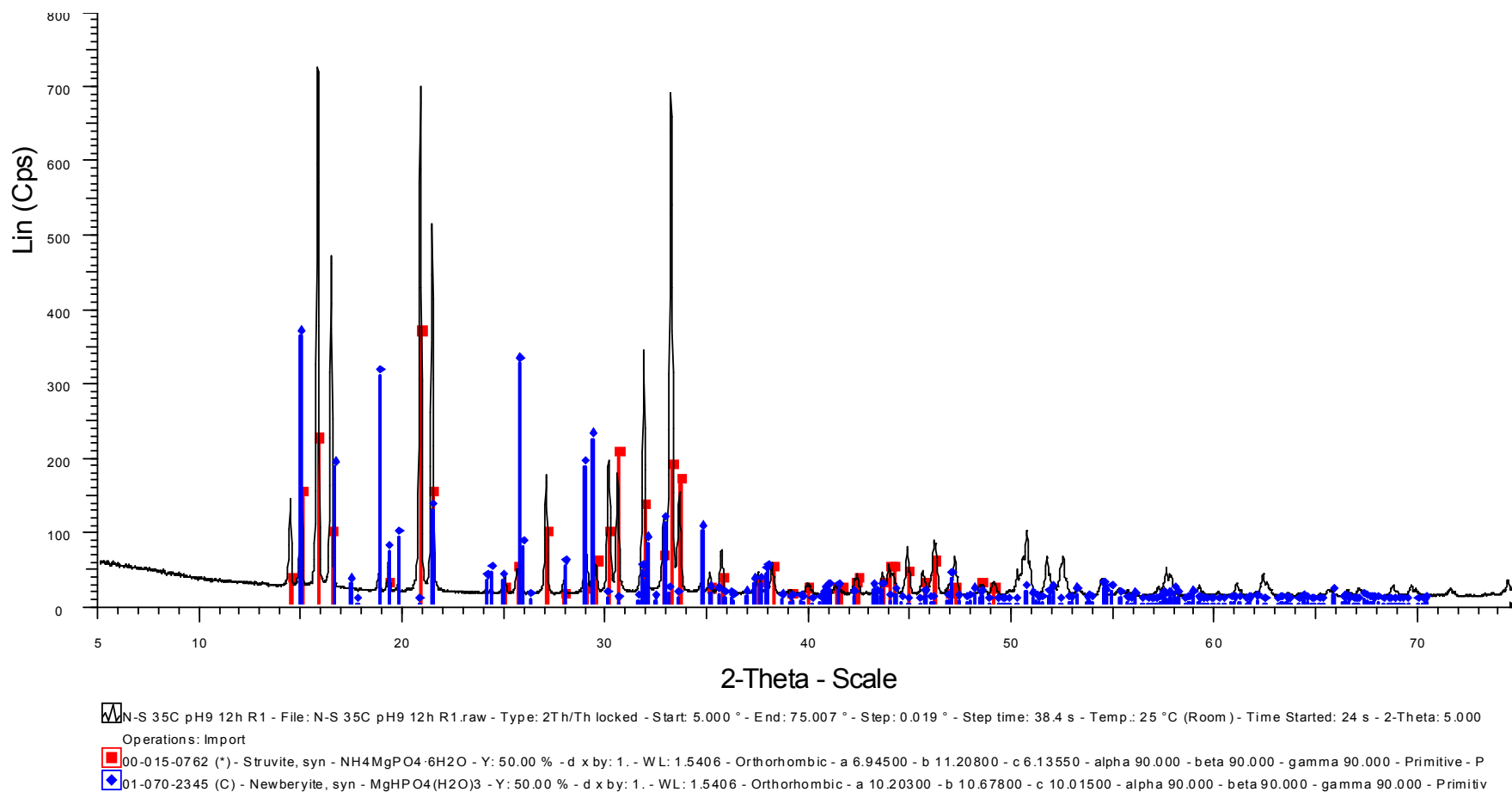


Figure C.10 – XRD output for Mg:N:P molar ratio 1:1.1:1, pH 9, 35° C, 12 h

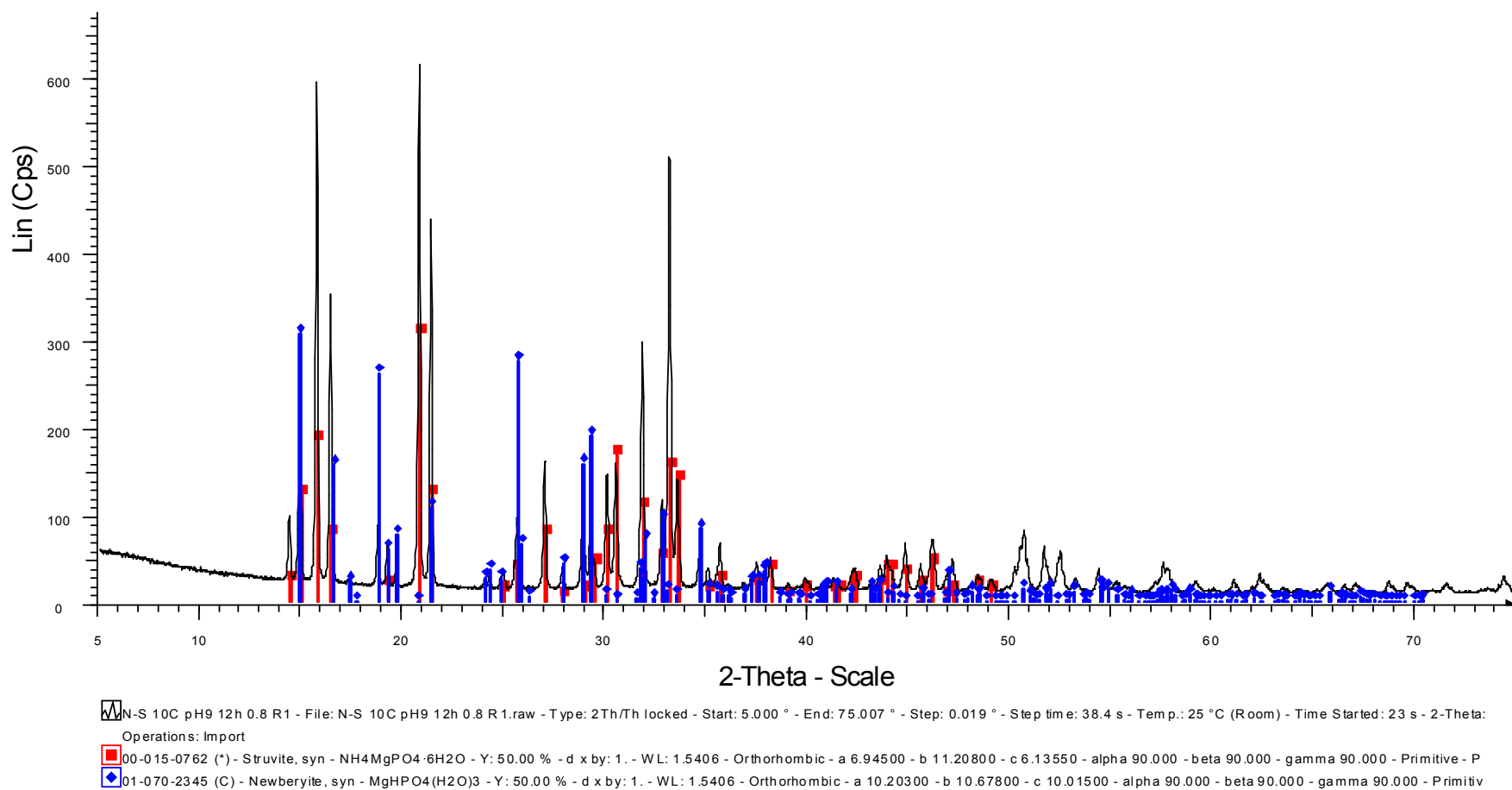


Figure C.11 – XRD output for Mg:N:P molar ratio 1:1.4:1, pH 9, 10° C, 12 h

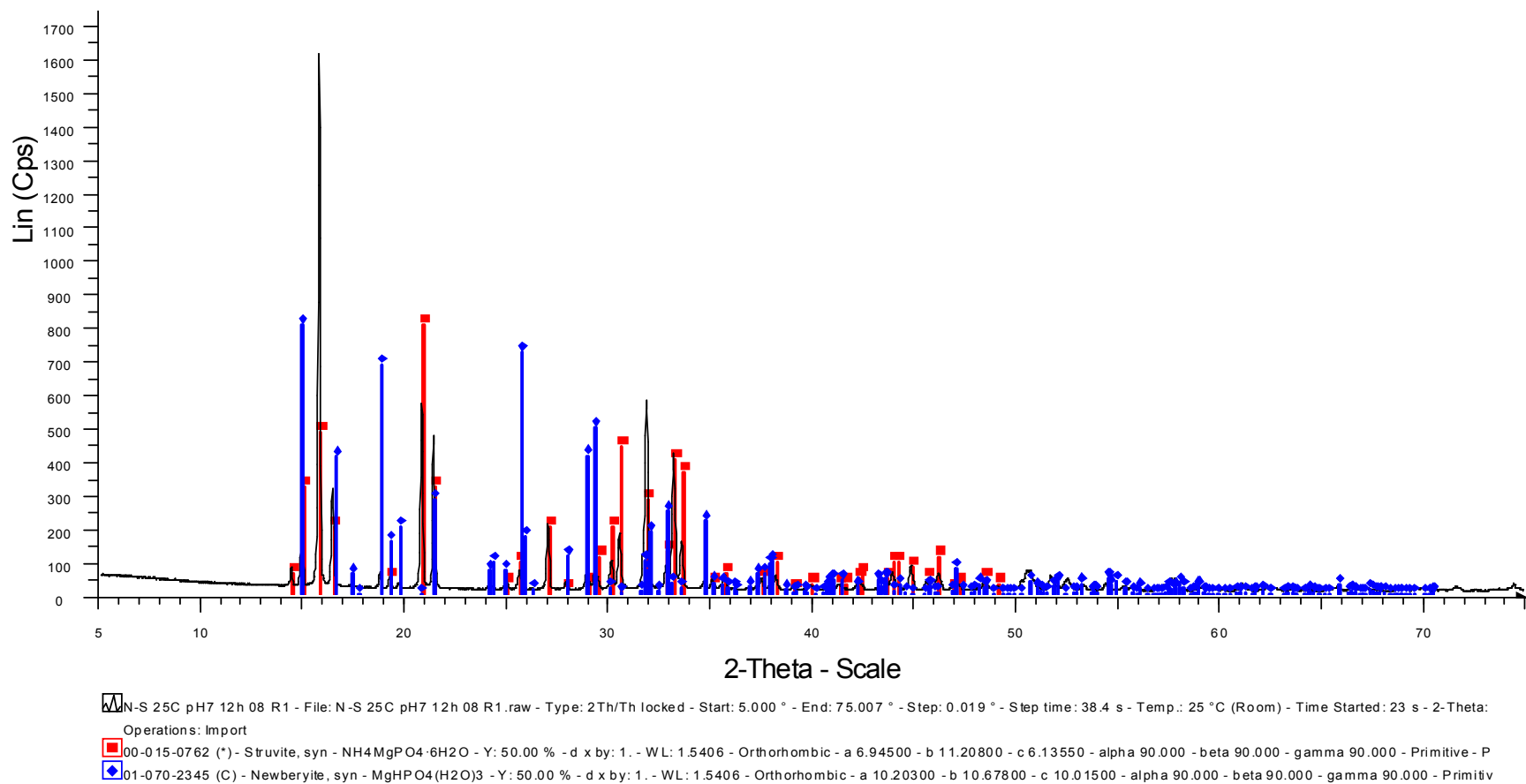


Figure C.12 – XRD output for Mg:N:P molar ratio 1:1.4:1, pH 7, 25° C, 12 h

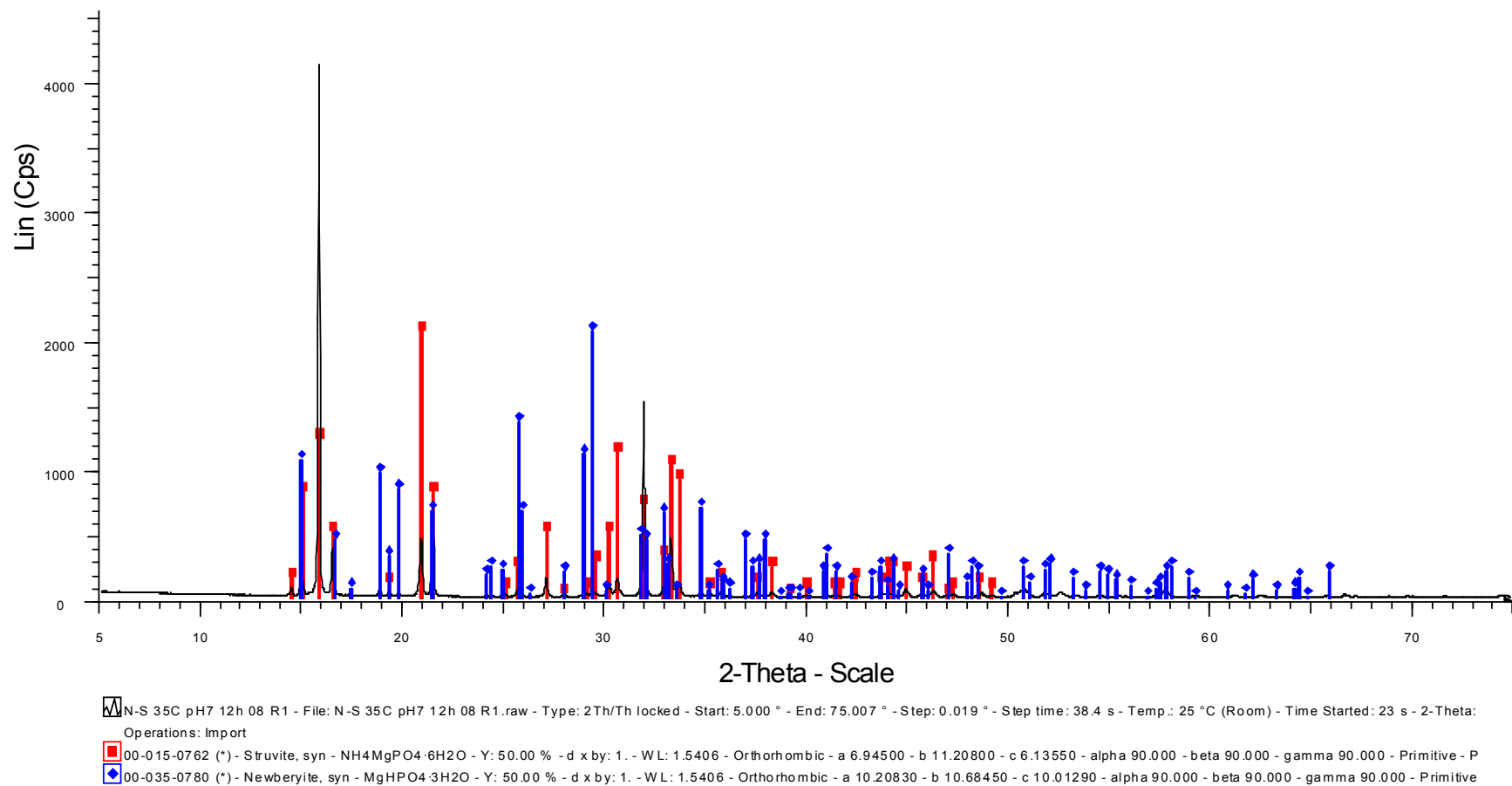


Figure C.13 – XRD output for Mg:N:P molar ratio 1:1.4:1, pH 7, 35 °C, 12 h

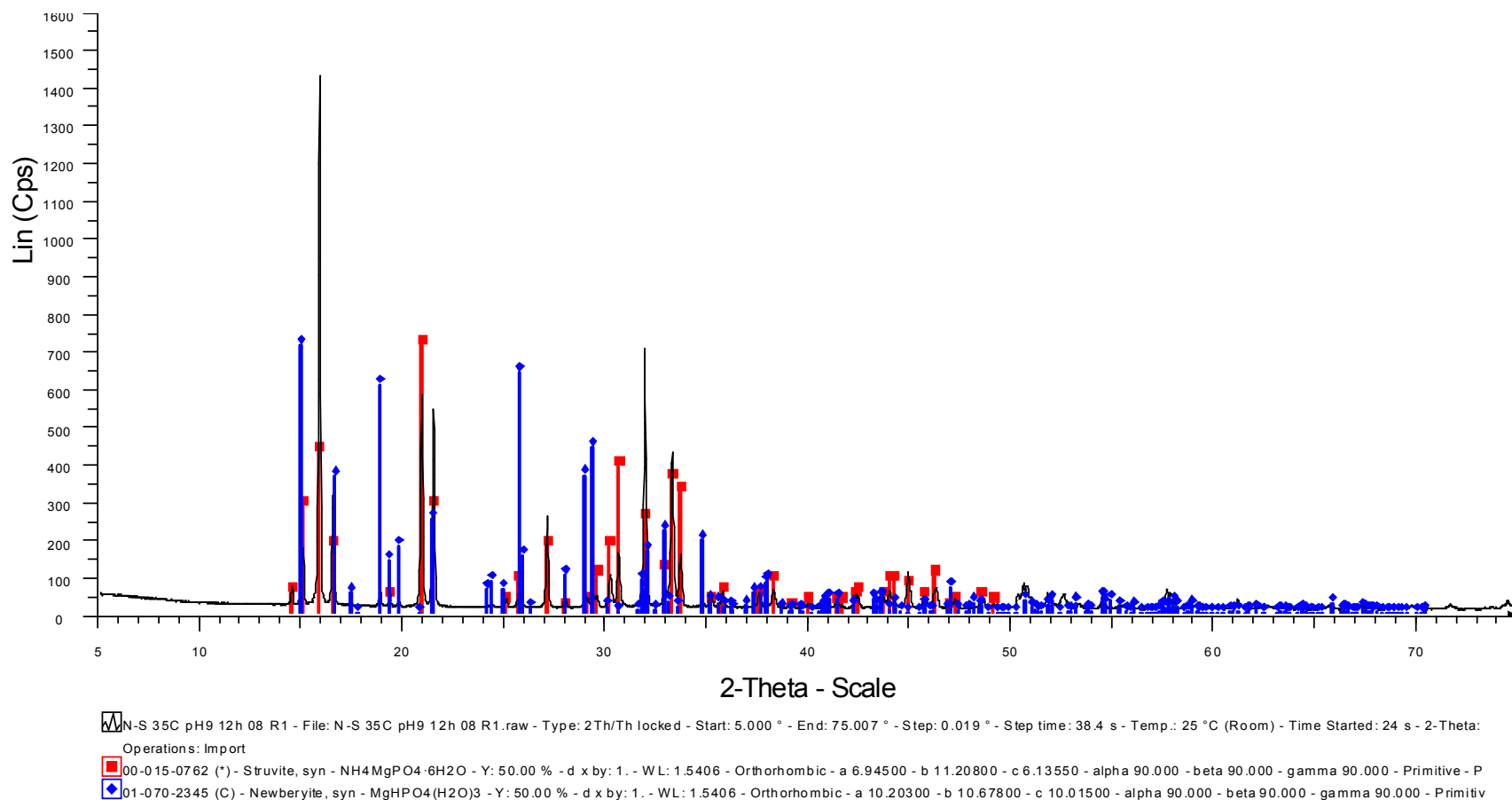


Figure C.14 – XRD output for Mg:N:P molar ratio 1:1.4:1, pH 9, 35° C, 12 h

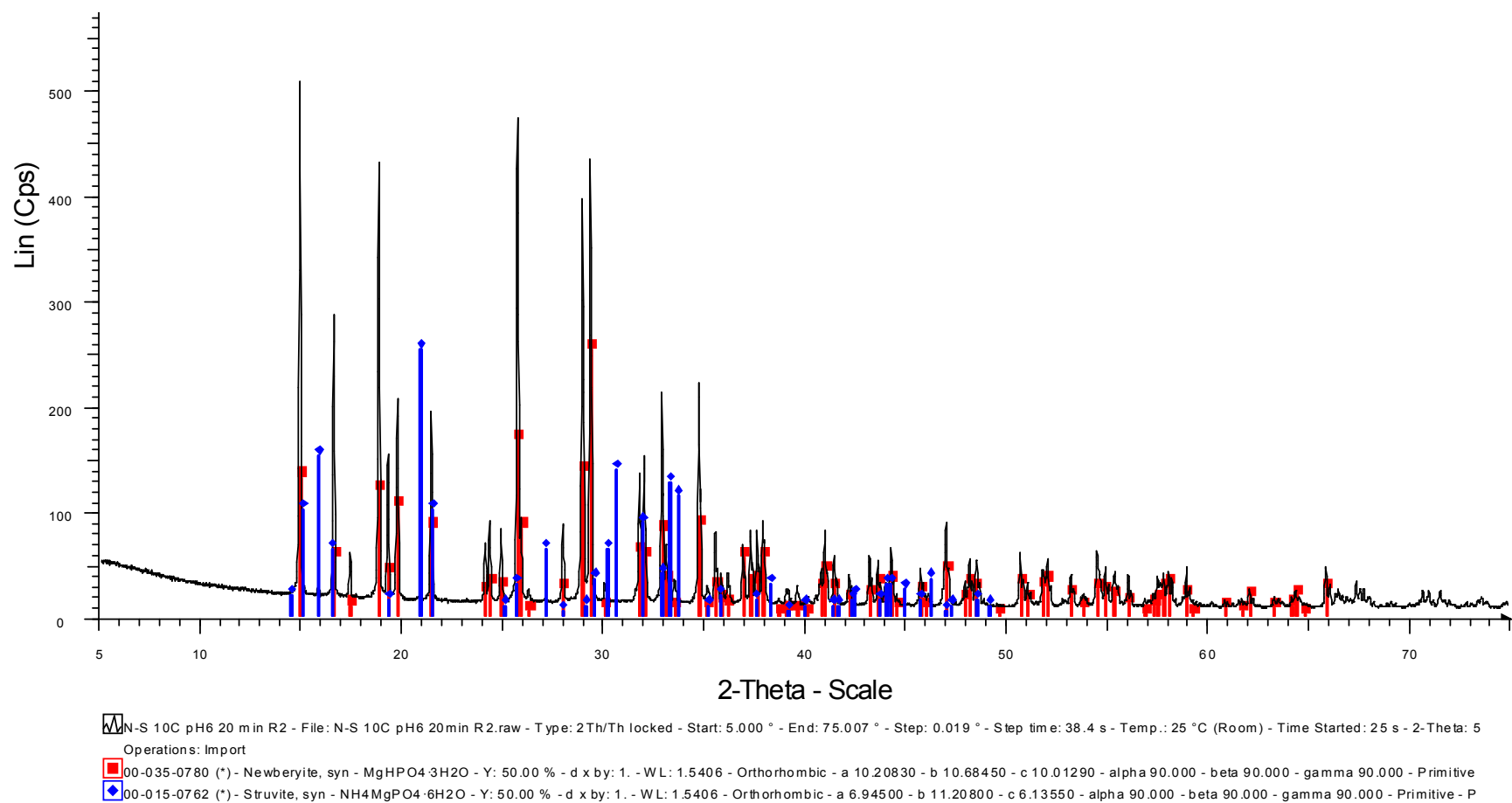


Figure C.15 – XRD output for Mg:N:P molar ratio 1:1.1:1, no pH control, 10° C, 20 mins

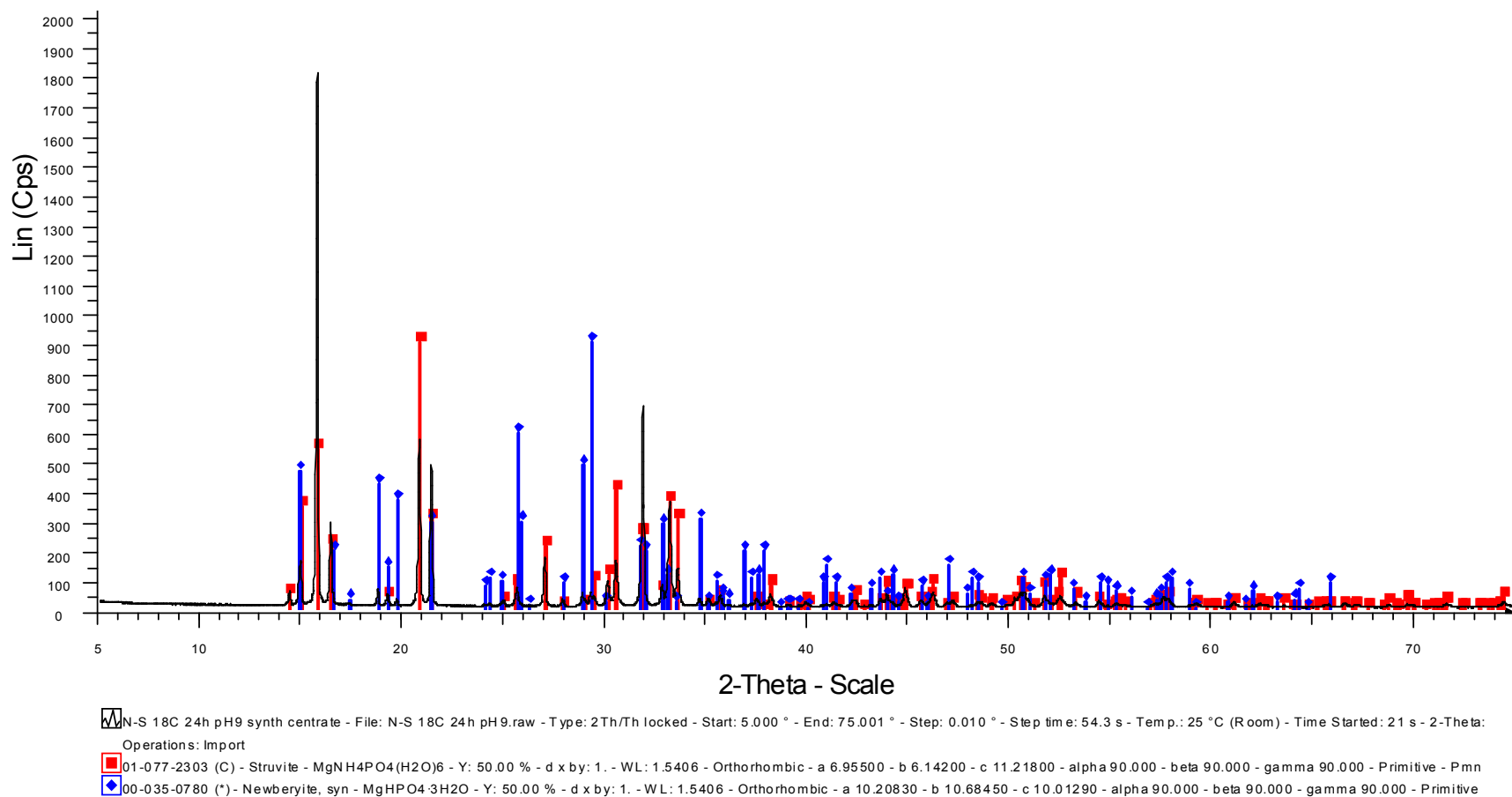


Figure C.16 – XRD output for Mg:N:P molar ratio 1:1:1 in synthetic crystallizer effluent, pH 9, 18° C, 24 h

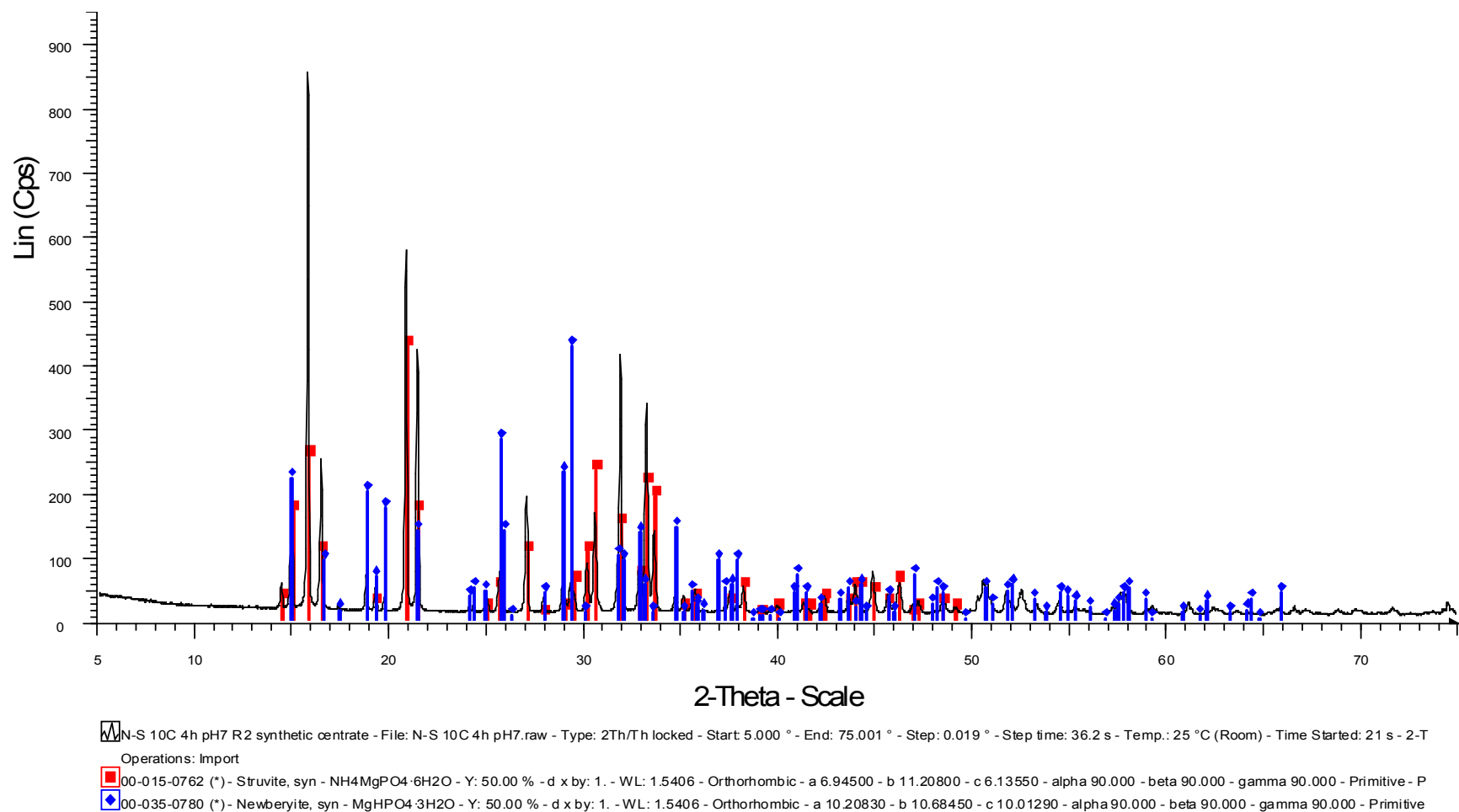


Figure C.17 – XRD output for Mg:N:P molar ratio 1:1.05:1 in synthetic centrate, pH 7, 10° C, 4 h

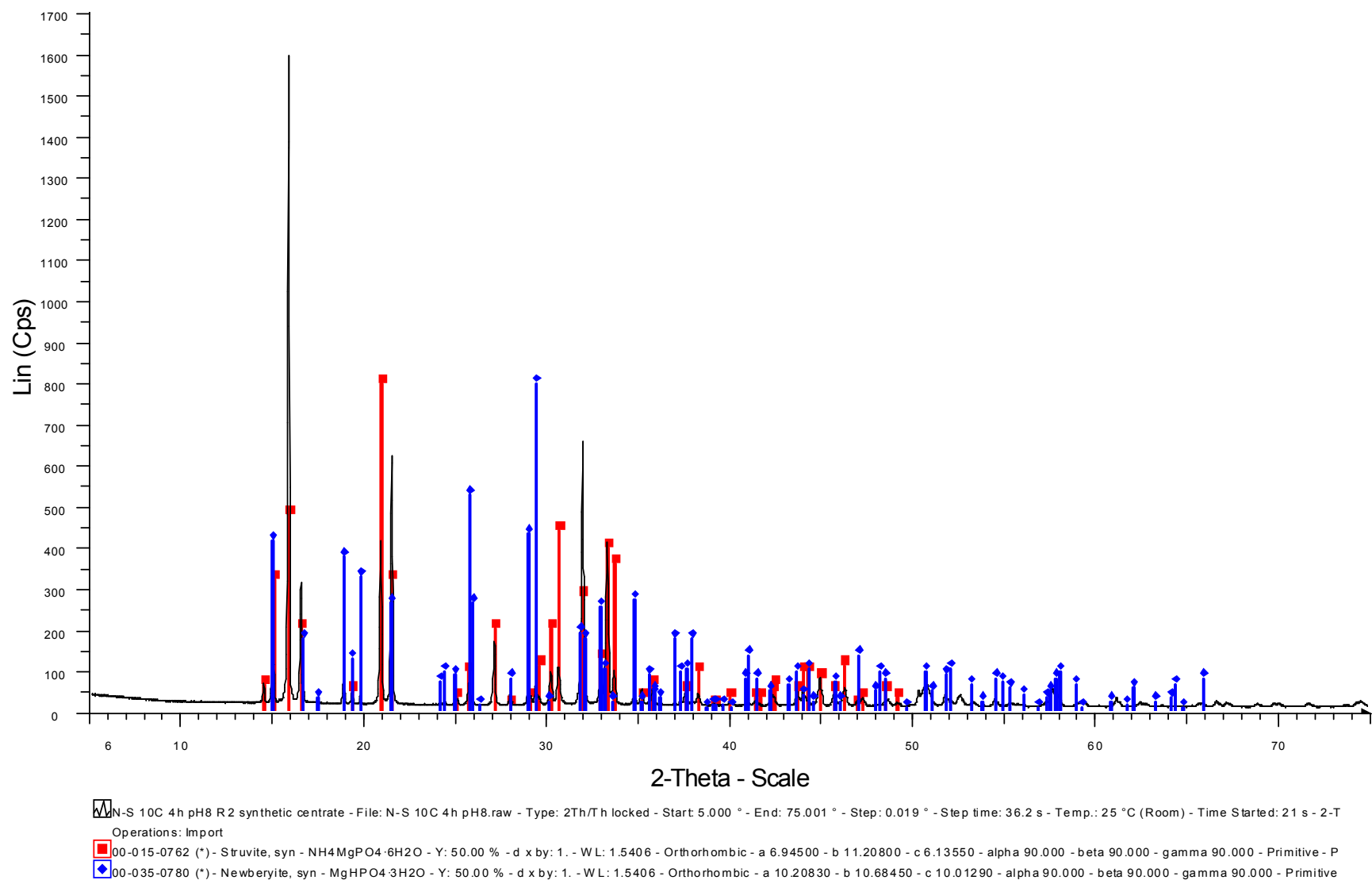


Figure C.18 – XRD output for Mg:N:P molar ratio 1:1.05:1 in synthetic centrate, pH 8, 10° C, 4 h

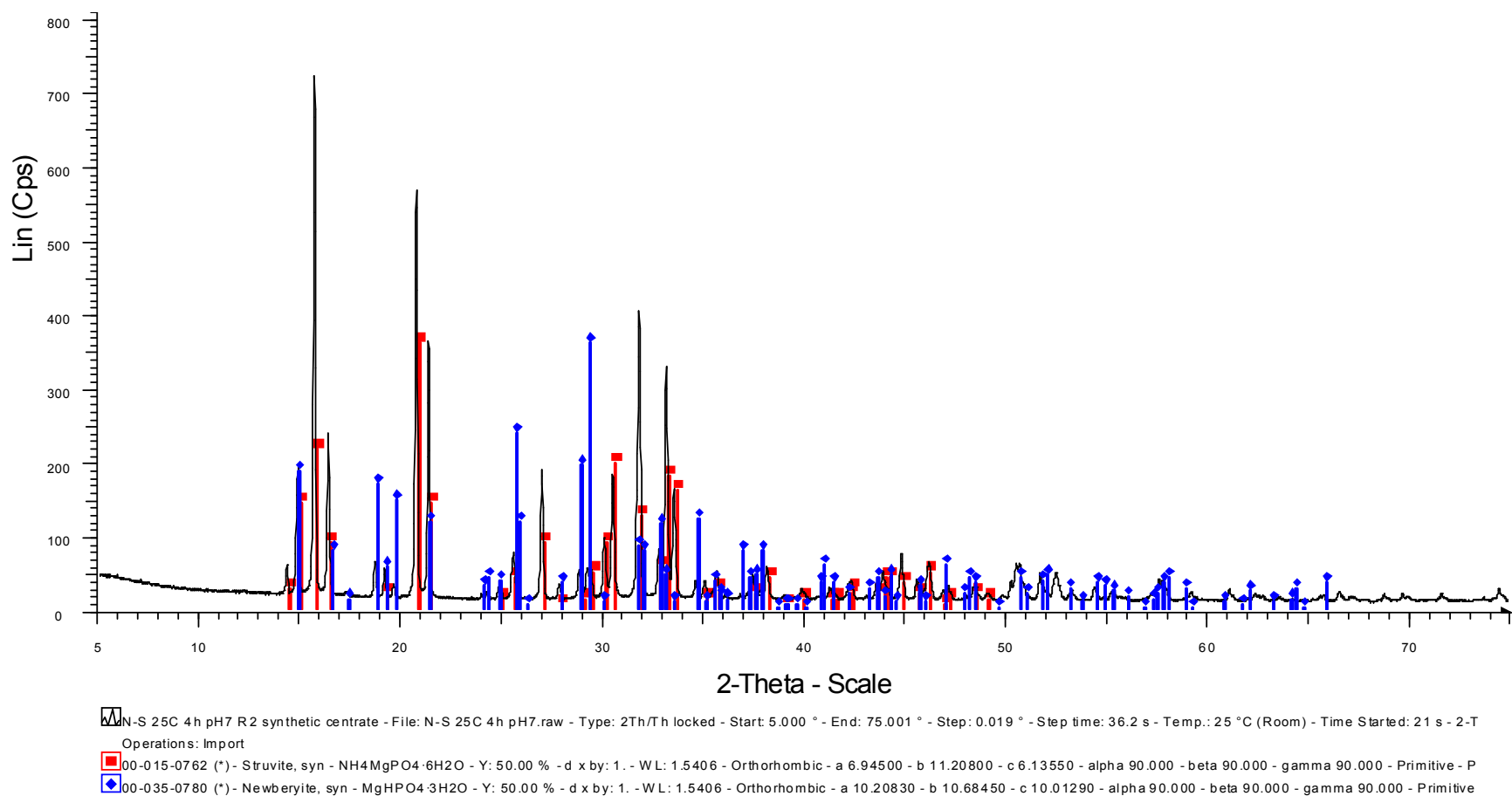


Figure C.19 – XRD output for Mg:N:P molar ratio 1:1.05:1 in synthetic centrate, pH 7, 25° C, 4 h

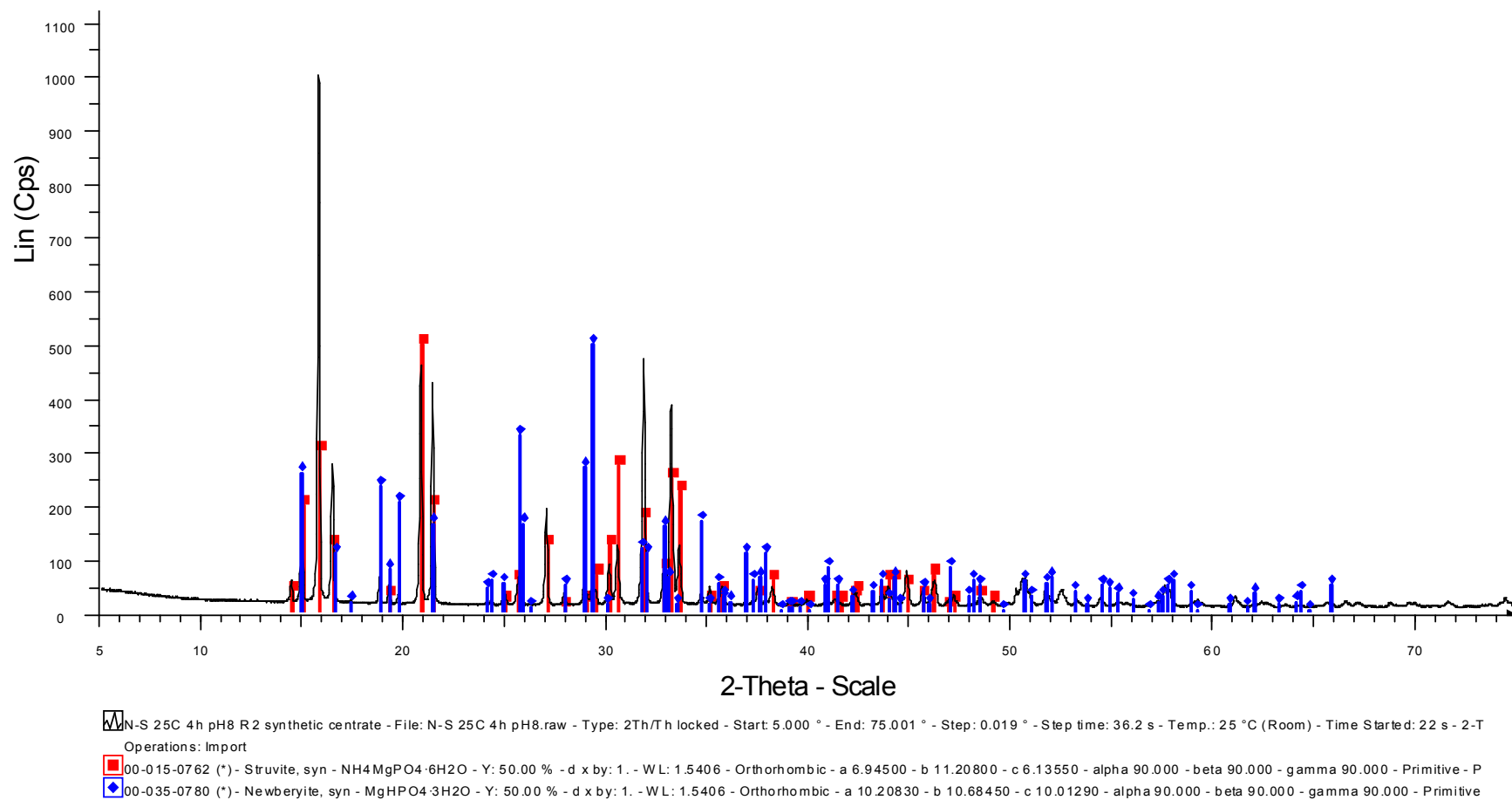


Figure C.20 – XRD output for Mg:N:P molar ratio 1:1.05:1 in synthetic centrate, pH 8, 25° C, 4 h

## APPENDIX D: MODELLING RESULTS

Table D.1 – Model equilibrium prediction for newberyite in ammonia solution at 35° C and Mg:N:P molar ratio 1:1.1:1 with consideration of bobbierite

Conditions		Concentration (mg/L)				
		Solid Species		Aqueous Species		
Temp (°C)	pH	Bobbierite	Struvite	Mg	NH <sub>4</sub> -N	PO <sub>4</sub> -P
35	7.04	591	8453	48	256	168
	8.09	232	10339	12	141	57
	9.26	249	10368	2	147	47

Table D.2 – Model equilibrium prediction for newberyite in ammonia solution at Mg:N:P molar ratio 1:1.1:1 without consideration of bobbierite

Conditions		Concentration (mg/L)				
		Solid Species		Aqueous Species		
Temp (°C)	Final pH	Newberyite	Struvite	Mg	NH <sub>4</sub> -N	PO <sub>4</sub> -P
10	5.88	3063	3247	380	553	491
	7.05	0	10707	72	127	93
	8.18	0	11280	16	95	20
	9.21	0	11388	5	88	7
25	6.20	5676	1432	198	657	256
	7.02	0	10491	93	140	120
	8.18	0	11236	20	97	26
	9.48	0	11373	6	89	8
35	6.44	6626	766	132	695	170
	7.04	437	9859	95	176	122
	8.09	0	11162	27	101	35
	9.26	0	11334	10	91	14

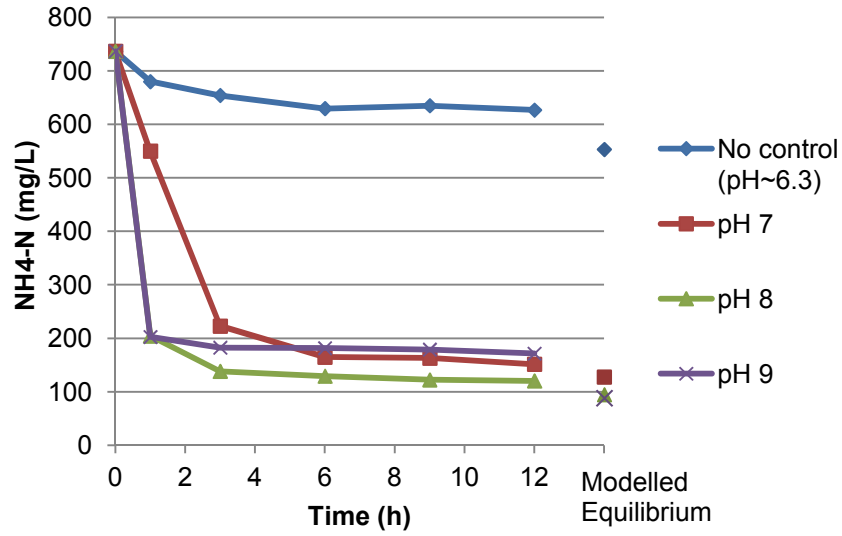


Figure D.1 – Comparison of real and model-predicted  $\text{NH}_4\text{-N}$  for newberyite in ammonia solution at 10° C and Mg:N:P molar ratio 1:1.1:1

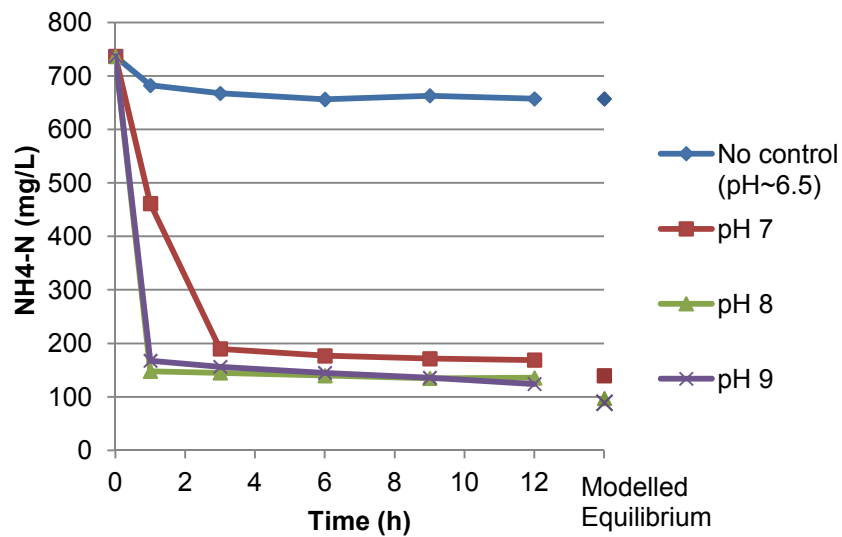


Figure D.2 – Comparison of real and model-predicted  $\text{NH}_4\text{-N}$  for newberyite in ammonia solution at 25° C and Mg:N:P molar ratio 1:1.1:1

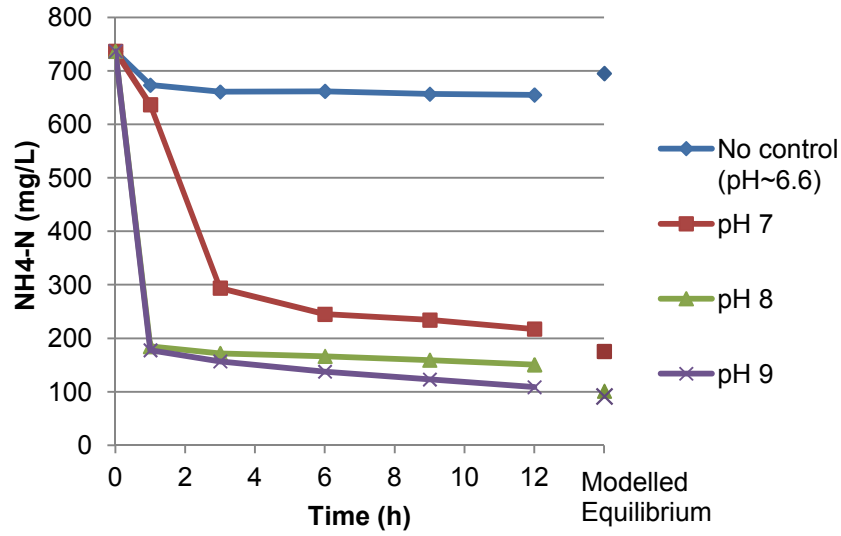


Figure D.3 – Comparison of real and model-predicted NH<sub>4</sub>-N for newberyite in ammonia solution at 35° C and Mg:N:P molar ratio 1:1.1:1

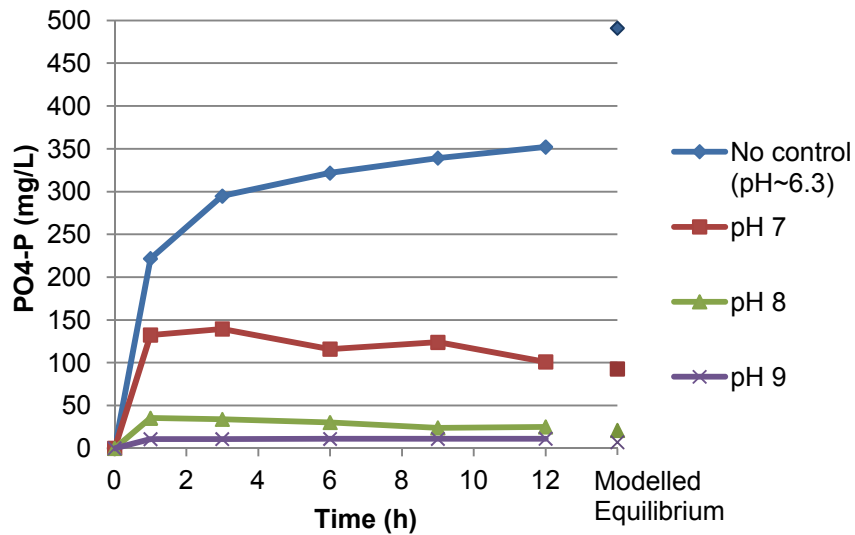


Figure D.4 – Comparison of real and model-predicted PO<sub>4</sub>-P for newberyite in ammonia solution at 10° C and Mg:N:P molar ratio 1:1.1:1

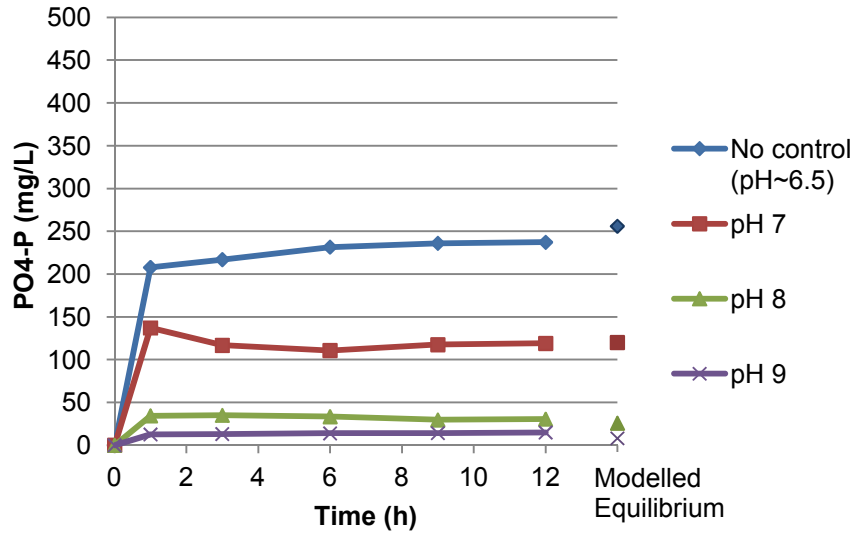


Figure D.5 – Comparison of real and model-predicted PO<sub>4</sub>-P for newberyite in ammonia solution at 25° C and Mg:N:P molar ratio 1:1.1:1

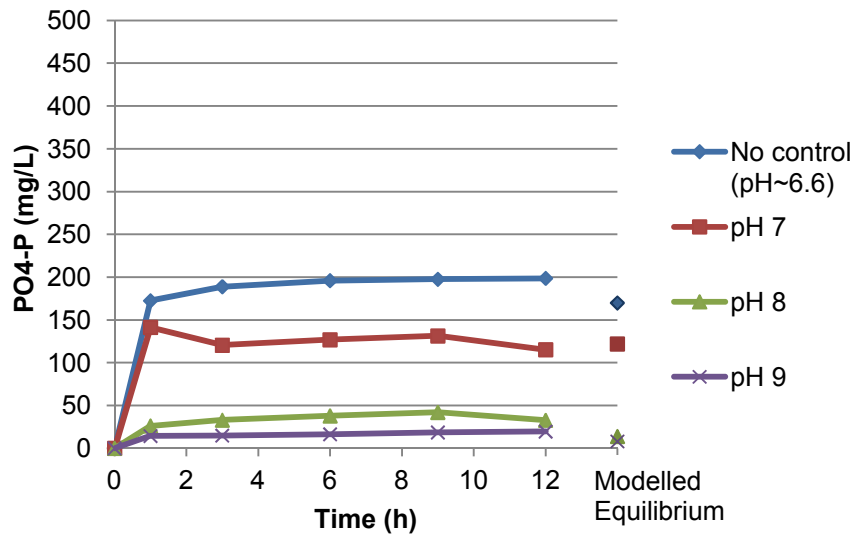


Figure D.6 – Comparison of real and model-predicted PO<sub>4</sub>-P for newberyite in ammonia solution at 35° C and Mg:N:P molar ratio 1:1.1:1

**Table D.3 – Model equilibrium prediction for newberyite in ammonia solution at 35° C and Mg:N:P molar ratio 1:1.4:1 with consideration of bobbierite**

Conditions		Concentration (mg/L)				
		Solid Species		Aqueous Species		
Temp (°C)	pH	Bobbierite	Struvite	Mg	NH <sub>4</sub> -N	PO <sub>4</sub> -P
35	7.07	398	7855	56	290	103

**Table D.4 – Model equilibrium prediction for newberyite in ammonia solution at Mg:N:P molar ratio 1:1.4:1 without consideration of bobbierite**

Conditions		Concentration (mg/L)				
		Solid Species		Aqueous Species		
Temp (°C)	Final pH	Newberyite	Struvite	Mg	NH <sub>4</sub> -N	PO <sub>4</sub> -P
10	5.88	1434	3247	380	553	491
	7.07	0	8653	49	245	63
	8.08	0	9031	12	223	15
	9.16	0	9114	3	219	4
25	6.20	4047	1432	198	657	256
	6.99	0	8448	69	256	89
	8.14	0	9006	14	224	18
	9.07	0	9094	5	220	7
35	6.44	4997	766	132	695	170
	7.07	0	8423	71	258	92
	8.16	0	8982	16	226	21
	9.01	0	9070	8	221	10

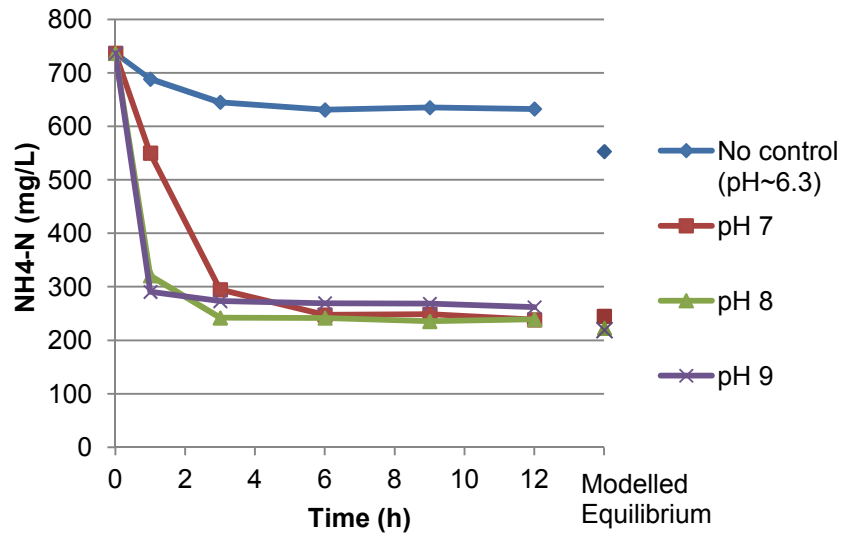


Figure D.7 – Comparison of real and model-predicted  $\text{NH}_4\text{-N}$  for newberyite in ammonia solution at 10° C and Mg:N:P molar ratio 1:1.4:1

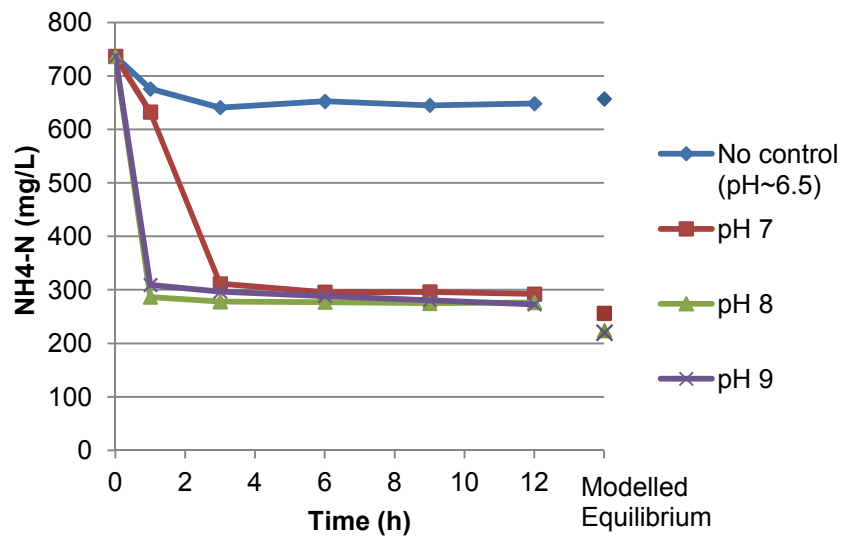


Figure D.8 – Comparison of real and model-predicted  $\text{NH}_4\text{-N}$  for newberyite in ammonia solution at 25° C and Mg:N:P molar ratio 1:1.4:1

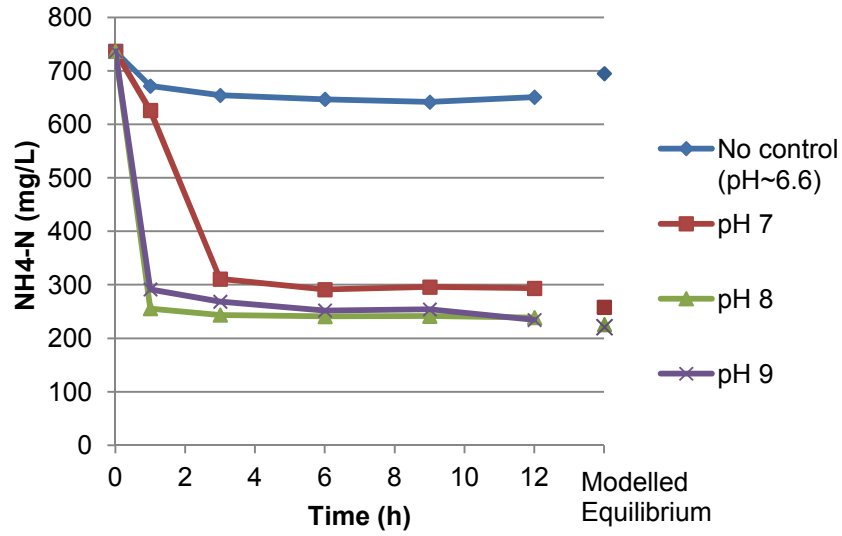


Figure D.9 – Comparison of real and model-predicted NH<sub>4</sub>-N for newberyite in ammonia solution at 35° C and Mg:N:P molar ratio 1:1.4:1

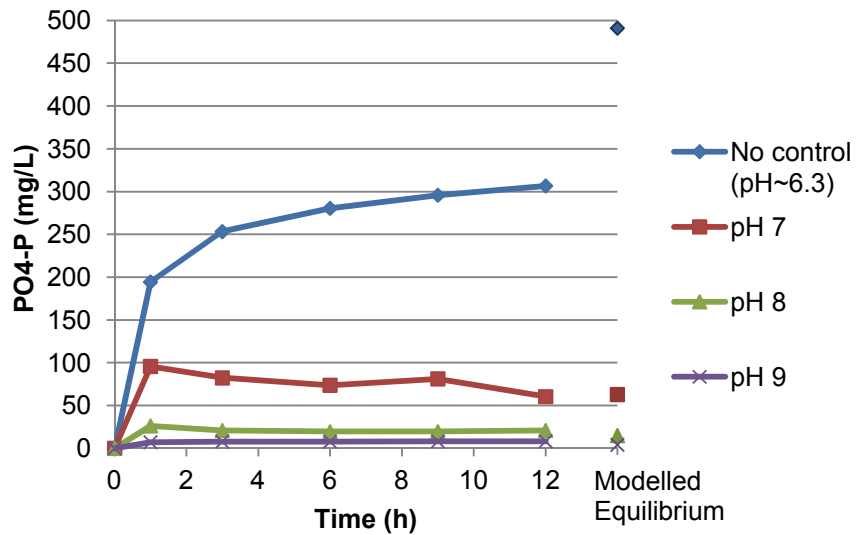


Figure D.10 – Comparison of real and model-predicted PO<sub>4</sub>-P for newberyite in ammonia solution at 10° C and Mg:N:P molar ratio 1:1.4:1

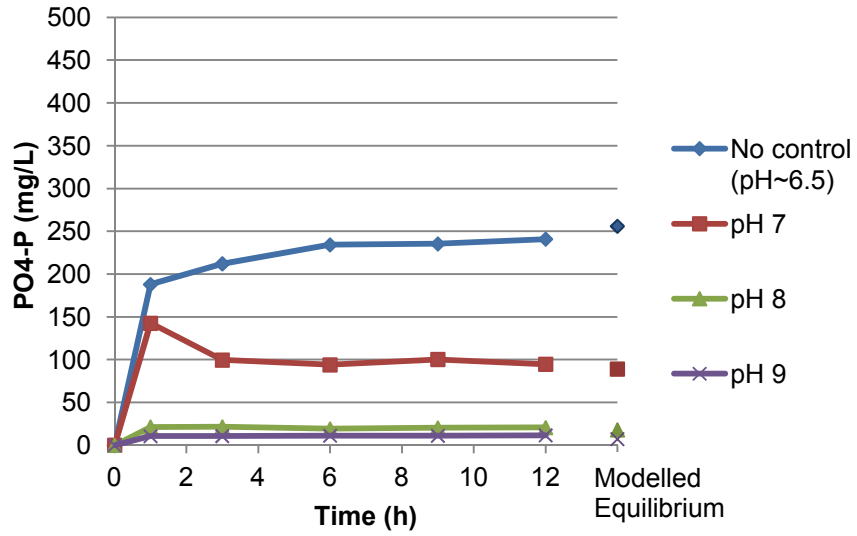


Figure D.11 – Comparison of real and model-predicted PO<sub>4</sub>-P for newberyite in ammonia solution at 25° C and Mg:N:P molar ratio 1:1.4:1

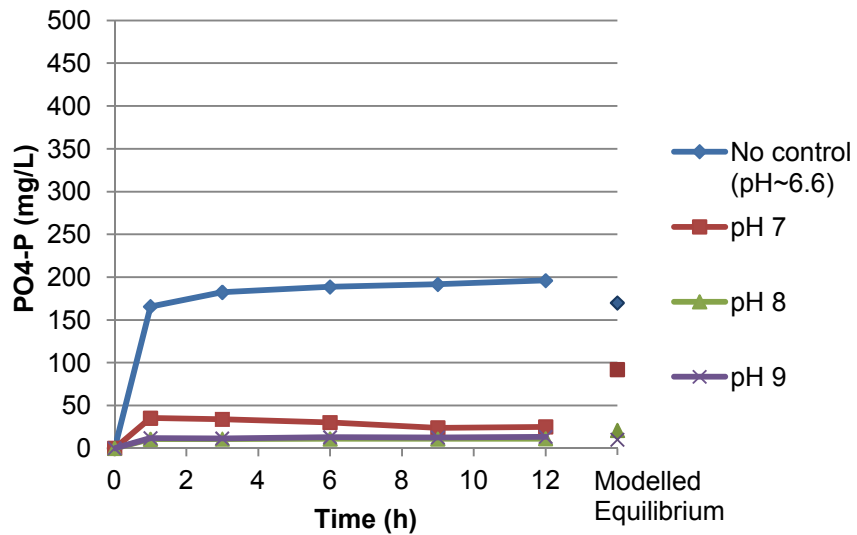


Figure D.12 – Comparison of real and model-predicted PO<sub>4</sub>-P for newberyite in ammonia solution at 35° C and Mg:N:P molar ratio 1:1.4:1

**Table D.5 – Model equilibrium prediction for newberyite in synthetic crystallizer effluent at Mg:N:P molar ratio 1:1:1 with consideration of magnesite and bobbierite**

Conditions		Concentration (mg/L)				
		Solid Species		Aqueous Species		
Temp (°C)	pH	Magnesite	Struvite	Mg	NH <sub>4</sub> -N	PO <sub>4</sub> -P
10	7.00	344	14382	69	102	216
	7.99	428	14774	7	80	167
25	7.01	680	13558	54	149	321
	8.07	704	13990	5	125	266

**Table D.6 – Model equilibrium prediction for newberyite in synthetic crystallizer effluent at Mg:N:P molar ratio 1:1:1 without consideration of magnesite and bobbierite**

Conditions		Concentration (mg/L)				
		Solid Species		Aqueous Species		
Temp (°C)	pH	Newberyite	Struvite	Mg	NH <sub>4</sub> -N	PO <sub>4</sub> -P
10	7.00	0	14823	125	77	161
	7.99	0	15626	46	31	59
25	7.01	310	14308	132	106	171
	8.07	0	15562	52	35	67

**Table D.7 – Model equilibrium prediction for synthetic newberyite in synthetic centrate at Mg:N:P molar ratio 1:1.05:1 with consideration of magnesite and bobbierite**

Conditions		Concentration (mg/L)				
		Solid Species		Aqueous Species		
Temp (°C)	pH	Magnesite	Struvite	Mg	NH <sub>4</sub> -N	PO <sub>4</sub> -P
10	7.01	271	15347	60	136	174
	8.10	337	15714	5	115	128
25	7.05	620	14504	42	184	281
	8.06	627	14872	4	163	234

**Table D.8 – Model equilibrium prediction for synthetic newberyite in synthetic centrate at Mg:N:P molar ratio 1:1.05:1 without consideration of magnesite and bobbierite**

Conditions		Concentration (mg/L)				
		Solid Species		Aqueous Species		
Temp (°C)	pH	Newberyite	Struvite	Mg	NH <sub>4</sub> -N	PO <sub>4</sub> -P
10	7.01	0	15734	99	114	125
	8.10	0	16474	27	71	31
25	7.05	592	15577	115	123	145
	8.06	0	16386	35	76	42